

AD-A100 836

NATIONAL AERONAUTICAL ESTABLISHMENT OTTAWA (ONTARIO)

F/G 17/7

A KALMAN FILTER APPROACH TO NAVIGATION ON THE NAE CONVAIR 580 A-ETC(U)

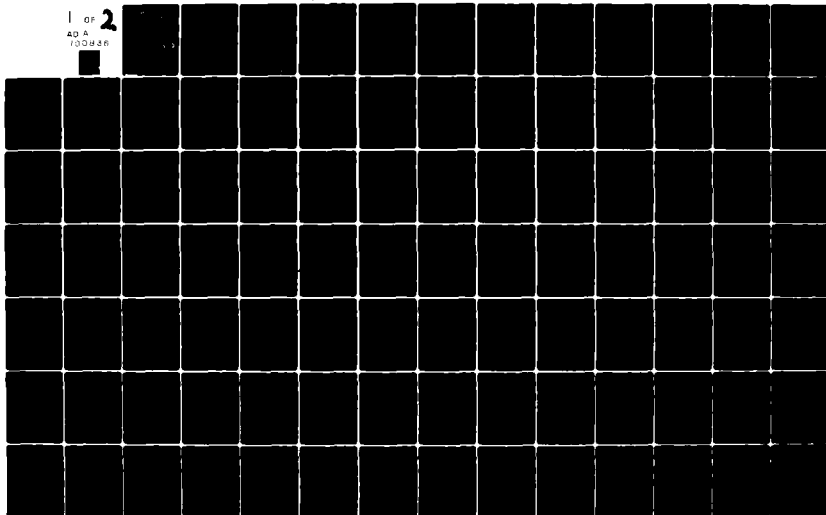
FEB 81 B W LEACH

UNCLASSIFIED NAE-LR-604

NRC-19271

NL

1 OF 2
AD A
100836





National Research
Council Canada

Conseil national
de recherches Canada

⑥ LEVEL

A KALMAN FILTER APPROACH TO NAVIGATION ON THE NAE CONVAIR 580 AEROMAGNETICS RESEARCH AIRCRAFT

by

B.W. Leach

National Aeronautical Establishment

OTTAWA

FEBRUARY 1981

DISTRIBUTION STATEMENT A

Approved for public release;
Distribution Unlimited

AERONAUTICAL REPORT

LR-604

NRC NO. 19271

Canada

81 6 29 273

DTIC FILE COPY

AD A110 603 86

DTIC
ELECTE
JUN 30 1981
S B D

**A KALMAN FILTER APPROACH TO NAVIGATION ON THE
NAE CONVAIR 580 AEROMAGNETICS RESEARCH AIRCRAFT**

**(L'APPORT DU FILTRE KALMAN DANS LE SYSTÈME DE NAVIGATION
DE L'AÉRONEF DE RECHERCHE AÉROMAGNÉTIQUE NAE CONVAIR 580**

by/par

B.W./Leach

A.D. Wood, Head/Chef
Flight Research Laboratory/
Laboratoire des recherches en vol

G.M. Lindberg
Director/Directeur

(i/ii)

ABSTRACT

Doppler radar, compass heading, and VLF communications station phase difference information are combined in an optimal fashion to form an integrated navigation system based on the concepts of Kalman filtering. A ten-state Doppler/VLF Kalman filter navigation algorithm is designed for use onboard the NAE Convair 580 aeromagnetics research aircraft, with simulation studies conducted using computer programs written in FORTRAN for the IBM 3032 TSS operating environment. Results from the studies show the unique features of a Kalman filtering approach to the navigation task. Various contingencies, or anomalous situations, that can arise when handling the VLF data are considered, and solutions are offered in the context of the Kalman filter approach being used. A comparison study involving simulated navigation data demonstrates the superiority of the Kalman filter navigator compared to simpler navigation algorithms, especially when significant bias errors occur in the basic quantities being measured. A further comparison study based on navigation data collected onboard the Convair verifies that the proposed Kalman filter navigation algorithm operates properly when using typical 'real world' data.

SOMMAIRE

Des données de radar Doppler, de cap au compas et de déphasage entre stations de télécommunications VLF sont combinées de façon optimale dans un nouveau système de navigation intégré fondé sur les principes du filtrage Kalman. On a en effet élaboré un algorithme de navigation pour filtre Kalman Doppler/VLF à dix états utilisé à bord de l'aéronef de recherche aéromagnétique NAE Convair 580; des études de simulation ont été menées à l'aide de programmes informatiques rédigés en FORTRAN pour le milieu de fonctionnement du système TSS IBM 3032. Les résultats de ces études font ressortir l'apport unique du filtrage Kalman dans un système de navigation. Diverses contingences ou anomalies pouvant se présenter lors du traitement des données VLF sont mises en évidence, et des solutions faisant appel au filtrage Kalman sont proposées. Une étude comparative portant sur des données de navigation simulées démontre la supériorité du navigateur à filtre Kalman par rapport à des algorithmes de navigation plus simples, surtout lorsque se présentent des erreurs non centrées importantes dans les grandeurs de base mesurées. Une autre étude comparative reposant sur des données de navigation recueillies à bord du Convair confirme l'efficacité de l'algorithme de navigation pour filtre Kalman lorsque des données typiques et 'réelles' sont utilisées.

on For	<input checked="" type="checkbox"/>
BA&I	<input checked="" type="checkbox"/>
B	<input type="checkbox"/>
need	<input type="checkbox"/>
action	<input type="checkbox"/>

By	PER LETTER
Distribution	
Availability	
Availability	
Dist	
A	

CONTENTS

	Page
ABSTRACT	(iii)
ILLUSTRATIONS	(v)
APPENDICES	(vii)
SYMBOLS	(vii)
1.0 INTRODUCTION	1
2.0 THEORY OF KALMAN FILTERING	1
2.1 Elementary Statistical Concepts	1
2.2 State Variable Formulation for a Linear Kalman Filter	3
2.2.1 Scalar Kalman Filter	3
2.2.2 General Form of the Linear Kalman Filter	6
2.3 A Quasi-Linear Approach for Nonlinear Systems	9
2.4 Practical Aspects of Designing and Running a Kalman Filter	10
2.4.1 System and Statistical Modelling	10
2.4.2 Numerical Accuracy and Stability	11
3.0 A DOPPLER/VLF KALMAN FILTER NAVIGATOR	12
3.1 Description of the Basic Navigation Transducers	12
3.2 Mathematical Development for the Kalman Filter Navigator	13
4.0 SIMULATION EXPERIMENTS WITH THE DOPPLER/VLF KALMAN FILTER	21
4.1 Details Concerning the Simulation Algorithm	21
4.2 Transient and Steady State Nature of the Kalman Filter	21
4.3 Bias Estimation and Linear Dependency Problems	24
4.4 Handling VLF Bias Drifting	25
4.5 Contingency Planning for VLF	28
4.5.1 VLF Data Management Problems	28
4.5.2 In-Flight Measurement of VLF Phase Variance	30
4.5.3 Detecting VLF Bias Shifts	31
5.0 A COMPARISON OF FIVE DIFFERENT NAVIGATION ALGORITHMS	32
5.1 Description of the Five Navigation Algorithms	32
5.2 Description of the Different Types of Simulated Navigation Data	37
5.3 Results from Simulating Best Quality Data	39
5.4 Results from Simulating Large Doppler/Heading Biases	40
5.5 Results from Simulating Large VLF Station Biases	41
5.6 Results from Simulating VLF Station Drift	41
5.7 Results from Using Real Data	41
5.8 Summary of Results	15

CONTENTS (Cont'd)

		Page
6.0	CONCLUSIONS	46
	6.1 Assessment of the Kalman Filter Approach to Navigation.....	46
	6.2 Future Work	46
7.0	ACKNOWLEDGEMENTS.....	47
8.0	REFERENCES	47

TABLES

Table		Page
4.1	Simulated Navigation Conditions	22
4.2	Kalman Filter Initial Conditions for Transient Response Study	23
4.3	Simulated Navigation Conditions for a Drifting VLF Station Experiment	26
4.4	Kalman Filter Initial Conditions for Drifting VLF Station Experiment.....	27
5.1	Initial Conditions for Naive Kalman Filter	37
5.2	Information on the Visual Reference Points for the Navigation Study	42
5.3	VLF Station Information for the Navigation Study	43
5.4	Real Data Initial Conditions for the Naive Kalman Filter	43
5.5	Changes to Initial Conditions for the Smart Kalman Filter	44

ILLUSTRATIONS

Figure		Page
1	Proposed Doppler/VLF Navigator.....	51
2	Detailed Doppler/VLF Kalman Filter Navigation Scheme.....	52
3	Block Diagram of Kalman Navigation Filter Simulator	53
4	Flowchart of Kalman Filter Simulator	54
5	Kalman Filter Output Errors for Small Initial Error Variances	55

ILLUSTRATIONS (Cont'd)

Figure		Page
6	Kalman Filter Output Errors for Medium Initial Error Variances	56
7	Kalman Filter Output Errors for Large Initial Error Variances	57
8	Stabilization of P and K Matrices with Time for Small \underline{P}_0	58
9	Stabilization of P and K Matrices with Time for Medium \underline{P}_0 ..	59
10	Stabilization of P and K Matrices with Time for Large \underline{P}_0	60
11	Kalman Filter Output Errors for Large Initial Bias Error Variances — No VLF Biases Simulated in Data	61
12	Kalman Filter Output Errors for Large Initial Bias Error Variances — Davis Strait Location.	62
13	Stabilization of P and K Matrices with Time for Large \underline{P}_0 and Davis Strait Location	63
14	VLF Geometry — Projection Centred in Ottawa Area.	64
15	VLF Geometry — Projection Centred in Davis Strait Area	65
16	Kalman Filter Run with Four out of Six VLF Biases Being Estimated from Poor Initial Conditions	66
17	Kalman Filter Output Errors Showing Effect of Linear Drift in Two VLF Stations.	67
18	Kalman Filter Output Errors — Two Drifting VLF Stations with Appropriate \underline{P}_0 Elements Fixed	68
19	Kalman Filter Output Errors — Two Drifting VLF Stations Weighted Out	69
20	Comparison of Total Position Errors Using Best Quality Data.	70
21	Comparison of Total Position Errors Using Best Quality Data and Circular Track	71
22	Comparison of Total Position Errors Using Data with Large Doppler Biases	72
23	Comparison of Total Position Errors Using Data with Large Doppler Biases and Circular Track	73
24	Doppler Bias Error Plots — Large Doppler/Heading Biases Simulated	74
25	Comparison of Total Position Errors Using Data with Large VLF Biases.	75
26	Naive Kalman Filter Output Errors for Large Doppler/Heading Biases and Large VLF Biases	76

ILLUSTRATIONS (Cont'd)

Figure		Page
27	Smart Kalman Filter Output Errors for Large Doppler/Heading Biases and Large VLF Biases	77
28	Comparison of Total Position Errors Using Data with a Large VLF Drift	78
29	Naive Kalman Filter Output Errors for VLF Drift in Station O	79
30	Smart Kalman Filter Output Errors for VLF Drift in Station O	80
31	VLF Geometry — Stations Available During Navigation Flight	81
32	Naive Kalman Filter Outputs for Real Data.	82
33	Position Errors for Naive Kalman Filter Run.	83
34	Smart Kalman Filter Outputs for Real Data	84
35	Position Errors for Smart Kalman Filter Run	85
36	Comparison of Total Position Errors Using Real Data.	86
37(a)	VLF Geometry for Latitude Variations.	87
37(b)	VLF Geometry for Longitude Variations	87

APPENDICES

Appendix		Page
A	Algorithm for Handling Doppler Beam Frequency Data	89
B	VLF Communications Station Information.	91
C	Development of Plant Noise Equations	93
D	Evaluation of $\partial d\phi_i/\partial \text{PLAT}$; $\partial d\phi_i/\partial \text{PLONG}$	99

SYMBOLS

Symbol	Definition
\underline{x}_k	n^{th} -- order state vector of a discrete process at time t_k
$\underline{\Phi}_k$	$n \times n$ state transition matrix of a linear discrete process, or quasi-linear state transition matrix for a nonlinear process
\underline{u}_k	m^{th} -- order Gaussian plant noise vector

SYMBOLS (Cont'd)

Symbol	Definition
$\underline{\underline{Q}}_k$	$m \times m$ covariance matrix of \underline{u}_k
$\underline{\underline{G}}_k$	$n \times m$ gain matrix operating on plant noise vector
\underline{y}_{k+1}	ℓ^{th} -- order measurement vector at time t_{k+1}
$\underline{\underline{H}}_{k+1}$	$\ell \times n$ matrix operating on \underline{x}_{k+1} representing relationship between state variables and measurements
\underline{v}_{k+1}	ℓ^{th} -- order Gaussian measurement noise vector
$\underline{\underline{R}}_{k+1}$	$\ell \times \ell$ covariance matrix for \underline{v}_{k+1}
$\hat{\underline{x}}_k$	best estimate of \underline{x} from Kalman filter at time t_k
$\underline{\underline{P}}_k$	$n \times n$ covariance matrix of $\hat{\underline{x}}_k$
\underline{x}'_{k+1}	state vector update based on $\hat{\underline{x}}_k$
$\underline{\underline{P}}'_{k+1}$	covariance matrix of \underline{x}'_{k+1}
$\underline{\underline{K}}_{k+1}$	$n \times \ell$ Kalman gain matrix at time t_{k+1}
$\underline{f}(\underline{x}_k)$	n^{th} -- order nonlinear plant update vector for a discrete process
$\underline{h}(\underline{x}_k)$	ℓ^{th} -- order nonlinear observation vector for a discrete process
f_a, f_b, f_c	RF beam frequencies of Doppler radar system
θ, ϕ	pitch and roll attitude of aircraft
V_{DOP}	aircraft groundspeed derived from Doppler
α	aircraft drift angle derived from Doppler
ψ	magnetic heading of aircraft
VAR	magnetic variation

SYMBOLS (Cont'd)

Symbol	Definition
β	true heading of aircraft: i.e. $\psi - \text{VAR}$
$\alpha + \beta$	true track of aircraft
ϕ_i	phase difference measurement of VLF station i
PLAT, PLONG	aircraft location in geographical latitude and longitude
B_V	bias in groundspeed
B_α	bias in drift angle
B_β	bias in true heading
$B_{\alpha+\beta}$	bias in true track
B_{ϕ_i}	bias in phase measurement of VLF station i
u_V, σ_V^2	random noise in V_{DOP} and associated variance
$u_\alpha, \sigma_\alpha^2$	random noise in α and associated variance
u_β, σ_β^2	random noise in β and associated variance
$u_{\alpha+\beta}, \sigma_{\alpha+\beta}^2$	random noise in $\alpha + \beta$ and associated variance
$v_{\phi_i}, \sigma_{\phi_i}^2$	random noise in ϕ_i and associated variance
u_V^*, σ_V^{*2}	equivalent plant noise process associated with random noise in V_{DOP}
$u_{\alpha+\beta}^*, \sigma_{\alpha+\beta}^{*2}$	equivalent plant noise process associated with random noise in $\alpha + \beta$
$d\phi_i$	theoretical VLF phase difference for station i as derived from Sodano inverse

A KALMAN FILTER APPROACH TO NAVIGATION ON THE NAE CONVAIR 580 AEROMAGNETICS RESEARCH AIRCRAFT

1.0 INTRODUCTION

The NAE Convair 580 research aircraft has onboard various navigation aids, including Doppler radar, C-12 compass heading, VLF station phase difference information, LORAN-C, OMEGA station phase difference information, a Litton LTN-51 inertial navigator, and the possibility of a GPS (Global Positioning System) receiver at some time in the near future (Refs. 1 and 2). With so much redundant navigation data available, it is important to try to use it as effectively as possible. A Kalman filter approach (or some extension of it) becomes almost essential in such a situation in order to 'blend', in some optimal fashion, the various types of navigation information.

At the Flight Research Laboratory, a study was initiated in May 1978 to look at a simple Doppler/VLF navigation filter employing the Kalman filter technique. The purpose of this study was three-fold:

- i) to gain an understanding of basic Kalman filter concepts through analyzing a relatively simple version of a Kalman filter;
- ii) to compare the Doppler/VLF Kalman filter to the Doppler/VLF complementary filter being used at present; and
- iii) to demonstrate the possible advantages of the Kalman filter approach for other applications at Flight Research — a multi-sensor hybrid navigation system and aircraft attitude sensing are just two of the possibilities.

2.0 THEORY OF KALMAN FILTERING

The mathematical theory behind the concept of Kalman filtering involves probability and statistics together with linear systems theory in a state vector formulation. In this chapter, the basic theory will be outlined very briefly — many references are available for a more complete analysis of the theory (e.g. Ref. 3 is an excellent textbook on the subject).

2.1 Elementary Statistical Concepts

References 4 and 5 serve as a very good source for gaining a quick understanding of the underlying principles of a Kalman filter. In its very simplest form, the Kalman filtering process consists of combining two independent estimates of a random variable to form a weighted average. The optimal weighting factor is chosen so as to produce a weighted average having the *minimum variance*. Let x_1 and x_2 be two independent estimates of a Gaussian random variable, x , having variances $\sigma_{x_1}^2$ and $\sigma_{x_2}^2$ respectively (see Ref. 6 for basic statistical definitions). Furthermore, assume that x_2 is estimated by measuring $y_2 = h \cdot x_2$, where y_2 has the variance $\sigma_{y_2}^2 = h^2 \cdot \sigma_{x_2}^2$. Now, a general form for the weighted average of x_1 and x_2 would be,

$$\begin{aligned}\hat{x} &= (1 - K \cdot h) \cdot x_1 + K \cdot h \cdot x_2 \\ (1 - K \cdot h) \cdot x_1 + K \cdot y_2; 0 < K \cdot h < 1\end{aligned}\tag{2.1}$$

with $K \cdot h$ the 'weighting' on x_2 and $(1 - K \cdot h)$ the 'weighting' on x_1 — K is the weighting factor

From Equation (2.1), the statistical expectation (i.e. mean value) of \bar{x} , $E(\bar{x})$, can be expressed as,

$$E(\bar{x}) = (1 - K \cdot h) \cdot E(x_1) + K \cdot E(y_2) \quad (2.2)$$

By definition, the variance of \bar{x} , $\sigma_{\bar{x}}^2$, would be,

$$\sigma_{\bar{x}}^2 \equiv E\left\{\left[\bar{x} - E(\bar{x})\right]^2\right\} \quad (2.3)$$

The following expansion of Equation (2.3) can then be developed:

$$\begin{aligned} \sigma_{\bar{x}}^2 &= E\left\{\left[\bar{x} - E(\bar{x})\right]^2\right\} = E\left\{\left[(1 - K \cdot h) \cdot x_1 \right. \right. \\ &\quad \left. \left. + K \cdot y_2 - (1 - K \cdot h) \cdot E(x_1) - K \cdot E(y_2)\right]^2\right\} \\ &= E\left\{\left[(1 - K \cdot h) \cdot (x_1 - E(x_1)) + K \cdot (y_2 - E(y_2))\right]^2\right\} \\ &= E\left\{(1 - K \cdot h)^2 \cdot [x_1 - E(x_1)]^2 + K^2 \cdot [y_2 - E(y_2)]^2 \right. \\ &\quad \left. + 2 \cdot K \cdot (1 - K \cdot h) \cdot [x_1 - E(x_1)] \cdot [y_2 - E(y_2)]\right\} \\ &= (1 - K \cdot h)^2 \cdot E\left\{[x_1 - E(x_1)]^2\right\} + K^2 \cdot E\left\{[y_2 - E(y_2)]^2\right\} \\ &\quad + 2 \cdot K \cdot (1 - K \cdot h) \cdot E\left\{[x_1 - E(x_1)] \cdot [y_2 - E(y_2)]\right\} \end{aligned} \quad (2.4)$$

Now, $E\{|x_1 - E(x_1)| \cdot |y_2 - E(y_2)|\} \equiv 0$ because x_1 and $y_2 \equiv h \cdot x_2$ are assumed to be independent estimates; hence, $|x_1 - E(x_1)|$ and $|y_2 - E(y_2)| \equiv h \cdot |x_2 - E(x_2)|$ must be uncorrelated. The expansion of $\sigma_{\bar{x}}^2$ then reduces to

$$\sigma_{\bar{x}}^2 = (1 - K \cdot h)^2 \cdot \sigma_{x_1}^2 + K^2 \cdot \sigma_{y_2}^2 \quad (2.5)$$

To determine the minimum variance, $\hat{\sigma}_{\bar{x}}^2$, as a function of weighting factor, K , simply differentiate Equation (2.5) with respect to K and set the result to zero. Thus,

$$\frac{\partial \sigma_{\bar{x}}^2}{\partial K} = 2 \cdot h \cdot (1 - K \cdot h) \cdot \sigma_{x_1}^2 + 2 \cdot K \cdot \sigma_{y_2}^2 = 0 \quad (2.6)$$

which yields the optimum value of K , \hat{K} , as

$$\hat{K} = \frac{h \cdot \sigma_{x1}^2}{\sigma_{y2}^2 + h^2 \cdot \sigma_{x1}^2} \quad (2.7)$$

From Equation (2.1), the expression for the best estimate, \hat{x} , can be written as,

$$x = (1 - \hat{K} \cdot h) \cdot x1 + \hat{K} \cdot h \cdot x2 = x1 - \hat{K} \cdot (h \cdot x1 - y2) \quad (2.8)$$

and, from Equations (2.5) and (2.7), the expression for the variance of \hat{x} , $\hat{\sigma}_x^2$, becomes,

$$\begin{aligned} \hat{\sigma}_x^2 &= (1 - \hat{K} \cdot h)^2 \cdot \sigma_{x1}^2 + \hat{K}^2 \cdot \sigma_{y2}^2 \\ &= \left[\frac{\sigma_{y2}^2}{h^2 \cdot \sigma_{x1}^2 + \sigma_{y2}^2} \right]^2 \cdot \sigma_{x1}^2 + \left[\frac{h \cdot \sigma_{x1}^2}{h^2 \cdot \sigma_{x1}^2 + \sigma_{y2}^2} \right]^2 \cdot \sigma_{y2}^2 \\ &= \frac{\sigma_{x1}^2 \cdot \sigma_{y2}^2}{h^2 \cdot \sigma_{x1}^2 + \sigma_{y2}^2} \\ &= \sigma_{x1}^2 \cdot \frac{\sigma_{y2}^2}{h^2 \cdot \sigma_{x1}^2 + \sigma_{y2}^2} = \sigma_{x1}^2 \cdot (1 - \hat{K} \cdot h) = \sigma_{x1}^2 - \hat{K} \cdot h \cdot \sigma_{x1}^2 \end{aligned} \quad (2.9)$$

If one assumes that $y2 = h \cdot x2$ is a measurement used to improve an updated estimate, $x1$, then Equations (2.8) and (2.9) indicate just how the estimate and its variance are improved by the measurement.

2.2 State Variable Formulation for a Linear Kalman Filter

In order to apply Kalman filtering technique to any particular physical problem involving a dynamic process, the equations of motion of the process must be expressed in a state variable formulation, with any random noise processes included as well — the underlying statistical theory will be that of a Markov process. Furthermore, sampled data versions of the various equations will be used in order to reflect the more practical situation of having to deal with measurement data in digital form. First, a scalar (i.e. one-dimensional) Kalman filter will be developed to outline the basic principles of state variable formulations and Markov processes; then, an extension to the general multi-dimensional Kalman filter algorithm will take place.

2.2.1 Scalar Kalman Filter

In the ensuing mathematical development a 'system state' formulation is assumed, in which the actual state of the physical system is to be estimated using a Kalman filter. An alternative to this

would be the so-called 'error state' formulation, in which it is only the error in the particular process state which is to be estimated via a Kalman filter (see Ref. 5 for an interesting example of an error state formulation).

Assume a first-order physical system exists in the form of a Markov process (see Ref. 3 for definition), as follows:

$$x_{k+1} = f_k \cdot x_k + g_k \cdot u_k \quad (2.10)$$

where

- x_k \equiv true state of the process at time t_k
- f_k \equiv transition term representing the dynamics, or equation of motion, of the system
- u_k \equiv random noise input with zero mean and variance q_k , assumed to be Gaussian
- g_k \equiv scalar multiplier reflecting the effect of the random noise process, u , on the state x

Equation (2.10) is known as the plant equation, with u_k the so-called plant noise.

As well as a scalar plant equation, it is assumed that a measurement process exists in which the quantity being measured, y , is some linear function of the state of the system. Thus,

$$y_{k+1} = h_{k+1} \cdot x_{k+1} + v_{k+1} \quad (2.11)$$

where

- y_{k+1} \equiv quantity being measured
- h_{k+1} \equiv scalar multiplier reflecting the relationship between the measurement and the state
- v_{k+1} \equiv random measurement noise with zero mean and variance r_{k+1} , assumed to be Gaussian

Equation (2.11) is called the observation (or measurement) equation, with v_{k+1} the observation (or measurement) noise. Note that f_k , g_k , h_k , q_k , and r_k are all allowed to vary from one sample time to the next in this formulation.

In order to relate this first-order mathematical development to what was discovered in Section 2.1 (i.e. about optimally combining an update and a measurement), it is necessary to express the variance of the update, p'_k , properly. For this purpose, define the following quantities:

- \hat{x}_k \equiv best estimate of the true state after k samples of data
- x'_{k+1} \equiv state update based on \hat{x}_k , i.e. $x'_{k+1} = f_k \cdot \hat{x}_k$

- $p_k \equiv \text{variance of } \hat{x}_k$
- $p'_{k+1} \equiv \text{variance of the update } x'_{k+1}$
- $\epsilon_k \equiv \text{random error in } \hat{x}_k, \text{ namely } \hat{x}_k - x_k$
- $\epsilon'_{k+1} \equiv \text{random error in } x'_{k+1}, \text{ namely } x'_{k+1} - x_{k+1}$

The best update from the plant equation can be expressed as,

$$\begin{aligned} x'_{k+1} &= f_k \cdot \hat{x}_k = f_k \cdot (x_k + \epsilon_k) = f_k \cdot x_k + f_k \cdot \epsilon_k \\ &= x_{k+1} - g_k \cdot u_k + f_k \cdot \epsilon_k \end{aligned} \quad (2.12)$$

Since x_{k+1} represents the true value of x at t_{k+1} , the error in x'_{k+1} , ϵ'_{k+1} , must be

$$\epsilon'_{k+1} \equiv x'_{k+1} - x_{k+1} = -g_k \cdot u_k + f_k \cdot \epsilon_k \quad (2.13)$$

Also, the variance of ϵ'_{k+1} , $\text{var} \{ \epsilon'_{k+1} \}$, is precisely the variance of x'_{k+1} , p'_{k+1} , because $x_{k+1} \equiv E(x_{k+1})$ (i.e. the true value has no variance, by definition). Therefore,

$$\begin{aligned} p'_{k+1} &\equiv \text{var} \{ \epsilon'_{k+1} \} = \text{var} \{ -g_k \cdot u_k + f_k \cdot \epsilon_k \} \\ &= \text{var} \{ -g_k \cdot u_k \} + \text{var} \{ f_k \cdot \epsilon_k \} \end{aligned} \quad (2.14)$$

because u_k and ϵ_k are assumed to be independent random processes. With $\text{var} \{ u_k \} \equiv q_k$, and $\text{var} \{ \epsilon_k \} \equiv \text{var} \{ \hat{x}_k \} = p_k$, Equation (2.14) becomes,

$$\begin{aligned} p'_{k+1} &= f_k^2 \cdot p_k + g_k^2 \cdot q_k \\ &= f_k \cdot p_k \cdot f_k + g_k \cdot q_k \cdot g_k \end{aligned} \quad (2.15)$$

It is now possible to make comparisons based on the previous developments of Section 2.1. At step $k+1$ identify

$$\begin{aligned} x1 &\equiv x'_{k+1}; \quad \sigma_{x1}^2 \equiv p'_{k+1} = f_k \cdot p_k \cdot f_k + g_k \cdot q_k \cdot g_k \\ y2 &\equiv y_{k+1}; \quad \sigma_{y2}^2 \equiv r_{k+1}; \quad h \equiv h_{k+1} \\ \hat{x} &\equiv \hat{x}_{k+1}; \quad \hat{K} \equiv K_{k+1} \end{aligned} \quad (2.16)$$

Equations (2.7), (2.8), and (2.9) from Section 2.1 can then be rewritten as,

$$K_{k+1} = \frac{p'_{k+1} \cdot h_{k+1}}{h_{k+1} \cdot p'_{k+1} \cdot h_{k+1} + r_{k+1}} \quad (2.17)$$

$$\hat{x}_{k+1} = x'_{k+1} - K_{k+1} \cdot (h_{k+1} \cdot x'_{k+1} - y_{k+1}) \quad (2.18)$$

and

$$p_{k+1} = p'_{k+1} - K_{k+1} \cdot h_{k+1} \cdot p'_{k+1} \quad (2.19)$$

respectively. Thus, the best estimate of the first-order system state, \hat{x}_k , and its variance, p_k , can be updated for minimum variance at each step by sequencing, recursively, through the following so-called Kalman update equations:

$x'_{k+1} = f_k \cdot \hat{x}_k$	plant update	
$p'_{k+1} = f_k \cdot p_k \cdot f_k + g_k \cdot q_k \cdot g_k$	variance of update	
$K_{k+1} = p'_{k+1} \cdot h_{k+1} \cdot [h_{k+1} \cdot p'_{k+1} \cdot h_{k+1} + r_{k+1}]^{-1}$	Kalman gain	(2.20)
$\hat{x}_{k+1} = x'_{k+1} - K_{k+1} \cdot (h_{k+1} \cdot x'_{k+1} - y_{k+1})$	optimal state estimate after k+1 samples	
$p_{k+1} = p'_{k+1} - K_{k+1} \cdot h_{k+1} \cdot p'_{k+1}$	variance of optimal state estimate	

Note that, in order to initiate the Kalman recursion formulas of Equation (2.20), it is necessary to establish initial conditions for \hat{x} and p -- i.e. \hat{x}_0 and p_0 . These initial best estimates for the state and its variance are sometimes difficult to determine precisely and, so, must be approximated in some manner to 'start off' the filter.

2.2.2 General Form of the Linear Kalman Filter

The general form of the linear Kalman filter for the multi-dimensional situation is simply an extension of the foregoing scalar case using matrix formulation. A general n^{th} -order physical process is assumed to have the following sampled data version of the plant equation:

$$x_{k+1} = \Phi_k \cdot x_k + G_k \cdot u_k \quad (2.21)$$

where

$\underline{x}_k \equiv$ nth-order state of the process at time t_k , with the dimension $(n \times 1)$

$\Phi_k \equiv$ $(n \times n)$ transition matrix representing the known dynamics of the process

$\underline{u}_k \equiv$ mth-order $(m \leq n)$ vector representing zero mean, random disturbances, or plant noise, in the system -- dimension $(m \times 1)$

$G_k \equiv$ $(n \times m)$ matrix representing the effects of the m noise sources on the n states of the system

The plant noise vector, \underline{u}_k , is usually assumed to correspond to a set of m zero mean, random noise processes with *constant* variances, $\sigma_{u_i}^2$; $i = 1, \dots, m$; all noise processes are assumed to be independent of each other. These assumptions of Gaussian noise result in an $(m \times m)$ covariance matrix for \underline{u}_k , Q_k , of the following form:

$$\underline{Q}_k = Q \equiv \begin{bmatrix} \sigma_{u_1}^2 & 0 & \cdot & \cdot & \cdot & \cdot & 0 \\ 0 & \sigma_{u_2}^2 & 0 & \cdot & \cdot & \cdot & 0 \\ \cdot & \cdot & \cdot & \cdot & \cdot & \cdot & \cdot \\ \cdot & \cdot & \cdot & \cdot & \cdot & \cdot & \cdot \\ \cdot & \cdot & \cdot & \cdot & \cdot & \cdot & \cdot \\ \cdot & \cdot & \cdot & \cdot & \cdot & \cdot & 0 \\ 0 & 0 & \cdot & \cdot & \cdot & 0 & \sigma_{u_m}^2 \end{bmatrix} \quad (2.22)$$

In conjunction with this general multi-dimensional linear plant, assume that a multi-dimensional measurement process exists as follows:

$$\underline{y}_{k+1} = H_{k+1} \cdot \underline{x}_{k+1} + \underline{v}_{k+1} \quad (2.23)$$

where

$\underline{y}_{k+1} \equiv$ $(\ell$ th-order $(\ell \leq n)$ set of measurements at time t_{k+1} , with the dimension $(\ell \times 1)$

$H_{k+1} \equiv$ $(\ell \times n)$ matrix which operates on \underline{x}_{k+1} to represent the relationship between state variables and measurements

$\underline{v}_{k+1} \equiv$ $(\ell \times 1)$ measurement noise vector representing zero mean, random disturbances (i.e. observation noise) in each of the measured quantities

The measurement noise vector, \underline{v}_{k+1} , is normally assumed to be a set of ℓ zero mean, random noise processes having *constant* variances, $\sigma^2_{v_i}$; $i = 1, \dots, \ell$ - each noise process is also assumed to be independent of the others. The $(\ell \times \ell)$ covariance matrix, \underline{R}_{k+1} , for \underline{v}_{k+1} then becomes,

$$\underline{R}_{k+1} = \underline{R} \triangleq \begin{bmatrix} \sigma^2_{v_1} & 0 & \cdot & \cdot & \cdot & 0 \\ 0 & \sigma^2_{v_2} & & & & \cdot \\ \cdot & & \cdot & & & \cdot \\ \cdot & & & \cdot & & \cdot \\ \cdot & & & & \cdot & 0 \\ 0 & \cdot & \cdot & \cdot & 0 & \sigma^2_{v_\ell} \end{bmatrix} \quad (2.24)$$

For the foregoing multi-dimensional process and measurement configuration, the Kalman filter task is to compute the best estimate of \underline{x}_k , $\hat{\underline{x}}_k$, and the covariance matrix of $\hat{\underline{x}}_k$, \underline{P}_k , at each time t_k ; $k = 1, 2, \dots$. As in the scalar case, define \underline{x}'_{k+1} as the state update based on \underline{x}_k (i.e. $\underline{x}'_{k+1} = \underline{\Phi}_k \cdot \underline{x}_k$); and define \underline{P}'_{k+1} as the covariance matrix associated with \underline{x}'_{k+1} . The general form for the Kalman update of $\hat{\underline{x}}_k$ and \underline{P}_k (proof given in Ref. 4) is then,

$$\begin{aligned} \underline{x}'_{k+1} &= \underline{\Phi}_k \cdot \hat{\underline{x}}_k && \text{plant update} \\ \underline{P}'_{k+1} &= \underline{\Phi}_k \cdot \underline{P}_k \cdot \underline{\Phi}_k^T + \underline{G}_k \cdot \underline{Q}_k \cdot \underline{G}_k^T && \text{covariance of update} \\ \underline{K}_{k+1} &= \underline{P}'_{k+1} \cdot \underline{H}_{k+1}^T \cdot \left[\underline{H}_{k+1} \cdot \underline{P}'_{k+1} \cdot \underline{H}_{k+1}^T + \underline{R}_{k+1} \right]^{-1} && \text{Kalman gain matrix} \\ \hat{\underline{x}}_{k+1} &= \underline{x}'_{k+1} - \underline{K}_{k+1} \cdot \left[\underline{H}_{k+1} \cdot \underline{x}'_{k+1} - \underline{y}_{k+1} \right] && \text{optimal state estimate after } k+1 \text{ samples} \\ \underline{P}_{k+1} &= \underline{P}'_{k+1} - \underline{K}_{k+1} \cdot \underline{H}_{k+1} \cdot \underline{P}'_{k+1} && \text{covariance of optimal state estimate} \end{aligned} \quad (2.25)$$

Note the strong similarity between the scalar form of the update, given in Equation (2.20), and the above matrix form. The matrix recursion formula given in Equation (2.25) corresponds to a minimization of \underline{P}_{k+1} at each step, i.e. the optimal state estimate is always the one having minimum error variance in the Kalman filter approach to the problem.

Now the Kalman filter update equations define a set of recursion relationships, readily implemented on a digital computer, for computing the optimal state estimate of a physical process *in real time* - this is the essence of the benefit to be derived from a Kalman filter. Assuming that the

plant and measurement processes are well-known (i.e. accurate knowledge of Φ_k , G_k , Q_k , H_k , and R_k) then all that is required to get the Kalman filter started is knowledge of the initial state vector estimate, \underline{x}_0 , and its initial, or so-called a priori, covariance, P_0 . Often it is difficult to specify an accurate estimate of P_0 — it really reflects the possible variance of the error in the initial state estimate. The covariance matrix, P_k , is quite important because its diagonal elements are a measure of the error variance of the individual optimal state estimates as a function of time. Usually the estimation error of each state is reduced dramatically during the first part of a Kalman filter run and then, eventually, a steady state error condition is reached. In the steady state region, the elements of both the Kalman gain matrix, K_k , and the covariance matrix, P_k , become small and near-constant.

2.3 A Quasi-Linear Approach for Nonlinear Systems

Many practical problems for which a Kalman filter approach would be quite useful involve nonlinear plant equations and/or nonlinear measurement equations. In most cases, it would be too inaccurate to linearize the equations completely, so some quasi-linear approach must be found. Friedland and Bernstein (Ref. 7) and Richman and Friedland (Ref. 8) have suggested one approximate quasi-linear technique which will be outlined here; there are also other possible extensions of the Kalman filter to include nonlinearities (see Ref. 3, Ch. 8).

Maintaining the same notation as in Subsection 2.2.2, define a nonlinear sampled data plant equation,

$$\underline{x}_{k+1} = \underline{f}(\underline{x}_k) + \underline{G}_k \cdot \underline{u}_k \quad (2.26)$$

so that, in general, an $(n \times 1)$ vector, \underline{f} , with elements consisting of nonlinear functions of the state, \underline{x} , replaces the linear vector function, $\underline{\Phi}_k \cdot \underline{x}_k$, of Equation (2.21). In similar fashion, a nonlinear observation equation,

$$\underline{y}_{k+1} = \underline{h}(\underline{x}_{k+1}) + \underline{v}_{k+1} \quad (2.27)$$

is assumed, where the $(l \times 1)$ vector, \underline{h} , has elements consisting of nonlinear functions of \underline{x} ; and \underline{h} replaces $\underline{H}_{k+1} \cdot \underline{x}_{k+1}$ of Equation (2.23). The noise process vectors, \underline{u}_k and \underline{v}_k , are assumed to have the same general statistics as those defined in Subsection 2.2.2.

Consider now a quasi-linear state transition matrix, $\underline{\Phi}_k$, whose elements are defined as,

$$\left[\underline{\Phi}_k \right]_{ij} = \left. \frac{\partial f_i(\underline{x})}{\partial x_j} \right|_{\underline{x} = \underline{x}_k} \quad i = 1, \dots, n; j = 1, \dots, n \quad (2.28)$$

and a quasi-linear observation matrix, \underline{H}_k , having the elements,

$$\left[\underline{H}_k \right]_{ij} \equiv \left. \frac{\partial h_i(\underline{x})}{\partial x_j} \right|_{\underline{x} = \underline{x}_k} \quad ; i = 1, \dots, \ell; j = 1, \dots, n \quad (2.29)$$

The Kalman filter update equations for the quasi-linear best estimate, $\hat{\underline{x}}_k$, then become,

$$\begin{aligned} \underline{x}'_{k+1} &= f(\hat{\underline{x}}_k) && \text{nonlinear plant update} \\ \underline{P}'_{k+1} &= \underline{\Phi}_k \cdot \underline{P}_k \cdot \underline{\Phi}_k^T + \underline{G}_k \cdot \underline{Q}_k \cdot \underline{G}_k^T && \text{covariance of update, or} \\ &&& \text{a priori covariance of} \\ &&& \text{state estimate} \\ \underline{K}_{k+1} &= \underline{P}'_{k+1} \cdot \underline{H}_{k+1}^T \cdot \left[\underline{H}_{k+1} \cdot \underline{P}'_{k+1} \cdot \underline{H}_{k+1}^T + \underline{R}_{k+1} \right]^{-1} && \text{quasi-linear Kalman} \\ &&& \text{gain} \\ \hat{\underline{x}}_{k+1} &= \underline{x}'_{k+1} + \underline{K}_{k+1} \cdot \left[h(\underline{x}'_{k+1}) - \underline{y}_{k+1} \right] && \text{optimal quasi-linear} \\ &&& \text{state estimate after} \\ &&& \text{k+1 samples} \\ \underline{P}_{k+1} &= \underline{P}'_{k+1} - \underline{K}_{k+1} \cdot \underline{H}_{k+1} \cdot \underline{P}'_{k+1} && \text{covariance of optimal} \\ &&& \text{state estimate, or a} \\ &&& \text{posteriori covariance} \end{aligned} \quad (2.30)$$

Note that the quasi-linear approximations are used only to calculate the Kalman gain matrix and the various covariance matrices. The true nonlinear relationships are still used for defining the plant update, \underline{x}' , and the theoretical observation vector, h .

2.4 Practical Aspects of Designing and Running a Kalman Filter

Before a presentation of the quasi-linear Kalman filter algorithm designed for the Doppler VLF navigation task, a few general comments can be made about the practicalities involved in implementing a Kalman filter. A more detailed look at the practical aspects of Kalman filtering is reserved for the later chapters on the Doppler VLF navigation filter.

2.4.1 System and Statistical Modelling

The following are some of the practical considerations that have to be confronted when modelling for any Kalman filter application.

- (i) One must define the essential state variables that are required to describe the process adequately. Including additional variables that define obscure second order effects (with an associated increase in the number of states being estimated) can actually cause difficulties - the computational burden per filter cycle could become excessive, and there is a very good chance that linear dependencies could occur among certain state variables, resulting in poor state estimation overall.

- ii) Bias state estimation can be quite important and can be implemented quite readily. Assume an arbitrary variable, v , of a physical process has a bias which is to be estimated. A so-called bias state variable, B_v , can be defined; and the corresponding state update equation for B_v would be: $B_{v,k+1} = B_{v,k}$, with no plant noise assumed. Several such bias state equations could be included as part of the overall plant equation, and optimal estimation of the assumed biases would take place.
- iii) Modelling the statistical characteristics of the various noise processes accurately is essential for proper operation of any Kalman filter. Even the basic assumption of constant variance, zero mean noise processes is suspect at times. For example, a correlated noise process modelling might be desirable and certainly could be implemented if required. Statistical modelling of the measurement noise processes is fairly straightforward, since one usually has direct access to the basic measurement errors. However, correct modelling of plant noise processes can be more of a fine art than a science. It is often difficult to gain access to the basic error quantities that correspond to the plant noise as defined in the plant equation. Sometimes the basic error processes of the physical system, for which statistical information is known, are modified significantly to get them into the configuration prescribed by Equation (2.26). The main concern is to arrive at some 'ball park' figure for plant noise variance which in some way reflects the randomness that can be expected in the chosen mathematical description of the dynamics of the physical process.
- iv) Proper initialization of the Kalman filter is also quite important in order to have accurate filter estimates as soon as possible after filtering action begins. As already mentioned in Subsection 2.2.2, to initialize the Kalman filter one must specify an initial state estimate, \hat{x}_0 , and its corresponding a priori covariance matrix, P_0 . P_0 is simply a diagonal matrix consisting of the various individual initial state error variances, $\sigma_{x_{i0}}^2$, $i = 1, \dots, n$. It is not so important that \hat{x}_0 be perfectly accurate — what is important is that P_0 correctly reflects the expected uncertainty of the individual elements of \hat{x}_0 . In other words, P_0 'tells' the filter how much weight to place on the update of the initial state estimate relative to the incoming measurement information. If P_0 does not represent the true situation, then the filter state estimates will not be as accurate as they could be — also, the filter might take more time to stabilize to its steady state estimation condition.
- v) The Kalman filter configuration is such that it can handle various contingencies (e.g. sudden changes in the quality of the data) through modifications to Q_k , R_k , or even P_k . To take advantage of this capability, one must have continuous, real-time knowledge of the characteristics of the various sensors involved. It may take a great deal of ingenuity and forethought to devise appropriate monitoring schemes for the data transducers. However, the effort would reap dividends by keeping the Kalman filter 'optimally tuned' through refreshing it with the best statistical information available at any point in time.

2.1.2 Numerical Accuracy and Stability

One important consideration that must be addressed when implementing any Kalman filter in a digital computer is the numerical accuracy of the computations. Any potential accuracy problem becomes more acute as the number of physical states to be estimated increases. Basically, the source of the difficulty is the requirement to propagate the P matrix accurately (via the matrix operations defined in Equations (2.25) or (2.30)) as the elements of P decrease to very small values with time. Numerical analysts have found various ways to combat the problem by redefining the update equations in a numerically more efficient manner. Two possible approaches receiving a lot of attention in the literature are square root filtering (Refs. 9 to 11) and U-D factorization (Refs. 12 to 14). These particular techniques, compared to the normal Kalman update, are equivalent to doubling the word length used in any given computer — resulting in an obvious improvement in numerical accuracy. The computational effort involved in these more advanced numerical techniques is somewhat greater, but is demonstrated to be well worthwhile in a high dimension Kalman filter situation.

Closely associated with the numerical accuracy problem is the basic stability of the Kalman filter. Under certain circumstances it has been shown that a Kalman filter can be unstable -- the state estimation errors actually diverge with time. Many times, this instability is associated with ill-conditioning inherent in the problem and aggravated by the numerical inaccuracy of the ordinary Kalman update equations. Two solutions to this problem that are commonly used are the following:

- i) In the statistical modelling, include a sufficient level of plant noise to ensure that the covariance matrix, P , never gets so small that it causes a numerical instability problem (which would show up as one or more negative eigenvalues in P at some sample time). Sometimes plant noise is included, even with a very accurate plant update equation, for this very purpose.
- ii) Use alternatives to the Kalman update equations, such as square root filtering or U-D factorization, which tend to propagate a more accurate P that remains positive definite (i.e. positive eigenvalues) and, hence, circumvents the stability problem.

3.0 A DOPPLER/VLF KALMAN FILTER NAVIGATOR

Based on the quasi-linear technique described in Section 2.3, a Kalman filter is designed for optimal blending of Doppler radar, compass heading, and VLF station phase difference information, with an update rate of once every ten seconds. The primary outputs of the Kalman filter navigator will be the optimal estimates of aircraft position and velocity. The mathematical modelling is developed for the navigation equipment presently onboard the NAE Convair 580 research aircraft, with the basic navigation parameters sampled and processed using an Interdata 7-32 minicomputer onboard. The digitized data is presently stored on magnetic tape for post flight analysis; but, eventually, it is intended that the Kalman filter would run in real-time onboard the Convair, using the Interdata computer (see Refs. 1, 2 for computing capabilities onboard the Convair).

3.1 Description of the Basic Navigation Transducers

The following navigation transducers are included in the present design of the Kalman filter navigator:

- i) Decca Doppler Radar -- a three-beam Doppler radar measures the three components of aircraft velocity relative to aircraft-fixed axes. The raw RF beam frequency information is sampled every half second. In order to resolve aircraft-fixed velocities into 'straight and level' earth-fixed components (required for navigation), the angular attitudes of the aircraft, pitch (θ) and roll (ϕ), are also measured. Appendix A gives a complete description of the mathematics involved in converting the beam frequency data into the more typical Doppler groundspeed (V_{DOP}) and drift angle (α) quantities that are required.
- ii) Sperry C-12 Magnetic Compass -- a dual compass heading system onboard the Convair measures magnetic heading, ψ , which is sampled at a rate of twice per second. The true heading with respect to geographic north, β , is then computed as $\beta = \psi - VAR$, where VAR is the magnetic variation for the given geographical area.
- iii) Global Navigation GNS-200 VLF Receiver -- this VLF receiver is used in conjunction with a Rb frequency standard onboard the Convair to measure the phase difference between the transmissions from the various U.S. Navy Communications stations and the Rb clock. These phase-stable measurements can be directly related to the distances from the aircraft to each of the VLF stations -- the phase measurements for all stations are sampled simultaneously every ten seconds. Appendix B is a table listing the essential features of each of the VLF Communications stations that can be received by the Convair's GNS 200 unit. For more details about the operation of the GNS 200, and VLF navigation in general, see References 15 and 16.

3.2 Mathematical Development for the Kalman Filter Navigator

The basic task is to design a mathematical algorithm, suitable for use in a computer, which blends together the Doppler radar, heading, and VLF information in an optimal fashion, along the lines of the quasi-linear Kalman filter approach described in Section 2.3. Figure 1 is a very simple block diagram representation of what the proposed navigator would do. Each of the basic navigation inputs shown in Figure 1 is assumed to be corrupted with bias errors and noise -- the job of the Doppler/VLF navigator is to compute the best estimates (in the minimum variance sense) of position and velocity based on this imperfect data. The specifications defining the proposed Doppler/VLF Kalman filter implementation are categorized as follows:

- i) Raw Navigation Parameters -- the following parameters comprise the set of inputs, either measured or calculated, that the Kalman navigation filter will use:

f_a, f_b, f_c	-- RF beam frequencies of the Doppler radar, measured in hertz (hz).
θ, ϕ	-- aircraft pitch and roll attitude respectively, measured in radians (rad).
V_{DOP}	-- Doppler-derived groundspeed (from Appendix A) measured in nautical miles per second (nm/sec; converted from knots).
α	-- Doppler-derived drift angle (from Appendix A) measured in radians.
ψ	-- magnetic heading from C-12 compass, measured in radians (converted from degrees).
β	-- true heading, ψ -VAR, in radians.
$\alpha + \beta$	-- true track angle of aircraft, in radians.
$\phi_i, i = 1, \dots, 6$	-- VLF station phase difference between station i and Rb clock, a total of six stations assumed, measured in micro-seconds (μ sec; ϕ_i is actually the time it takes for the VLF signal to travel from station i to the aircraft; $d = ct$ implies that one μ sec is equivalent to a distance of 0.162 nm).

- ii) Biases Assumed -- for modelling purposes, the following biases are assumed to exist in the navigation parameters:

B_V	-- bias in groundspeed, V_{DOP} (nm/sec), assumed to originate with the biases in f_a, f_b, f_c and possibly θ, ϕ .
B_α	-- bias in drift angle, α (rad), assumed to originate with biases in f_a, f_b, f_c and possibly θ, ϕ .
B_β	-- bias in true heading, β (rad); a combination of any bias in measurement of ψ plus a possible bias in the specification of variation, VAR.
$B_{\alpha\beta}$	-- the combination $B_\alpha + B_\beta$, i.e. bias in true track, $\alpha + \beta$ (rad).
$B_{\phi_i}, i = 1, \dots, 6$	-- bias in the phase difference measurement of station i (μ sec).

- iii) Noise Processes Assumed — the measured and computed parameters are assumed to have the following zero mean, constant variance noise processes:

u_v	random noise in the measurement of V_{DOP} , with variance σ_v^2 (nm ² /sec ²).
u_α	random noise in the measurement of α , with variance σ_α^2 (rad ²).
u_β	random noise in the measurement of β , with variance σ_β^2 (rad ²).
$u_{\alpha\beta}$	combination of noise processes, $u_\alpha + u_\beta$, with variance $\sigma_{\alpha\beta}^2 = \sigma_\alpha^2 + \sigma_\beta^2$ (rad ²).
$v_{\phi i}, i = 1, \dots, 6$	random noise in the measurement of ϕ_i , with variance $\sigma_{\phi i}^2$ (μ sec ²).

Doppler Note: the Doppler biases and noise processes could have been defined in terms of the beam frequencies (i.e. f_a, f_b, f_c) and possible biases plus random noise in their measurement; however, it was felt that this procedure would be unduly complicated. Computer simulation has demonstrated that the simpler error modelling defined above is perfectly adequate for the types of aircraft trajectory expected (i.e. mostly near-constant velocity straight line or, possibly, shallow curved tracks).

- (iv) Digital Sampling Rates — there are two basic rates of sampling the incoming navigation data: every half second on the Doppler/heading data and every ten seconds on the VLF phase difference information.
- (v) Process and State Variables Chosen — the physical process assumed for the quasi-linear Kalman filter is the Doppler equation for updating geographical position every ten seconds based on integrating Doppler velocity components over that period of time. A vector set of ten discrete state variables, \underline{x} , is defined as follows:

PLAT	=	x1	⇒	geographical latitude of aircraft (deg).
PLONG	=	x2	⇒	geographical longitude of aircraft (deg).
B_v	=	x3	⇒	bias in Doppler groundspeed (nm/sec).
$B_{\alpha\beta}$	=	x4	⇒	bias in true track (rad).
$B_{\phi 1}$	=	x5	⇒	bias in measurement of station 1 phase (μ sec).
$B_{\phi 2}$	=	x6	⇒	bias in measurement of station 2 phase (μ sec).
$B_{\phi 3}$	=	x7	⇒	bias in measurement of station 3 phase (μ sec).
$B_{\phi 4}$	=	x8	⇒	bias in measurement of station 4 phase (μ sec).
$B_{\phi 5}$	=	x9	⇒	bias in measurement of station 5 phase (μ sec).
$B_{\phi 6}$	=	x10	⇒	bias in measurement of station 6 phase (μ sec).

- vi) State Equations of the Dynamic Process — recall that the discrete form of the dynamic process is the vector difference equation,

$$\underline{x}_{k+1} = \underline{f}(\underline{x}_k) + \underline{G}_k \cdot u_k \quad (3.1)$$

According to the state variables and process chosen, the elements of \underline{f} will be as follows (see Appendix C for more details):

$$\begin{aligned} f1(\underline{x}_k) &\equiv \text{PLAT}_k + [A1_k - A3_k \cdot B_{V,k}] \cdot \sin(B_{\alpha,k}) \\ &\quad + [A2_k - A4_k \cdot B_{V,k}] \cdot \cos(B_{\alpha,k}) \\ &= x1_k + [A1_k - A3_k \cdot x3_k] \cdot \sin(x4_k) \\ &\quad + [A2_k - A4_k \cdot x3_k] \cdot \cos(x4_k) \\ f2(\underline{x}_k) &\equiv \text{PLONG}_k - \frac{[A1_k - A3_k \cdot B_{V,k}]}{\cos[\text{PLAT}_k \cdot \pi/180]} \cdot \cos(B_{\alpha,k}) \\ &\quad - \frac{[A4_k \cdot B_{V,k} - A2_k]}{\cos[\text{PLAT}_k \cdot \pi/180]} \cdot \sin(B_{\alpha,k}) \\ &= x2_k - \frac{[A1_k - A3_k \cdot x3_k]}{\cos[x1_k \cdot \pi/180]} \cdot \cos(x4_k) \\ &\quad - \frac{[A4_k \cdot x3_k - A2_k]}{\cos[x1_k \cdot \pi/180]} \cdot \sin(x4_k) \end{aligned} \quad (3.2)$$

$$f3(x_k) = B_{V,k} - x3_k$$

$$f4(x_k) = B_{\alpha,k} - x4_k$$

$$f5(x_k), \dots, f10(x_k) = B_{\gamma_1,k}, \dots, B_{\gamma_6,k} - x5_k, \dots, x10_k$$

where

$$\begin{aligned}
 A1_k &= \frac{1}{60} \cdot \int_{t_k}^{t_k + 10} V_{DOP} \cdot \sin(\alpha + \beta) dt \\
 A2_k &= \frac{1}{60} \cdot \int_{t_k}^{t_k + 10} V_{DOP} \cdot \cos(\alpha + \beta) dt \\
 A3_k &= \frac{1}{60} \cdot \int_{t_k}^{t_k + 10} \sin(\alpha + \beta) dt \\
 A4_k &= \frac{1}{60} \cdot \int_{t_k}^{t_k + 10} \cos(\alpha + \beta) dt
 \end{aligned} \tag{3.3}$$

The integrations required in Equation (3.3) are computed digitally using trapezoidal integration (Ref. 17) on the 20 samples of Doppler heading data that occur in each ten second update interval.

- vii) Plant Noise Processes - Appendix C shows the details of how plant noise can be modelled as a function of the original Doppler noise processes u_V , u_{α} , and u_{β} . The result is the two-element vector,

$$u_k = \begin{bmatrix} u_{V,k}^* & u_{\alpha,\beta,k}^* \end{bmatrix}^T \tag{3.4a}$$

where

$$\begin{aligned}
 u_{V,k}^* &= \int_{t_k}^{t_k + 10} u_V dt \\
 u_{\alpha,\beta,k}^* &= \int_{t_k}^{t_k + 10} (u_{\alpha} + u_{\beta}) dt
 \end{aligned} \tag{3.4b}$$

The noise processes, u_V and $u_{\alpha,\beta}$, are assumed to be zero mean, constant variance random noise with variances σ_V^2 and $\sigma_{\alpha,\beta}^2$ respectively - once again, the integrations are accomplished digitally via trapezoidal integration. The auto-covariance matrix associated with u_k , Q_k , is identified as the (2 x 2) matrix,

$$Q_k = Q = \begin{bmatrix} \sigma_{V_k}^2 & 0 \\ 0 & \sigma_{\alpha\beta}^2 \end{bmatrix} \quad (3.5)$$

Also, from Appendix C (i.e. Equation (C15)), the G_k matrix is shown to be the (10×2) matrix,

$$G_k = \begin{bmatrix} A6_k & A5_k \\ A8_k & A7_k \\ 0 & 0 \\ \cdot & \cdot \\ \cdot & \cdot \\ \cdot & \cdot \\ 0 & 0 \end{bmatrix} \quad (3.6)$$

where

$$\begin{aligned} A5_k &= \frac{1}{60} \cdot (V_{DOP} - B_{V_k}) \cdot \sin(\alpha + \beta - B_{\alpha\beta k}) \bigg|_{t_k+5} \\ A6_k &= \frac{1}{60} \cdot \cos(\alpha + \beta - B_{\alpha\beta k}) \bigg|_{t_k+5} \\ A7_k &= \frac{(V_{DOP} - B_{V_k}) \cdot \cos(\alpha + \beta - B_{\alpha\beta k})}{60 \cdot \cos[PLAT_k + \pi/180]} \bigg|_{t_k+5} \\ A8_k &= \frac{\sin(\alpha + \beta - B_{\alpha\beta k})}{60 \cdot \cos[PLAT_k + \pi/180]} \bigg|_{t_k+5} \end{aligned} \quad (3.7)$$

viii) Observation Equations -- recall that the discrete version of the measurement process has the form,

$$y_{k+1} = h(x_{k+1}) + v_{k+1} \quad (3.8)$$

In this case, the measurement vector, y , will consist of the six VLF phase difference readings:

$$y_k = \begin{bmatrix} \phi 1_k & \phi 2_k & \dots & \phi 6_k \end{bmatrix}^T \quad (3.9)$$

The six elements of h are identified as follows:

$$\begin{aligned} h1(x_k) &= d\phi 1(PLAT_k, PLONG_k) + B_{\phi 1k} = d\phi 1(x1_k, x2_k) + x5_k \\ h2(x_k) &= d\phi 2(PLAT_k, PLONG_k) + B_{\phi 2k} = d\phi 2(x1_k, x2_k) + x6_k \\ &\vdots \\ h6(x_k) &= d\phi 6(PLAT_k, PLONG_k) + B_{\phi 6k} = d\phi 6(x1_k, x2_k) + x10_k \end{aligned} \quad (3.10)$$

where $d\phi i$; $i = 1, \dots, 6$ represents the theoretical phase difference (measured in μ sec) for station i at the geographical location (PLAT, PLONG). The relationship expressed by $d\phi$ is not explicit — rather, it is embodied in a computer algorithm known as the Sodano inverse routine (Refs. 18, 19) which must be included as part of the Kalman filter algorithm.

ix) Observation Noise Processes — the measurement noise is modelled as the six-element vector,

$$v_k = \begin{bmatrix} v_{\phi 1k} & v_{\phi 2k} & \dots & v_{\phi 6k} \end{bmatrix}^T \quad (3.11)$$

having an associated (6×6) auto-covariance matrix,

$$R_k = R = \begin{bmatrix} \sigma^2_{\phi 1} & 0 & 0 & \cdot & \cdot & \cdot & 0 \\ 0 & \sigma^2_{\phi 2} & & & & & \cdot \\ & & \cdot & & & & \\ \cdot & & & \cdot & & & \cdot \\ & & & & \cdot & & \\ \cdot & & & & & \cdot & \cdot \\ 0 & 0 & \cdot & \cdot & \cdot & \cdot & \sigma^2_{\phi 6} \end{bmatrix} \quad (3.12)$$

- (x) Quasi-Linear State Transition Matrix, $\underline{\Phi}$ -- recall, from Equation (2.28), that the elements of $\underline{\Phi}$ will be defined as,

$$\left[\Phi_k \right]_{ij} = \left. \frac{\partial f_i(x)}{\partial x_j} \right|_{x = x_k} ; i = 1, \dots, 10; j = 1, \dots, 10 \quad (3.13)$$

From the definition of the f_i 's given in Equation (3.2), $\underline{\Phi}_k$ can be identified as the (10×10) matrix,

$$\underline{\Phi}_k = \begin{bmatrix} 1 & 0 & \partial f_1/\partial x_3 & \partial f_1/\partial x_4 & 0 & \cdot & \cdot & \cdot & 0 \\ \partial f_2/\partial x_1 & 1 & \partial f_2/\partial x_3 & \partial f_2/\partial x_4 & 0 & \cdot & \cdot & \cdot & 0 \\ 0 & 0 & 1 & 0 & \cdot & \cdot & \cdot & \cdot & 0 \\ 0 & 0 & 0 & 1 & 0 & \cdot & \cdot & \cdot & 0 \\ \cdot & \cdot & \cdot & \cdot & \cdot & \cdot & \cdot & \cdot & \cdot \\ \cdot & \cdot & \cdot & \cdot & \cdot & \cdot & \cdot & \cdot & \cdot \\ \cdot & \cdot & \cdot & \cdot & \cdot & \cdot & \cdot & 1 & 0 \\ 0 & \cdot & \cdot & \cdot & \cdot & \cdot & \cdot & 0 & 1 \end{bmatrix} \quad (3.14)$$

where

$$\begin{aligned} \partial f_1/\partial x_3 &= A3_k \cdot \sin(x4_k) - A1_k \cdot \cos(x4_k) \\ \partial f_1/\partial x_4 &= (A1_k - A3_k \cdot x3_k) \cdot \cos(x4_k) - (A2_k - A4_k \cdot x3_k) \cdot \sin(x4_k) \\ \partial f_2/\partial x_1 &= \left[(A1_k - A3_k \cdot x3_k) \cdot \cos(x4_k) + (A4_k \cdot x3_k - A2_k) \cdot \sin(x4_k) \right] \\ &\quad \cdot \frac{\pi \sin(x1_k \cdot \pi/180)}{180 \cdot \cos^2(x1_k \cdot \pi/180)} \\ \partial f_2/\partial x_3 &= \left[A3_k \cdot \cos(x4_k) - A1_k \cdot \sin(x4_k) \right] \cdot \frac{1}{\cos(x1_k \cdot \pi/180)} \\ \partial f_2/\partial x_4 &= \left[(A1_k - A3_k \cdot x3_k) \cdot \sin(x4_k) - (A4_k \cdot x3_k - A2_k) \cdot \cos(x4_k) \right] \\ &\quad \cdot \frac{1}{\cos(x1_k \cdot \pi/180)} \end{aligned} \quad (3.15)$$

with $A1_k = A4_k$ already defined in Equation (3.3).

- xi) Quasi-Linear Observation Matrix, H_k - based on Equation (2.29), the elements of H will be defined as

$$\left[H_k \right]_{ij} = \left. \frac{\partial h_i(x)}{\partial x_j} \right|_{x=x_k} \quad ; i = 1, \dots, 6; j = 1, \dots, 10 \quad (3.16)$$

From the definition of the h_i 's given in Equations (3.10), H_k can be identified as the (6×10) matrix,

$$H_k = \begin{bmatrix} \partial d\phi_1/\partial x_{1k} & \partial d\phi_1/\partial x_{2k} & 0 & 0 & 1 & 0 & \cdot & \cdot & 0 \\ \partial d\phi_2/\partial x_{1k} & \partial d\phi_2/\partial x_{2k} & 0 & 0 & 0 & 1 & 0 & \cdot & 0 \\ \cdot & \cdot & \cdot & \cdot & \cdot & \cdot & \cdot & \cdot & \cdot \\ \cdot & \cdot & \cdot & \cdot & \cdot & \cdot & \cdot & \cdot & \cdot \\ \cdot & \cdot & \cdot & \cdot & \cdot & \cdot & \cdot & \cdot & 0 \\ \partial d\phi_6/\partial x_{1k} & \partial d\phi_6/\partial x_{2k} & 0 & \cdot & \cdot & \cdot & \cdot & 0 & 1 \end{bmatrix} \quad (3.17)$$

Appendix D shows details of the explicit computation of partial derivatives $\partial d\phi_i/\partial x_{1k}$, $\partial d\phi_i/\partial x_{2k}$; $i = 1, \dots, 6$ based on output information from the Sodano inverse routine.

- xii) Detailed Block Diagram Representation - the complete mathematical development for the proposed Kalman filter navigator has been outlined in this section. Figure 2 shows a detailed block diagram representation of the Doppler/VLF Kalman filter navigation scheme indicating the individual inputs and outputs - essentially an expansion of Figure 1. The following points summarize the main operating features of this proposed hybrid navigation algorithm:
- Doppler radar and compass heading information are used by the Kalman filter to define the basic plant process (i.e. to resolve and integrate Doppler velocity components in order to get position updates).
 - VLF station phase difference information becomes the so-called measurement, or observation, process.
 - All the available data is used to compute optimum estimates of position every ten seconds, plus calculate the various Doppler heading and VLF biases.
 - The estimates of bias in Doppler groundspeed (\hat{B}_V) and true track angle (\hat{B}_{θ}) can be used to correct V_{DOP} and $\alpha + \beta$ in order to arrive at improved velocity estimates, \hat{V}_{LAT} and \hat{V}_{LONG} .
 - The estimates of bias in VLF phase (\hat{B}_ϕ) can be used to correct the raw VLF phase measurements (ϕ_0), resulting in improved VLF phase data, $\hat{\phi}_0$; $i = 1, \dots, 6$.

- f) If either the Doppler/heading or VLF subsystems become inoperative during the navigation task, the bias errors will have been updated by the Kalman filter to that point in time. This should mean more accurate navigation in the degraded mode compared to no estimation of biases in the system.

4.0 SIMULATION EXPERIMENTS WITH THE DOPPLER/VLF KALMAN FILTER

The important features of a computer program used to simulate operation of the Kalman navigation filter are given in Section 4.1. Other sections in this chapter are devoted to identifying, through various simulation experiments, the rather unique characteristics of the proposed Kalman filter design.

4.1 Details Concerning the Simulation Algorithm

A computer program for simulating the running of the Doppler/VLF Kalman filter in real time has been designed and written in the FORTRAN IV programming language for the IBM 3032 TSS operating environment. Figure 3 is a block diagram representation of the simulator and Figure 4 shows the associated computer program flowchart. Some of the pertinent features of this particular simulation routine are the following:

Simulated motion of the aircraft is either a straight-line trajectory with constant velocity, or a circular track with constant tangential velocity: velocity and track specified by the user.

The Doppler navigation simulator outputs groundspeed, heading, and drift angle rather than the more fundamental Doppler beam frequency data - it has been verified that the simpler approach used is sufficiently accurate for simulating the Doppler radar system.

Any level of bias and/or random noise can be simulated for the Doppler groundspeed, heading, drift angle, and VLF station phase difference measurements.

The VLF simulator uses a version of the Sodano inverse routine to compute the theoretical microsecond phase readings for the different VLF stations.

A variable number of VLF stations can be simulated; up to a maximum number of six.

A plotting routine has been developed to display the results from any Kalman filter simulation run. This routine allows a great deal of flexibility with respect to plotting interval, scaling, and desired information (i.e. Lat/Long position estimation errors, Doppler heading bias estimation errors, VLF bias estimation errors, or any combination).

The simulation routine also prints out the Kalman filter state estimates and the P, Φ , G, K matrices every ten seconds, mainly for debugging purposes.

A modified version of the simulation routine permits the use of real navigation data stored on magnetic tape, with the further option of being able to modify the data to simulate desired data conditions.

The modified routine also has options for various VLF contingency checks (to be described in Section 4.5).

4.2 Transient and Steady State Nature of the Kalman Filter

One of the first characteristics of the Doppler/VLF Kalman filter to be studied in some detail via simulation was the speed-of-response, or transient nature, of the filter as a function of the

specified initial conditions. Of particular interest was the nature of the bias estimation response as the diagonal elements of the initial state estimate covariance matrix, P_{α} , were varied in size. For this study, a straight-line, constant velocity trajectory was simulated for the aircraft motion-details of the simulated navigation conditions are summarized in Table 4.1. Note that large bias errors were simulated for every quantity of interest (i.e. groundspeed, true track angle, and six VLF station phase differences) in order to resolve the transient response of the bias estimates accurately.

TABLE 4.1
SIMULATED NAVIGATION CONDITIONS

True start position (Lat/Long) --	45.0/75.0 deg
Error in start position --	0.001/0.001 deg
True groundspeed (V_{DOP}) --	250.0 knots
Bias in measurement of V_{DOP} --	10.0 knots
True track ($\alpha + \beta$) --	45.0 deg
Bias in measurement of $\alpha + \beta$	10.0 deg
VLF stations --	O G M A D W
VLF measurement biases --	10.0 10.0 10.0 10.0 10.0 10.0 μ sec
Noise variance for V_{DOP} : σ^2_v --	1.0 knot ²
Noise variance for α : σ^2_{α} --	0.25 deg ²
Noise variance for β : σ^2_{β} --	0.25 deg ²
Noise variances for VLF stations: $\sigma^2_{\phi_i}$; (i = 1, . . . , 6)	1.0 μ sec ² ; all i

Recall that, in order to initialize the Kalman filter, it is necessary to specify a starting estimate of the state, \hat{x}_{α} , and the corresponding covariance matrix of that estimate, P_{α} . For this particular simulation study, the initial position estimates had an error of 0.001 deg in each of latitude and longitude while all the initial estimates of bias were set to zero. Sets of variances for the initial estimates of all the states were grouped into one of three categories: small, medium, or large. These initial conditions for the transient response study are all summarized in Table 4.2.

Figures 5 to 7 show the set of Kalman filter state estimate *errors* as a function of time for the three different initial error variance categories. A careful look at these plots reveals that the speed-of-response (in terms of decreasing the initial state errors) increases as the initial error variance levels increase (from small, to medium, to large). Conversely, one could say that the effective damping of the filter increases as the initial error variances decrease in size. For the particular initial error variances chosen, one almost has a situation akin to an overdamped (initial bias variances = 0.1), critically damped (initial bias variances = 5.0), or underdamped (initial bias variances = 100.0) response. Of course, the initial error variances should be chosen on the basis of a priori information available concerning possible errors in the initial state estimates. The foregoing analysis simply demonstrates how the transient response of the filter will be affected by the initial error covariances that are used

TABLE 4.2

KALMAN FILTER INITIAL CONDITIONS FOR TRANSIENT RESPONSE STUDY

Position: $\hat{P}LAT_{00}/\hat{P}LONG_{00}$	15.001/75.001 deg
Bias in Doppler groundspeed: $\hat{B}_{V_{00}}$	0.0 knot
Bias in true track: $\hat{B}_{\alpha_{00}}$	0.0 deg
Biases in VLF phase measurements: $\hat{B}_{\phi_{00}} (0 = 1, \dots, 6)$	0.0 μ sec; all 1
Noise variance levels	same as Table 4.1

Error covariance matrix, P_{00} :

	Small	Medium	Large
Variance of $\hat{P}LAT_{00} : P_{00}(1,1)$	0.00001	0.001	1.0 deg ²
Variance of $\hat{P}LONG_{00} : P_{00}(2,2)$	0.00001	0.001	1.0 deg ²
Variance of $\hat{B}_{V_{00}} : P_{00}(3,3)$	0.1	5.0	100.0 knot ²
Variance of $\hat{B}_{\alpha_{00}} : P_{00}(4,4)$	0.1	5.0	100.0 deg ²
Variance of $\hat{B}_{\phi_{00}} : P_{00}(5,5)$ + $P_{00}(10,10)$	0.1	5.0	100.0 μ sec ²

The results depicted in Figures 5 to 7 make sense intuitively, since it can be argued that specifying a very small initial error variance corresponds to telling the Kalman filter to place a great deal of emphasis on the initial state estimate and its update compared to what new information the incoming measurement data might be bringing. Thus, in particular, the Kalman filter is slow to react to the large initial errors of the bias estimates. On the other hand, a large initial error variance specification implies that very little weight should be put on the initial estimate compared to the measurement data. The filter then reacts quickly, on the basis of the incoming data, to reduce the large initial position or bias errors.

According to Figures 5 to 7, a steady state situation is eventually reached in which the various error quantities stabilize at relatively small values -- a typical response for a Kalman filter. Usually, during the course of any Kalman filter run, there is an initial transient region of relatively higher state estimation errors as the filter attempts to adapt to the incoming data (on the basis of the assumed model and initial conditions). In time, the adaptation phase is completed -- a steady state condition then prevails, corresponding to minimum error in the state estimates. Studying the matrices P and K as functions of time can also be instructive when it comes to understanding the operation of a Kalman filter. Figures 8 to 10 show $\|K\|K^{-1}$ and $\|P\|$ as functions of time for each of the small, medium, and large P_{00} cases already cited (the matrix norm, $\|\cdot\|$, is defined as the square root of the sum of the squares of the diagonal elements). The transient response nature of these quantities follows the same pattern as did the state estimates for the same categories of P_{00} . The Kalman gain matrix, K ,

reaches a small, steady state value (as measured by $\|K K^{-1}\|$), indicating that the plant update process has become quite accurate after all the biases have been estimated properly. Furthermore, the covariance matrix, P , also reaches a low level in the steady state, implying that the state estimate error variances have become quite small as the filter adapts to the incoming data (i.e. the accuracy of state estimation has improved with time).

4.3 Bias Estimation and Linear Dependency Problems

It became obvious very early in the analysis of the Doppler VLF Kalman filter that the biases in V_{DOP} and $\alpha + \beta$, B_A and B_B respectively, could be estimated quickly and accurately, with no noticeable interaction between the two Doppler heading biases being estimated. Figures 5 to 7 show this situation quite dramatically — steady state errors in the estimates of B_A and B_B are seen to be quite small, and the steady state error condition for them is reached sooner than for the VLF bias estimates of the same run.

Another phenomenon that was observed was an apparent linear dependency relationship among the various VLF bias estimates under certain conditions. For example, the Kalman filter runs depicted in Figures 5 to 7 can again be cited. Figures 5 and 6 show situations where the VLF phase bias estimation seems to be proceeding as expected — a monotonically decreasing phase bias estimation error for each of the six VLF stations as more and more data is processed by the filter. However, Figure 7, corresponding to the underdamped, fast transient response case, indicates a very different situation for VLF phase bias estimation. There is an initial, rapid improvement in VLF bias estimation for the time range 0 to 700 sec, as expected; then, suddenly, bias errors actually increase in five out of six of the stations during the time range 700 to 1800 sec (i.e. only VLF station A behaves as expected). Eventually, beyond 1800 sec, the VLF bias estimation errors decrease to acceptably small levels. Note that estimation of the biases in V_{DOP} and $\alpha + \beta$ is completely divorced from this effect whereas the position error, especially longitude error, is obviously strongly correlated to it.

In order to verify the suggested hypothesis of linear dependency among VLF phase bias estimates, another Kalman filter run was executed with all conditions the same as for the previous underdamped, fast transient response case of Figure 7 (i.e. large P_{11} in Table 4.2), except that no VLF biases were simulated in the measurement of VLF phase differences. The concern was that the effect being observed might simply be the result of having large initial discrepancies in the VLF bias estimates which somehow elicited this particular response. The results are shown in the plots of Figure 11 — comparisons with Figure 7 show that the VLF bias error responses of the two runs are virtually identical, apart from the first 500 sec or so. This would appear to reinforce the claim that there is some inherent linear relationship among the set of VLF stations chosen that causes the sudden increase in VLF bias errors when the filter damping is low.

The conjecture was also made that the observed interaction among VLF bias errors might be a function of geographical location — hence, it might be associated with the geometrical relationship between the VLF stations and the aircraft's position. To test out this theory, another Kalman filter run was made with all conditions the same as for the Figure 7 run except that the starting point was in the middle of the Davis Strait (i.e. 70° N, 60° W) instead of the Ottawa location (i.e. 45° N, 75° W). The results of this experiment are shown in the plots of Figure 12, and demonstrate vastly different VLF bias error and position error responses compared to the same results for the Ottawa location run, shown in Figure 7. Furthermore, plots of $\|K K^{-1}\|$ and $\|P\|$ as functions of time for the Davis Strait run (see Fig. 13) reveal significant differences when compared to the corresponding plots for the Ottawa run (see Fig. 10). These observed differences would then appear to be caused by a change in interaction among VLF bias estimates resulting from the significant shift in operating location.

In order to compare the geometries of the VLF stations for the two different operating locations being considered, a FORTRAN program was written which plots a map of a hemisphere centred at any specified geographical position. The projection used is an azimuthal equal area

(i.e. Lambert) projection, which allows accurate measurement of bearings and angles on the map. This type of map is quite useful for observing the geographical locations of the VLF stations relative to the operating position assumed for the aircraft. A linear dependency among certain VLF station bias estimates will probably occur if two or more VLF stations are almost in-line with the operating position. In such a case it would be very difficult for the Kalman filter to resolve the individual VLF station bias estimates accurately — a typical filter response would be large, correlated fluctuations in the bias errors for the VLF stations involved in the linear relationship.

Figures 14 and 15 show map projections centred at the Ottawa location and Davis Strait location respectively — the position of each of the six VLF stations is also indicated. A study of the projection centred at Ottawa (Fig. 14) reveals that VLF stations W, D, and M are roughly in-line with the Ottawa area operating location. Another look at the VLF phase bias error responses for the Ottawa area start location (i.e. Figs. 7 and 11) shows that the bias error responses of those three stations, in particular, correlate strongly during the 'large amplitude' region from 700 to 1800 sec. A series of Kalman filter experiments involving that same VLF geometry, where each VLF station in turn is programmed for no bias estimation (by setting the chosen VLF station's P_{ij} element value to zero), verifies that there is a consistently strong correlation among the bias error responses of stations W, D, and M. The projection centred in the Davis Strait area (Fig. 15), on the other hand, demonstrates a VLF geometry vastly different to that of the Ottawa projection. The Davis Strait projection reveals pairwise VLF station combinations that are nearly in-line with the projection centre — W-G, D-O, and A-M (to a lesser extent). A close look at the VLF bias error responses shown in Figure 12 indicates definite pairwise correlations for each of the three station pairs cited above. Moreover, further experimentation corroborates the existence of this set of correlations among VLF stations for the Davis Strait position.

Thorough investigation of the VLF linear dependency problem, under various conditions, has demonstrated that, in general, it is possible to estimate four out of six large VLF biases accurately and accurately without exciting the kind of linear dependency interaction that results in significant position error for a long period of time. For example, a Kalman filter experiment was run in which all conditions were as described in Tables 4.1 and 4.2 (i.e. the 'large' P_{ij} case), except that VLF stations A and D were simulated having no bias (instead of 10μ sec each) and the corresponding P_{ij} element values for A and D were set at 0.1μ sec² each (i.e. 'small' instead of 'large'). The net effect on the operation of the Kalman filter was to weight heavily the accurate initial condition information concerning the possible biases in A and D while deweighting the inaccurate initial condition information concerning biases in the other four VLF stations (i.e. note that the initial bias estimates of all VLF stations are set to zero). Figure 16 shows the plots of the error outputs for this particular run. It can be seen quite clearly how well the four large VLF biases are estimated while, at the same time, the bias estimates for A and D remain close to zero, as they should (note how much more sensitive the scaling is for the bias error plots of A and D).

4.1 Handling VLF Bias Drifting

One typical source of error in VLF measurements is caused by a phase shift in one or more station phase difference signals that has nothing to do with the true motion of the aircraft. The rate of this phase shifting can be fairly constant in time and a common cause is the so-called diurnal shift (see Ref. 15) as a result of the day-night terminator crossing a particular VLF station's transmission path. These diurnal shifts can have rates as high as 20μ sec per hour and can last for a couple of hours. Furthermore, various other ionospheric disturbances can cause phase shifts of a more random nature. It then becomes important to find out whether or not the Doppler VLF Kalman filter is configured to handle such VLF phase shifts.

In order to deal with the assumption of a drifting VLF station in the context of the Kalman filter, the concept of a VLF bias whose value could shift in time was considered. Different methods of tracking this time-variable bias were then tested. For example, Tables 4.3 and 4.4 outline the simulated navigation conditions and the Kalman filter initial conditions, respectively, for one series of experiments that were used to test out various ways of handling the drifting VLF station situation. Two VLF stations, G and M, were simulated to be drifting simultaneously at the rather high rates

of $36 \mu \text{ sec/hour}$ and $72 \mu \text{ sec/hour}$ respectively. The other four VLF stations were simulated to have only very small, fixed biases of $0.1 \mu \text{ sec}$ each. Both VLF station drifts started halfway through the Kalman filter run, at the 2500 sec point. Figure 17 shows the Kalman filter output error plots for this situation, with no use being made of any a priori information about the drifting VLF stations. The detrimental effect on all VLF bias estimates, as well as on basic position accuracy, is quite evident once the bias drifting starts.

TABLE 4.3
SIMULATED NAVIGATION CONDITIONS
FOR A DRIFTING VLF STATION EXPERIMENT

True start position (Lat/Long)	45.0 75.0 deg						
Error in start position	0.001, 0.001 deg						
True groundspeed (V_{DOP})	250.0 knots						
Bias in measurement of V_{DOP}	10.0 knots						
True track ($\alpha + \beta$)	45.0 deg						
Bias in measurement of $\alpha + \beta$	10.0 deg						
VLF stations	O	G	M	A	D	W	
VLF measurement biases	0.1	0.1	0.1	0.1	0.1	0.1	μ sec
VLF drift rates starting at $t = 2500$ sec		36.0	72.0				μ sec/hour
Noise variances	$\sigma^2_{\dot{\chi}} = 1.0 \text{ knot}^2$, $\sigma^2_{\dot{\beta}} = 0.25 \text{ deg}^2$ $\sigma^2_{\dot{\alpha}} = 0.25 \text{ deg}^2$, $\sigma^2_{\dot{\gamma}} = 1.0 \mu \text{ sec}^2$, all i						

In general, it was found from the simulation experiments that a drift in one or more of the VLF biases, if not somehow accounted for, would cause the other VLF bias estimates to drift away from their true values. Invariably, this would cause the LAT/LONG position errors to increase as well, as the VLF bias drifting continued. An intuitive explanation for this phenomenon will now be offered. In the Kalman filter experiment just described (results in Fig. 17), the filter first runs for 2500 sec, with no VLF bias drifts occurring. By $t = 2500 \text{ sec}$, all VLF biases are estimated accurately (equal to their true values of $0.1 \mu \text{ sec}$ each), so the associated P matrix (a posteriori covariance matrix) diagonal elements will all be quite small. In other words, by computing very small bias error variances, the Kalman filter itself considers all VLF bias estimates to be quite accurate at this point in time. At $t = 2500 \text{ sec}$, the biases in VLF stations G and M begin to drift at the specified rates. As the true biases in G and M increase, the errors in the Kalman filter estimates of these biases will also increase correspondingly. However, because the variances of all VLF bias estimates are quite small now, the bias errors of VLF stations G and M are accepted by the Kalman filter as "accurate" estimates for successive iterations. These errors build up and eventually cause the other VLF bias estimates to increase in error, due to the linear relationship existing among VLF station biases. Of course, the basic problem is due to the plant update equation for VLF bias states, which is not correct when bias drifting actually occurs.

TABLE 4.4

**KALMAN FILTER INITIAL CONDITIONS
FOR DRIFTING VLF STATION EXPERIMENT**

Position: $\hat{P}LAT_0/\hat{P}LONG_0$ —	45.001/75.001 deg
Bias in Doppler groundspeed: \hat{B}_{V_0} —	0.0 knot
Bias in true track: $\hat{B}_{\alpha\beta 0}$ —	0.0 deg
Biases in VLF phase measurements: $\hat{B}_{\phi_{i0}}$ ($i = 1, \dots, 6$) —	0.0 μ sec; all 1
Noise variance levels —	Same as Table 4.3
Error covariance matrix, P_0 :	
Variance of $\hat{P}LAT_0$: $P_0(1,1)$	1.0 deg ²
Variance of $\hat{P}LONG_0$: $P_0(2,2)$	1.0 deg ²
Variance of \hat{B}_{V_0} : $P_0(3,3)$	100.0 knot ²
Variance of $\hat{B}_{\alpha\beta 0}$: $P_0(4,4)$	100.0 deg ²
Variances of $\hat{B}_{\phi_{i0}}$: $P_0(5,5) \rightarrow P_0(10,10)$	0.1 μ sec ² ; all 1

In order to compensate for VLF bias drifting, without changing the plant update modelling, it became obvious that the appropriate P matrix diagonal elements would have to be adjusted during the drift period in order to counter this tendency of error build-ups in the Kalman filter. Two methods of P matrix adjustment were attempted:

- (i) Reset the appropriate VLF bias error covariance levels to large values at the beginning of the bias drift period in order to 'tell' the Kalman filter that these particular bias estimates would become inaccurate, but let P propagate normally after that. This technique proved to be unsuccessful in reducing the effects of bias drift. Unfortunately, after only a few iterations of the Kalman update equations, the (initially) large VLF bias covariance levels were once again at small values. Since the biases were still drifting at that point, significant errors in both VLF bias estimation and position estimation then occurred.
- (ii) Maintain the appropriate VLF bias error covariances in the P matrix at high values *throughout the entire drift period* — this forces the covariance elements of interest to remain at the same high level from one iteration to the next. Such a procedure was found to compensate for the bias drifts rather well. Because the particular VLF bias covariances were kept fixed at large values, the effects of the bias drifting were not transmitted to the other VLF bias estimates, nor to the position estimates. As soon as the bias drifting stopped, the P matrix was allowed to propagate normally again. The output error plots of Figure 18 are one example of this procedure being applied successfully. In this case, all the conditions are identical to those of the Kalman filter run shown in Figure 17 (and previously described).

except that P (6,6) and P (7,7), corresponding to biases in VLF stations G and M, are now fixed at $100 \mu \text{ sec}^2$ each for $t > 2500 \text{ sec}$. As a result, no appreciable error shows up in the estimation of the other VLF biases, and the position estimates remain accurate. Furthermore, the drifting biases of VLF stations G and M are actually estimated quite well on the average — the rather high noise levels in these estimates result from a lack of any smoothing effect for bias estimation when the P elements are set so high in value. Actually, the noise levels on the drifting bias estimates correspond to the variance specifications for the simulated VLF station noise processes (i.e. $1.0 \mu \text{ sec}^2$). Note that the success of this approach relies entirely on knowing when any particular VLF station is likely to be drifting — which is certainly feasible for the diurnal drift case, in particular.

Another modification within the Kalman filter can be used to eliminate any adverse effects from drifting VLF biases — namely, change the appropriate elements of the R matrix according. Recall that the R matrix indicates to the Kalman filter, via approximate statistics on the various VLF station noise processes, the relative weighting that should be placed on each of the incoming VLF phase difference measurements. By setting any particular R matrix diagonal element arbitrarily high in value, one can virtually eliminate the use of the corresponding VLF station's phase information. For example, in Figure 19 all the conditions for the Kalman filter experiment are identical to those of Figure 1, except that R (2,2) and R (7,7) corresponding to the noise variance of stations G and M have been reset to $10,000 \mu \text{ sec}^2$ for $t > 2500 \text{ sec}$. This action has the effect of eliminating the phase measurements of G and M from the Kalman filter solution for the remainder of the run. As a result, the drifting VLF biases have no influence on the other VLF bias estimates, and position accuracy is maintained. A comparison of the error plots from Figure 18 and Figure 19 indicates that, apart from the VLF bias errors of G and M, all other error signals show the same behavior between the two plots. Thus, modifying either the R matrix or the P matrix has the same effect on the other state estimates. The difference between the two approaches only shows up in the estimation responses of the drifting VLF station(s), G and M. Modification of the P matrix provides for "tracking" of the drifting VLF bias(s), whereas modification of R does not — as discussed in Figure 19, the VLF bias estimation error for G and M wind up rapidly once drifting starts. These estimation errors become exceedingly large after drifting begins because the corresponding P matrix diagonal elements stay small while the G and M VLF phase data is being weighted out — in fact, no further VLF bias estimation is attempted for the biases in G and M beyond $t = 2500 \text{ sec}$. The R matrix augmentation procedure should only be considered in a last resort situation, where one or more VLF stations are of such poor quality even to the point of loss of signal that they need be eliminated entirely from the Kalman filter solution.

1.5 Contingency Planning for VLF

1.5.1 VLF Data Management Problems

Past experience at NAE with using the VLF stations for navigation has revealed that definite data reliability problems are encountered and must be dealt with. In particular, the following three VLF problems are fairly common, and can occur with one or more of the stations at any time during a navigation flight:

- (a) The level of the random noise occurring in a particular VLF phase measurement may change suddenly.
- (b) A VLF station (receiver/transmitter) may develop a bias error in time, which may cause a propagation error in excess of 0.1 ft.
- (c) A VLF station may lose its signal.

- iii) A VLF station transmission may deteriorate in quality, even to the point of a 'loss-of-signal' status in the aircraft VLF receiver for a certain period of time. Eventually, the VLF signal will be re-acquired with either
 - a) an incorrect phase reading, or
 - b) the correct phase displaced by an integer multiple of wavelengths from what it should be (known as lane jumping).

In order to make effective use of the VLF data in the context of a Kalman navigation filter, it is imperative that some sort of contingency planning be determined for detecting and handling each of the VLF problems just described. To this end, consider the following five VLF 'scenarios' with suggested solutions:

- 1) Change in VLF noise character -- if one or more VLF stations are detected to have increased, or decreased, their phase measurement noise levels during flight, rough estimates of the new noise variance levels can replace the initial values in the appropriate R-matrix diagonal locations. A method of estimating VLF measurement noise variances in flight will be described subsequently.
- 2) Shift in VLF phase -- if a diurnal shift (or VLF bias change for any other reason) is detected, the appropriate P-matrix diagonal element can be fixed at a large value, such as $100 \mu\text{sec}^2$ -- the time-varying VLF bias can then be tracked accurately by the Kalman filter. When that particular bias stops drifting, the modified P-matrix element can be allowed to propagate normally again. A method for distinguishing between a sudden VLF bias shift and a VLF noise process increase will be suggested towards the end of this chapter.
- 3) Loss of VLF signal -- if a VLF station experiences a loss-of-signal situation, the associated R-matrix diagonal element should be increased to a very large value, such as 10^6 , in order to eliminate that station from the Kalman filter solution. Indication of a 'station down' status is transmitted to the Kalman filter algorithm by way of a VLF flag for each station (0 = station down, 1 = station up) that is inherent to the digital processing of the VLF phase data.
- 4) Re-acquisition of VLF signal -- if a VLF station comes back on line after being down, the following must be done before using that station again in the Kalman filter:
 - check nominal noise level of the station by measuring its approximate noise variance
 - check VLF phase measurements from that station for shifts and wavelength jumps
 - reset the appropriate VLF flag when it is verified that the station is permanently back on line.

When a VLF station's phase measurement data is to be brought back into the Kalman filter solution, the appropriate R- and P-matrix diagonal elements must be reset accordingly.

The VLF noise variance level check will yield a new value for the R-matrix diagonal element, and the wavelength check will sort out any gross bias error due to lane jumping. The wavelength check is automatically taken care of in the present digital processing of VLF onboard the Convair. When the VLF station is finally used in the filter again, the initial estimate of its bias should be zero. However, the corresponding initial VLF bias error variance should be large to reflect a feeling that there just might be some bias not accounted for in the phase measurements. Hopefully, then, the Kalman filter will respond quickly to estimate any nonzero bias that still exists in the station coming back up, even after VLF digital processing.

- 5) Complete loss of VLF signals — in such a case, all R matrix diagonal elements must be increased to values like 10^8 during the VLF outage; the Kalman filter is then navigating on Doppler heading information only. Assuming no accurate position reference exists at the time of VLF restart, such a situation would cause the most severe start-up problems. If all the VLF stations are down for only a short period of time (say ten minutes or less), Doppler heading navigation can be considered to be quite accurate — especially with the Doppler heading biases well estimated from the Kalman filter. When the VLF stations are reacquired, the check procedures outlined in 4) can be followed to null out any gross VLF biases and to establish new VLF noise variance levels, with Doppler heading updated position being used as the accurate reference. All VLF bias estimates would be re-initialized to zero, with the corresponding initial bias error variances set at relatively small values except, possibly, for a couple of stations that are known to exhibit bias shifting.

If all VLF stations are down for a long period of time (say an hour or more) then one can expect Doppler heading position error to increase at a nominal rate of 2×3 nm/hour. Thus, the Doppler heading position will be inaccurate when the VLF stations come up again. Without any other more accurate source of position information, the Kalman filter will simply have to continue on in a degraded mode of operation. The VLF stations must be re-initialized based on the inaccurate Doppler heading position; however, one consolation is the fact that the position error should not continue to increase once VLF is back on line.

4.5.2 In-Flight Measurement of VLF Phase Variance

The on-ground measurement of individual VLF station phase measurement statistics can be accomplished in a very straightforward manner. Since the aircraft is stationary, a series of VLF microsecond readings can be used directly for mean and variance calculations. A set of about 30 VLF measurements (i.e. a five minute collection of VLF data) would be sufficient to arrive at a reasonably accurate calculation of the mean value and variance. The mean value so calculated can be compared to the theoretical, constant, microsecond value for the known ground position, in order to determine any inherent phase bias for each VLF station. This phase bias is automatically nulled out in the basic preprocessing of raw VLF data; so the VLF phase biases, at the start of a navigation flight, are always close to zero.

In-flight measurement of VLF phase noise variance — a capability highly desired when running a Kalman filter — requires a procedure more elaborate than that just described. When the aircraft is flying, the raw VLF phase readings will, of course, vary according to the flight path, and a different quantity must be used for the calculation of noise variance. In the Kalman filter context, of Equation (2.30) recall that a new position update, $\hat{x}_{k+1|k+1}$, is calculated based on the Doppler heading plant process (with estimated Doppler heading biases taken into account). As well, the theoretical VLF microsecond distance must be determined for the calculation of the updated optimal state estimate, $\hat{x}_{k+1|k+1}$. VLF phase variance calculations can then proceed in flight as follows:

Recall the Kalman filter optimal state estimate equation,

$$\hat{x}_{k+1|k+1} = \hat{x}_{k+1|k} + K_{k+1} \cdot [h(x_{k+1|k}) - y_{k+1}] \quad (4.10)$$

Each y_{k+1} , $k = 0, 1, \dots$ is the actual measured VLF microsecond vector quantity whose elements are assumed to take the general form,

$$y = \mu_{\text{SECTED}} + \text{BIAS}_{\text{TRF}} + \text{NOISE}_{\text{TRF}} \quad (4.11)$$

The elements of \underline{h} represent the theoretical VLF microsecond distances plus estimates of phase bias evaluated at the updated Doppler heading position. Thus, in general,

$$\underline{h} = \mu \text{ sec}_{\text{DOP EST}} + \text{BIAS}_{\text{EST}} \quad (4.2)$$

for each VLF station being considered. Combining Equations (4.2) and (4.3), one can then write,

$$\begin{aligned} \underline{y} - \underline{h} &= \mu \text{ sec}_{\text{TRUE}} + \text{BIAS}_{\text{TRUE}} + \text{NOISE}_{\text{TRUE}} - \mu \text{ sec}_{\text{DOP EST}} \\ &\quad - \text{BIAS}_{\text{EST}} \approx \text{NOISE}_{\text{TRUE}} \end{aligned} \quad (4.4)$$

assuming the Kalman filter VLF bias estimate and Doppler heading position update are reasonably accurate. Thus, the error sequence, $\underline{y} - \underline{h}$, from the Kalman filter update equations actually approximates the VLF measurement noise vector, \underline{v} (Equation (3.8) shows this in a very straightforward manner).

The error sequence, $\underline{y} - \underline{h}$, can be used to acquire statistics that should reflect the approximate variances of the various VLF stations in-flight. Probably something like 30 VLF measurements, acquired over a five minutes period, would be needed for each station in order to get a valid statistic. Note that these VLF error sequences from Equation (4.4) will not, in general, be zero mean since the estimated bias might not exactly equal the true VLF bias. Very likely, then, the error sequence will contain some bias, requiring that a mean value be computed before a noise variance is evaluated.

4.5.3 Detecting VLF Bias Shifts

The error sequence, $\underline{y} - \underline{h}$, can also be used for detecting bias shifts in the different VLF station phase measurements. Recall that the noise process inherent to each of the VLF microsecond distance signals is assumed to have a zero mean and constant variance for the purposes of the Kalman filter implementation. Generally, however, the signal quality of any given VLF station varies with time, as does the associated VLF bias. Some of the VLF station signal quality possibilities during flight are the following:

- i) VLF noise variance level remains about the same as on the ground for the duration of the flight.
- ii) VLF noise variance level changes during the flight compared to ground run statistics.
- iii) A sudden bias shift occurs in the VLF station, but the noise variance stays the same.

Of particular interest is the distinction between a noise process change and a shift in VLF bias level. A change in the VLF noise statistics would not normally be accompanied by an associated change in bias -- the automatic in-flight monitoring of VLF noise variance would then indicate a change in noise level. On the other hand, a bias shift would assume the form of a sudden, or abrupt, change with time, and the random noise level is assumed to remain about the same. Monitoring $\underline{y} - \underline{h}$ as a function of time should detect any shift in bias that is not being tracked accurately by the Kalman filter in its usual configuration. One suggested algorithm for detecting bias shifts involves making use of Chebyshev's Theorem (Ref. 6) which states that the probability of any given data sample lying within $\pm n \sigma$ of the mean value is $(1 - 1/n^2)$. Conversely, the probability of a data sample lying outside $\pm n \sigma$ from the mean value is $1/n^2$. Hence, based on the measured VLF mean and variance, if any particular data point of $\underline{y} - \underline{h}$ departs significantly from the mean (e.g., exceeds 2σ),

then a possible bias shift will be suspected. In order to avoid confusion from momentary 'glitches' of large value, $y - h$ should be tested for a series of successive values before the decision is reached that a bias shift has occurred. For example, the mean and variance calculation from one set of 30 datapoints of $y - h$ could be used for comparison with the next 30 datapoints in order to check for a possible bias shift. If all 30 datapoints pass some sort of tolerance test when checked, then a new mean and variance are calculated. However, if one or more of the datapoints do not pass the tolerance test, a further test is done to verify that a bias shift has taken place.

A lot of 'fine tuning' will have to be done in order to have the suggested algorithm, and other algorithms for handling VLF problems, work properly with real data. Although most of the VLF contingency situations described in this section have been programmed as part of the Kalman filter simulation routine, most of the verification of the logic has been reserved for future work.

5.0 A COMPARISON OF FIVE DIFFERENT NAVIGATION ALGORITHMS

In this chapter, the navigation errors of various simpler alternatives to the Kalman navigation filter are analyzed and compared to the results using the Kalman filter approach. A set of simulation experiments is described which involves comparing five different navigation algorithms, with a range of accuracy specifications on the basic data quantities. The five navigation algorithms are further compared using real data acquired onboard the NAE Convair.

5.1 Description of the Five Navigation Algorithms

Five different navigation algorithms were considered for a comparison study and evaluation, namely

- i) Doppler/heading only,
- ii) VLF only,
- iii) Doppler/VLF complementary filter,
- iv) A 'naive' version of the Doppler/VLF Kalman filter,
- v) A 'smart' version of the Doppler/VLF Kalman filter navigator.

Brief descriptions of these navigation schemes are as follows:

- i) Doppler/Heading Navigation This form of navigation is also called simply, 'Doppler only', with the tacit assumption that compass heading is always available. A Doppler/heading navigation scheme is based on using the measured, or derived, quantities V_{DOP} , α , β , $\dot{\alpha}$, $\dot{\beta}$, $\dot{\alpha}$, $\dot{\beta}$, as described in Section 3.2. From these Doppler/heading quantities the rates of change of latitude and longitude, \dot{PLAT} and \dot{PLONG} respectively, can be expressed as,

$$\begin{aligned} \dot{PLAT} &= \frac{6077 \cdot V_{DOP} \cdot \cos(\alpha + \beta)}{60 \cdot \left[6077 - 31 \cdot \cos(\pi \cdot PLAT/90) \right]} \\ \dot{PLONG} &= \frac{- 6077 \cdot V_{DOP} \cdot \sin(\alpha + \beta)}{60 \cdot \cos(PLAT \cdot \pi/180) \cdot \left[6077 - 31 \cdot \cos(\pi \cdot PLAT/90) \right]} \end{aligned} \quad (5.1)$$

where PLAT and PLONG are in the dimensions of geographical degrees; V_{DOP} is in the dimensions of nm/sec; α and β are in the dimensions of radians.

For the Convair research aircraft, the Doppler/heading navigation parameters are sampled twice per second - this is then the sampling rate assumed in the navigation simulation. A trapezoidal version of digital integration is used to compute the Doppler/heading updates PLAT (j), PLONG (j) - at times $t_j = 0.2 \cdot j$ sec, as follows:

$$\begin{aligned} \text{PLAT}(j) &= \text{PLAT}(j-1) + \frac{0.5}{2} \cdot [\dot{\text{PLAT}}(j) + \dot{\text{PLAT}}(j-1)] \\ \text{PLONG}(j) &= \text{PLONG}(j-1) + \frac{0.5}{2} \cdot [\dot{\text{PLONG}}(j) + \dot{\text{PLONG}}(j-1)] \end{aligned} \quad (5.2)$$

The accuracy of this form of navigation is directly dependent on the accuracy of the assumed start position - PLAT(0), PLONG(0) - as well as the accuracy of the Doppler and heading data used in the integration algorithm. Any error in the specification of start position will always be retained; but, more importantly, any bias error in the basic Doppler/heading quantities will result in a diverging ramp position error with time.

- ii) VLF Navigation - For the purposes of the VLF algorithm designed, six stations are assumed to be operational. The following parameters used in the algorithm are defined:

- \underline{P}' : a known geographical position chosen to be close to the present VLF position (i.e. within a few nautical miles)
- \underline{P} : the latest VLF position - to be computed from incoming VLF phase measurement data
- P'_j : the microsecond distance from \underline{P}' to location of VLF station j ($j = 1, \dots, 6$), as calculated from the Sodano inverse routine
- α'_j : the azimuth angle from \underline{P}' to location of VLF station j ($j = 1, \dots, 6$), as calculated from the Sodano inverse routine
- P_j : the measured microsecond distance from \underline{P} to the location of VLF station j
- α_j : the azimuth angle from \underline{P} to the location of VLF station j - the approximation $\alpha_j \approx \alpha'_j$ is valid for the long distances involved
- x : the increment in longitude in going from \underline{P}' to \underline{P} , measured in microseconds (μ sec)
- y : the increment in latitude in going from \underline{P}' to \underline{P} , measured in microseconds (μ sec)

For any given VLF station, j, the equation expressing the x, y increments can be written as,

$$x = \sin \alpha_j \cdot (P_j - P'_j) \quad y = \cos \alpha_j \cdot (P_j - P'_j) \quad (5.3)$$

With six VLF stations in all, the following set of observation equations is available to calculate a solution for (x, y):

$$\begin{aligned} x \cdot \sin \alpha_1 + y \cdot \cos \alpha_1 &= P_1 - P'_1 \\ &\cdot \quad \quad \quad \cdot \quad \quad \quad \cdot \\ &\cdot \quad \quad \quad \cdot \quad \quad \quad \cdot \\ &\cdot \quad \quad \quad \cdot \quad \quad \quad \cdot \\ &\cdot \quad \quad \quad \cdot \quad \quad \quad \cdot \end{aligned} \quad (5.4)$$

$$x \cdot \sin \alpha_6 + y \cdot \cos \alpha_6 = P_6 - P'_6$$

Define $A_1 = \sin \alpha_1$; $B_1 = \cos \alpha_1$; $C_1 = P_1 - P'_1$; then Equation (5.4) becomes,

$$\begin{aligned} x \cdot A_1 + y \cdot B_1 &= C_1 \\ &\cdot \quad \quad \quad \cdot \quad \quad \quad \cdot \\ &\cdot \quad \quad \quad \cdot \quad \quad \quad \cdot \\ &\cdot \quad \quad \quad \cdot \quad \quad \quad \cdot \\ x \cdot A_6 + y \cdot B_6 &= C_6 \end{aligned} \quad (5.5)$$

having the least-squares solution,

$$\begin{bmatrix} x \\ y \end{bmatrix} = \begin{bmatrix} \sum_{i=1}^6 A_i^2 & \sum_{i=1}^6 A_i \cdot B_i \\ \sum_{i=1}^6 A_i \cdot B_i & \sum_{i=1}^6 B_i^2 \end{bmatrix}^{-1} \cdot \begin{bmatrix} \sum_{i=1}^6 A_i \cdot C_i \\ \sum_{i=1}^6 B_i \cdot C_i \end{bmatrix} \quad (5.6)$$

The solution from Equation (5.6) assumes that equal weighting is placed on the information from all six VLF stations being used. The position, P' , that is used in the calculations (i.e.

Eq. (5.4)) is usually the previously calculated VLF position — new VLF positions are calculated every ten seconds, so P' is always fairly close to P . Note that the (x, y) solution from Equation (5.6) has the units of microseconds, and must be converted to the equivalent in units of degrees LAT/LONG before the new PLAT, PLONG can be calculated. Then $PLAT = PLAT' + y$; $PLONG = PLONG' + x$.

Doppler/VLF Complementary Filter Navigation — The Doppler, heading, and VLF navigation data can be blended together into a very simple algorithm based on a digital version of

second-order complementary filtering. In essence, the Doppler/heading data is only used for high frequency contributions to position while the VLF data is used for 'dc' and low frequency tracking of position. The complementary filter design is such that there is a perfectly flat frequency response in the filter output. The basic sampling rate for the digital version of complementary filtering is 0.1 cps (i.e. the same as the VLF) and the input quantities used are VLF position (P_{VLF} : as computed from the VLF algorithm just defined) and the so-called ten second Doppler update, UD^* . Actually, two different sets of input quantities are used - $PLAT_{VLF}/UD^*_{LAT}$ and $PLONG_{VLF}/UD^*_{LONG}$ - so two digital complementary filters run in parallel, one for PLAT and one for PLONG.

The UD quantities are computed by accumulating, via trapezoidal integration, the half second Doppler velocity components over each ten second VLF sample interval. For the n th ten second VLF interval,

$$UD_{LAT}(j) = UD_{LAT}(j-1) + \frac{0.5}{2} \cdot [\dot{PLAT}(j) + \dot{PLAT}(j-1)] ; j = 1, \dots, 20 \quad (5.7)$$

$$UD_{LONG}(j) = UD_{LONG}(j-1) + \frac{0.5}{2} \cdot [\dot{PLONG}(j) + \dot{PLONG}(j-1)] ; j = 1, \dots, 20$$

with PLAT and PLONG defined in Equation (5.1). Define $UD^*_{LAT}(n) \equiv UD_{LAT}(20)$, $UD^*_{LONG}(n) \equiv UD_{LONG}(20)$ as the Doppler updates to be used at the n th ten second sample time in the complementary filter. The general recursion formula (for either PLAT or PLONG) has the form:

$$\begin{aligned} P_{OUT}(n) = & C_1 \cdot P_{OUT}(n-1) + C_2 \cdot P_{OUT}(n-2) \\ & + C_3 \cdot [P_{VLF}(n) + (1-a) \cdot P_{VLF}(n-1) - a \cdot P_{VLF}(n-2)] \\ & + C_4 \cdot [UD^*(n) - UD^*(n-2)] \end{aligned} \quad (5.8)$$

with

$$\begin{aligned} C_1 &= \frac{2 - 5 \cdot K \cdot (1-a)}{1 + 5 \cdot K} \\ C_2 &= \frac{5 \cdot a \cdot K - 1}{1 + 5 \cdot K} \\ C_3 &= \frac{5 \cdot K}{1 + 5 \cdot K} \\ C_4 &= \frac{0.5}{1 + 5 \cdot K} \end{aligned} \quad (5.9)$$

The values of parameters K and a are chosen to define a particular second-order filter characteristic that is required. From experimentation with real navigation data it has been determined that a damping ratio of $\zeta = 0.707$ and a break frequency of $f_c = 0.008$ hz gives good results (i.e. 23% overshoot and a 90 second settling time) -- this corresponds to $K = 0.0832$ and $a = 0.69952$. Based on these values for K and a , the coefficients in Equation (5.9) become,

$$\begin{aligned}C_1 &= 1.324152 \\C_2 &= - 0.500706 \\C_3 &= 0.293785 \\C_4 &= 0.353107\end{aligned}\tag{5.10}$$

The complementary filter defined above, using the particular set of coefficient values specified in Equation (5.10), is the one that is used in the navigation comparison studies.

- iv) **Naive Kalman Filter Navigation** -- The effective operation of the Kalman filter is highly dependent upon having good a priori knowledge concerning the nominal operating conditions of the various navigation sensors. For example, if one sensor degrades in accuracy, and that degradation is detectable, then that information is useful to the Kalman filter -- it can lead to more accurate state estimation than would occur if the degradation went undetected. Therefore, two different Kalman filter implementations are considered in the comparison study. The first implementation -- a so-called naive version of the Kalman filter -- involves establishing a set of nominal initial conditions for the filter which is held fixed no matter what the actual status of the various sensors might be. This version of the Kalman filter is completely oblivious to any changes in the quality of the incoming data. Obviously, if some aspect of the measured navigation data changes significantly, then the filter's performance will degrade accordingly. The initial condition specifications chosen for the naive Kalman filter used in the comparison studies are outlined in Table 5.1.
- v) **Smart Kalman Filter Navigation** -- This implementation of the Kalman filter assumes some method exists for monitoring the basic reliability of the individual navigation sensors. As soon as it becomes known that a particular sensor (e.g. Doppler, C-12 compass, or VLF station) has degraded, this information is used in the Kalman filter. Certain parameters of the filter are then modified to reflect the new knowledge about the status of the navigation sensors. Included in this version of the Kalman filter is the capability of fixing any particular P matrix diagonal element at a high value -- for accurate VLF bias drift estimation or, simply, very rapid VLF bias estimation. The majority of the initial condition specifications for the smart Kalman filter will be the same as those for the naive Kalman filter (as defined in Table 5.1), except where noted for the particular conditions on the data being used in the comparison study.

TABLE 5.1

INITIAL CONDITIONS FOR NAIVE KALMAN FILTER

Position: $\hat{P}LAT_o/\hat{P}LONG_o$	45.001/75.001 deg
Bias in Doppler groundspeed: \hat{B}_{V_o}	0.0 knot
Bias in true track: $\hat{B}_{\alpha_{\phi o}}$	0.0 deg
Biases in VLF phase measurements: $\hat{B}_{\phi_{10}}$ ($i = 1, \dots, 6$)	0.0 μ sec; all i
Noise variance for V_{DOP} : σ^2_V	1.0 knot ²
Noise variances for α, β : $\sigma^2_\alpha, \sigma^2_\beta$	0.25, 0.25 deg ²
Noise variances for VLF stations: $\sigma^2_{\phi_i}$ ($i = 1, \dots, 6$)	1.0 μ sec ² ; all i
Error covariance matrix: P_o	
Variance of $\hat{P}LAT_o, \hat{P}LONG_o$: $P_o(1, 1), P_o(2, 2)$	0.0001, 0.0001 deg ²
Variance of \hat{B}_{V_o} : $P_o(3, 3)$	10.0 knot ²
Variance of $\hat{B}_{\alpha_{\phi o}}$: $P_o(4, 4)$	5.0 deg ²
Variances of $\hat{B}_{\phi_{10}}$: $P_o(5, 5) \rightarrow P_o(10, 10)$	0.1 μ sec ² ; all i

5.2 Description of the Different Types of Simulated Navigation Data

The four different types of simulated navigation data to be considered are:

- best quality data,
- data with large Doppler/heading bias errors
- data with large VLF phase bias errors, and
- data involving VLF station drifts.

Two different aircraft trajectories are used in the simulation studies, namely,

- straight-line track with constant velocity and
- circular track with constant tangential velocity.

Detailed specifications on the various types of simulated data are as follows:

i) Best Quality Data -- The conditions simulated for the navigation transducers are:

a) Doppler radar system --

$$B_V = 1.0 \text{ knot}, \sigma_V^2 = 1.0 \text{ knot}^2$$

$$B_\alpha = 0.5 \text{ deg}, \sigma_\alpha^2 = 0.25 \text{ deg}^2$$

b) C-12 compass system --

$$B_\beta = 0.5 \text{ deg}, \sigma_\beta^2 = 0.25 \text{ deg}^2$$

c) VLF system -- stations used are O G M A D W

$$B_{\phi_i} = 0.1 \mu \text{ sec}, \sigma_{\phi_i}^2 = 1.0 \mu \text{ sec}^2; i = 1, \dots, 6$$

ii) Large Doppler/Heading Bias Errors -- The conditions simulated for the navigation transducers are:

a) Doppler radar system --

$$B_V = 10.0 \text{ knot}, \sigma_V^2 = 10.0 \text{ knot}^2$$

$$B_\alpha = 5.0 \text{ deg}, \sigma_\alpha^2 = 2.5 \text{ deg}^2$$

b) C-12 compass system

$$B_\beta = 5.0 \text{ deg}, \sigma_\beta^2 = 2.5 \text{ deg}^2$$

c) VLF system -- specifications same as in i).

iii) Large VLF Phase Bias Errors

a) Doppler radar system -- specifications same as in i).

b) C-12 compass system -- specifications same as in i).

c) VLF system -- specifications same as in i) *except*

$$B_{\phi_i} = 10.0 \mu \text{ sec}, \sigma_{\phi_i}^2 = 25.0 \mu \text{ sec}^2 \text{ for VLF stations O and/or G.}$$

iv) VLF Station Drifting

a) Doppler radar system -- specifications same as in i).

b) C-12 compass system -- specifications same as in i).

c) VLF system -- specifications same as in i) *except*

$$B_{\phi_i} \text{ changes linearly at } 10.0 \mu \text{ sec/hour}; \sigma_{\phi_i}^2 = 5.0 \mu \text{ sec}^2 \text{ for VLF station O or G.}$$

Information concerning the two different aircraft trajectories simulated is as follows:

a) Straight-Line Track, Constant Velocity --

Initial Position -- 45.0° LAT, 75.0° LONG

Error in Assumed Initial Position -- 0.001° LAT, 0.001° LONG

Groundspeed -- 250 knots

True Heading -- 45.0°

b) Circular Track, Constant Tangential Velocity -- This type of aircraft trajectory is useful for simulating a strong acceleration situation for the aircraft. Note, however, that this particular manoeuvring would never occur for any length of time under normal flying conditions.

Initial Position -- 45.0° LAT, 75.0° LONG

Tangential Velocity -- 250 knots, clockwise

Radius of Circular Track -- 10.0 nm

Centripetal Acceleration -- 2.93 ft/sec² or 1.735 knot/sec

5.3 Results from Simulating Best Quality Data

Simulation runs were conducted using the best quality navigation data on the five different navigation schemes being compared. Both the straight-line and circular tracks were considered as well. In the case of the straight-line, constant velocity trajectory there was no difference between the naive and smart versions of the Kalman filter, so only one of them was used. Figure 20 compares the total position errors for each navigation algorithm as a function of time, over a 3000 sec run (NOTE: total position error = $[(\text{LAT ERROR})^2 + (\text{LONG ERROR})^2]^{1/2}$). From Figure 20 it can be seen that navigating on Doppler heading alone, even with reasonably good Doppler heading data, results in a significant ramp type of position error due to the biases in groundspeed and heading. Navigating on VLF stations alone leads to a bounded error with time -- the error level shown here for VLF would correspond to a very good quality VLF situation. When the Doppler VLF complementary filter is used (i.e. COMPL in Fig. 20) the average error level decreases slightly, and there is a bit of a smoothing effect on the VLF error from the low-pass action of the filter. The bottom trace in Figure 20 shows the Kalman filter result -- clearly much superior to any of the other navigation schemes in terms of average error level and smoothness of error response. Notice the typical Kalman filtering action, which results in a slightly higher error during the first few hundred seconds of the run as the filter adapts to the incoming data.

Figure 21 shows similar results, again for the best quality data, when the circular track with constant tangential velocity is being simulated. In this case, both a naive and a smart version of the Kalman filter are considered in the comparison plots. The error behaviours for the Doppler alone, VLF alone, and Doppler VLF complementary filter cases are about what would be expected (Doppler error is constrained because of the circular trajectory); but the total position error plot for the naive Kalman filter is rather interesting. For that case, the position error actually increases with time to a rather significant level -- it even looks as though the error is slowly diverging with time. The reason for this becomes apparent when one considers the type of aircraft trajectory that is being simulated. Recall that the simulated circular track results in a constant centripetal acceleration of 2.93 ft/sec² or 1.735 knots/sec for the aircraft. This is a fairly significant acceleration level, so the Doppler heading plant, based on velocity measurements, will not be nearly as accurate as in the straight-line, constant velocity case. Nevertheless, the naive version of the Kalman filter assumes that the Doppler heading plant retains its nominal accuracy as defined by the noise variance specifications on V_{DOPPLER} , σ_v , and β (i.e. in Table 5.1). Obviously, these specifications are incorrect for the type of accelerating motion taking place, and a smart version of the Kalman filter has been developed to overcome this problem.

For the smart Kalman filter a poor quality plant is assumed, and this information is conveyed to the filter by respecifying $\sigma^2_{\lambda} = 100.0 \text{ knot}^2$, $\sigma^2_{\psi} = 25.0 \text{ deg}^2$, and $\sigma^2_{\theta} = 25.0 \text{ deg}^2$. These changes in initial conditions give a much better, and more stable, total position error plot (shown in the bottom trace of Fig. 21). This position error trace shows a significant improvement compared to all the others, but the improvement is not as dramatic as in the straight-line trajectory case (shown in Fig. 20). The reason for this is the fact that the basic plant update equations have deteriorated in accuracy for the circular track situation, and the Kalman filter cannot be expected to do as well under the circumstances. Specifying basic plant accuracy as a function of the type of aircraft trajectory taking place is only one of the capabilities that a smart Kalman filter must have, as will be shown subsequently.

5.4 Results from Simulating Large Doppler/Heading Biases

The simulation results from navigation data with large Doppler heading bias errors are displayed in Figures 22 and 23. Figure 22 compares the five different navigation schemes for the straight-line track case. For navigation with Doppler alone, the error build up due to large Doppler heading biases is quite dramatic. Navigation error results for VLF alone stay the same as before, as do the navigation errors for the Doppler/VLF complementary filter. The large Doppler heading bias errors do not affect the operation of the complementary filter because only the high frequency contribution from the Doppler heading system is used. The naive and smart versions of the Kalman filter produce about the same error level in the steady state, and both are a significant improvement over the other navigation algorithms. The only difference in the error responses of the two versions of the Kalman filter is that the transient response for the first 300 sec or so is a lot faster in the case of the smart version. This is due to the fact that, for the smart version of the filter, initial conditions are respecified as $\sigma^2_{\lambda} = 10.0 \text{ knot}^2$, $\sigma^2_{\psi} = 2.5 \text{ deg}^2$, $\sigma^2_{\theta} = 2.5 \text{ deg}^2$, $P_{(3,3)} = 100.0 \text{ knot}^2$, and $P_{(1,1)} = 50.0 \text{ deg}^2$ to take advantage of the a priori knowledge that Doppler heading biases will be significant (so that a faster transient response should be used when estimating them).

Figure 23 compares the five navigation algorithms for the circular track situation. Again, the error results for Doppler alone, VLF alone, and the Doppler/VLF complementary filter show no great surprises. In spite of the large Doppler heading biases, errors in Doppler only navigation remain reasonably bounded mainly because of the 10 nm radius circular track — otherwise, the Doppler navigation error would grow at a much faster rate. The naive and smart Kalman filter results are very similar to those shown in Figure 21 (i.e. for best quality data and a circular track). The nominal naive Kalman filter specifications on the Doppler/heading plant correspond to a plant update equation assumed by the filter to be more accurate than is really the case. As a consequence, the position error grows with time — in fact, the Kalman filter appears to be close to instability. Modified specifications on the plant for the smart Kalman filter (the same ones as for the best quality data circular track case) rectify the situation by increasing the level of plant noise assumed, which has a stabilizing influence on the filter response. Note that the smart Kalman filter error response is only a marginal improvement over that of the complementary filter approach — due, no doubt, to the poor quality plant updating for the circular manoeuvring.

For completeness, Figure 24 shows plots of the actual Doppler heading bias errors in attempting to estimate B_{λ} and B_{ψ} using the Kalman filter. The runs used correspond to the results from Figure 22 for large Doppler/heading biases with a straight-line track. Figure 24 indicates that the error response is much faster for the smart Kalman filter compared to the naive version, due to the change in initial conditions. Nevertheless, for both naive and smart versions of the filter the errors in estimating the large Doppler/heading biases are quite small. The same small bias error levels occur even when the circular track manoeuvre is used in the simulation runs. An obvious practical situation in which Doppler/heading biases become significant occurs when magnetic variation, VAR, is specified incorrectly — the Kalman filter will quickly estimate any obvious bias in $\alpha + \beta$ from this source of error.

5.5 Results from Simulating Large VLF Station Biases

Simulation results for navigation data involving large biases in certain VLF station phase measurements are compared in Figure 25 (for the straight-line trajectory), with VLF stations O and G simulated to have phase biases of $10 \mu \text{ sec}$ each. The effect of these two VLF biases is quite evident for the VLF alone and Doppler/VLF complementary filter runs. In both cases, an average total position error of 1.0 nm occurs because of the significant biases in the two VLF stations. Note that the complementary filter still tends to smooth out the VLF data, but it can do nothing about the VLF bias errors. On the other hand, both versions of the Kalman filter show position error improvement with time. The naive Kalman filter response is quite sluggish because of the nominal initial condition variance levels for all VLF bias estimates, $\sigma^2_{B_{i,j}} = 0.1 \mu \text{ sec}^2$, all i . However, with appropriately large initial condition variance levels for biases in VLF station O and G (i.e. $\sigma^2_{B_{O,G}} = 100.0 \mu \text{ sec}^2$), as defined for the smart Kalman filter, the speed of response of the error-versus-time plot is greatly enhanced, and the steady state total position error is quite low.

As a further check, navigation data for the straight-line trajectory was simulated with both large Doppler heading biases and large VLF biases in stations O and G. This was done in order to verify that the superimposed data response was essentially the same as the sum of the individual Kalman filter responses. With the VLF bias errors predominating, the output error response for the superimposed data was virtually identical to that shown in Figure 25 (the only exception being Doppler only navigation where, of course, the large Doppler heading bias errors dominate). Figures 26 and 27 show the complete set of Kalman filter error responses for each of the naive and smart versions of the filter — corresponding to this superimposed navigation data situation. From the naive Kalman filter error outputs of Figure 26 it can be seen that the Doppler heading biases are estimated quickly and accurately, while VLF bias estimation is much more sluggish. There is also an obvious interaction among various VLF stations as a result of the linear dependencies that are known to exist. On the other hand, the smart Kalman filter error outputs (Fig. 27) look good right across the board — the advantage of having accurate a priori knowledge, especially concerning VLF, is quite evident!

5.6 Results from Simulating VLF Station Drift

Simulated navigation data with VLF station O drifting at the rate of $10 \mu \text{ sec/hour}$ was used for the comparison plots of total position error shown in Figure 28. The effect of the constant VLF drift rate is clearly seen in the VLF and complementary filter plots. A naive version of the Kalman filter produces an output error which appears to stabilize at a level of about 0.3 nm. However, a properly programmed smart Kalman filter (i.e. with $P(5, 5)$ fixed at $100.0 \mu \text{ sec}^2$ for the entire run) results in a very small total position error, as shown in the bottom trace of Figure 28. Similar results occur if VLF station G is drifting instead of station O. Figure 29 shows the complete set of estimation errors for the naive Kalman filter run with VLF station O drifting. The associated VLF bias error plots indicate that there is a strong interaction among the various VLF bias estimates caused by the drifting of station O. Figure 30 displays the same error quantities, but for the smart Kalman filter case. Notice now the VLF bias errors are much more stable and hardly drift at all compared to the naive Kalman filter case. Note also that the procedure of fixing $P(5, 5)$ at $100.0 \mu \text{ sec}^2$ means that the basic noise process of VLF station O ($\sigma^2 = 5.0 \mu \text{ sec}^2$) is present in the estimation error of $B_{O,O}$. Thus, the normal smoothing effect of the recursion formula for estimating $B_{O,O}$ (eq. (2.3)) is bypassed, causing $B_{O,O}$ to be estimated in a noisy fashion. Just the same, the average error in estimating $B_{O,O}$ is close to zero in spite of the large drift rate being simulated.

5.7 Results from Using Real Data

About an hour's worth of real navigation data, collected onboard the Convair 580 research aircraft, has been analyzed using the various navigation algorithms already defined (i.e. Doppler heading navigation, VLF navigation, Doppler/VLF complementary filter navigation, naive and smart Kalman filter navigators). The navigation data was collected in the vicinity of Ottawa, and the type of aircraft trajectory involved was a series of racetrack patterns passing over well-known visual landmarks such as airport beacons, airport VOR's and runway intersections. These visual on tops are

necessary, of course, in order to have reference points for establishing navigation error as a function of time in the case of the real data. Table 5.2 shows a list of the visual on-tops in the sequence in which they were overflowed, together with the time and correct geographical location. Note that the accuracy of these on tops is felt to be within 0.10 nm. The table indicates that there are about 57 minutes of useable navigation data from the known start position to the final on-top.

TABLE 5.2

INFORMATION ON THE VISUAL REFERENCE POINTS FOR THE NAVIGATION STUDY

Type of On-Top	Time from Start	Geographical Location
Intersection RW 25-32	0 secs	45 18'57" 75 39'55"
Ottawa VOR	290 secs	45 26'30" 75 53'50"
Kinburn Beacon	540 secs	45 25'00" 76 08'58"
Arnprior Bridge	1130 secs	45 26'06" 76 21'00"
Kinburn Beacon	1310 secs	45 25'00" 76 08'58"
Ottawa VOR	1520 secs	45 26'30" 75 53'50"
Intersection RW 25-32	1790 secs	45 18'57" 75 39'55"
Uplands Beacon	1980 secs	45 13'45" 75 29'36"
Uplands Beacon	2240 secs	45 13'45" 75 29'36"
Ottawa Beacon	2790 secs	45 21'36" 75 33'41"
Intersection RW 25-32	2970 secs	45 18'57" 75 39'55"
Rideau-Carleton Racetrack	3130 secs	45 17'48" 75 36'15"
Ottawa Beacon	3413 secs	45 21'56" 75 33'41"

For the particular navigation data collected, the VLF stations available were L, M, D, G, W, and R. Figure 31 shows the relative locations of these VLF stations using a Lambert projection centred at Ottawa. It can be seen from this projection that the VLF geometry is not the best, with many of the stations almost in-line. The possibility of VLF linear dependencies will then be quite real, and this fact must be taken into account when using the Kalman filter approach. VLF groundrun statistics, based on 42 samples for each station, were computed by monitoring the VLF receiver just prior to the navigation flight. As well, a comparison of the raw VLF was made between the start time data and the VLF data at the 2970 sec point (both of these positions are the RW 25-32 intersection) to see whether or not any VLF bias drifting was taking place. The results could then be compared with the estimates of VLF bias arrived at by using the Kalman filter. The noise variance estimates and raw VLF data comparisons are displayed in Table 5.3. From this table it can be seen that the VLF groundrun noise variances differ widely from one station to the next, but all are well below the nominal $1.0 \mu \text{ sec}^2$ level. The VLF phase bias shifts (i.e. $1 \mu \text{ sec}$), based on VLF measurements taken about 50 minutes apart, are all fairly small except for the bias shift of VLF station R. A closer look at station R's phase readings reveals that a fixed drift rate of about $17.0 \mu \text{ sec hour}$ exists, apparently due to inaccuracies in the frequency of transmission. It was felt that it would be an ideal test for the Kalman filter to try to track the known drifting VLF station. This particular real VLF data was considered to be quite representative of what to expect in the way of typical VLF data during the course of a flight

TABLE 5.3

VLF STATION INFORMATION FOR THE NAVIGATION STUDY

Station	Groundrun Variance	Phase Measurement at T = 0 Sec	Phase Measurement at T = 2970 Sec	Δ , μ Sec
L	$0.012 \mu \text{ sec}^2$	$9850.5 \mu \text{ sec}$	$9852.5 \mu \text{ sec}$	2.0
M	$0.005 \mu \text{ sec}^2$	$3661.4 \mu \text{ sec}$	$3660.0 \mu \text{ sec}$	1.4
D	$0.103 \mu \text{ sec}^2$	$4138.9 \mu \text{ sec}$	$4140.0 \mu \text{ sec}$	1.1
G	$0.093 \mu \text{ sec}^2$	$2104.1 \mu \text{ sec}$	$2103.4 \mu \text{ sec}$	0.7
W	$0.011 \mu \text{ sec}^2$	$6236.6 \mu \text{ sec}$	$6236.9 \mu \text{ sec}$	0.3
R	$0.614 \mu \text{ sec}^2$	$6783.5 \mu \text{ sec}$	$6797.6 \mu \text{ sec}$	14.1

TABLE 5.4

REAL DATA INITIAL CONDITIONS FOR THE NAIVE KALMAN FILTER

Position: $\hat{\text{PLAT}}_0 / \hat{\text{PLONG}}_0$	45.3158 / 75.6653 deg
Bias in Doppler Groundspeed: $\hat{\text{B}}_{\text{V}_0}$	0.0 knot
Bias in true track: $\hat{\text{B}}_{\text{true}}$	0.0 deg
Biases in VLF phase measurements: $\hat{\text{B}}_{\text{VLF}} (i = 1, \dots, 6)$	0.0 μ sec; all i
Noise variance for V_{DOP} : σ^2_{V}	1.0 knot ²
Noise variances for α/β : $\sigma^2_{\alpha}/\sigma^2_{\beta}$	2.5, 2.5 deg ²
Noise variances for VLF stations: σ^2_{VLF}	as per Table 5.3
Error covariance matrix, P_0 :	
Variances of $\hat{\text{PLAT}}_0 / \hat{\text{PLONG}}_0$: $\text{P}_0 (1, 1) / \text{P}_0 (2, 2)$	0.0001 / 0.0001 deg ²
Variance of $\hat{\text{B}}_{\text{V}_0}$: $\text{P}_0 (3, 3)$	100.0 knot ²
Variance of $\hat{\text{B}}_{\text{true}}$: $\text{P}_0 (4, 4)$	100.0 deg ²
Variances of $\hat{\text{B}}_{\text{VLF}}$: $\text{P}_0 (5, 5) \dots \text{P}_0 (10, 10)$	0.01 $\mu \text{ sec}^2$; all i

Table 5.4 indicates the initial condition specifications for a naive version of the Kalman filter that was run using the real navigation data. Specification of VLF noise variances based upon groundrun measurements was felt to be quite valid, even for the naive Kalman filter, since these measurements can be accomplished quite simply before the start of any navigation flight. Moreover, noise variances for α, β — namely $\sigma_{\alpha}^2, \sigma_{\beta}^2$ — were specified as 2.5 deg^2 each, based on examining the raw Doppler/heading data — again, something that would normally be available. The variances on $\hat{B}_{V_{\alpha}}$ and $\hat{B}_{V_{\beta}}$ were set quite high in order to estimate any Doppler/heading biases very quickly. However, the variances on all the $\hat{B}_{\phi_{ijk}}$'s were set fairly low to avoid a strong interaction among VLF bias estimates because of the linear dependencies known to exist. Figure 32 shows the Kalman filter outputs based on the specifications defined in Table 5.4. In Figure 33, the associated position errors are displayed, based on the 13 visual fixes available during the course of the flight. It can be seen from these position error plots that the overall error is fairly small for over half the flight and then it starts to increase. The increasing error is felt to be due to the effect of VLF station R's drifting — eventually, the phase drifting begins to effect the Kalman filter accuracy. Judging from the VLF phase bias estimates in Figure 32, the filter is attempting to follow the drifting in station R but just cannot keep up. The information from Table 5.3 suggests that estimation of the VLF biases in L and M is at least proceeding in the right direction. However, the other VLF bias estimates appear to be incorrect — no doubt the linear dependency problem is manifesting itself. In sharp contrast, Figure 32 shows that the Doppler/heading bias estimates are resolved rather quickly and then remain at reasonably constant values.

In order to alleviate the detrimental effect of VLF station R drifting, a smart Kalman filter was designed specifically to track station R's shifting bias. As well, this version of the Kalman filter concentrated on estimating the two largest VLF biases (as determined from Table 5.3), namely, those of VLF stations L and M. The changes that were made to the initial conditions in order to define this smart Kalman filter are outlined in Table 5.5. Note that the error covariance diagonal elements corresponding to VLF bias estimates in stations D, G, and W (i.e. $P_{ij}(7, 7) \rightarrow P_{ij}(9, 9)$) are set to zero, which means that VLF bias estimation is not even being attempted for these particular stations. Figure 34 displays the various smart Kalman filter estimates as a function of time while Figure 35 shows the resulting position errors at the 13 visual check-points. From Figure 34 it can be seen that the smart version of the Kalman filter is tracking the drift in station R's bias quite accurately (recall that the drift rate is about $-17 \mu \text{ sec./hour}$). Moreover, bias estimation for VLF stations L and M appears to be proceeding in the right direction. The results in Figure 35 indicate that the position error increases somewhat during the initial, transient region of Kalman filtering action and then appears to settle down quite nicely, as expected for proper operation of the Kalman filter. Notice that, here, Doppler/heading bias estimation is almost identical to that of the naive filter case. The rather small Doppler/heading biases estimated suggest that the Doppler/heading dead reckoning navigation system is reasonably accurate for this particular flight data.

TABLE 5.5

CHANGES TO INITIAL CONDITIONS FOR THE SMART KALMAN FILTER

Error covariance matrix, P_{ij}

Variances of $B_{\phi_{ijk}}$'s:

$P_{ij}(5, 5) + P_{ij}(6, 6)$	$100.0 - 100.0 \mu \text{ sec}^2$
$P_{ij}(7, 7) \rightarrow P_{ij}(9, 9)$	$0.0 \mu \text{ sec}^2$
$P_{ij}(10, 10)$	$100.0 \mu \text{ sec}^2$, fixed for duration of flight

A comparison study was conducted, for the same set of real navigation data, involving the various possible navigation algorithms (i.e. Doppler alone, VLF alone, and Doppler VLF complementary filter as well as the different versions of the Kalman filter). The results of this study are summarized in the comparison plots shown in Figure 36. Navigation using Doppler alone is surprisingly accurate, with the total position error rising to a little over 2.0 nm after one hour. Most likely, the position errors would have been higher for Doppler only navigation if a straight-line aircraft trajectory had been used instead of the racetrack patterns that were flown — recall from the simulation studies how the Doppler heading errors tended to be bounded for the circular track case. The second plot in Figure 36 shows Doppler VLF complementary filter position error results — VLF alone is not shown because the results are virtually identical to those of the complementary filter. The total position error of the complementary filter rises to almost 2.0 nm after one hour — due, no doubt, to the various VLF biases and, of course, the constant drift rate of VLF station R. The naive Kalman filter and smart Kalman filter (i.e. SMART KF1) results refer to the versions of the Kalman filter described earlier in this section. From Figure 36 it can be seen that the Kalman filter approach certainly improves the overall positional error very significantly.

The results of one other Kalman filter run are displayed as the bottom trace in Figure 36 (i.e. SMART KF2). Experimentation revealed this to be the most accurate result attainable and the particular initial conditions that produce this result are rather interesting. For this case, all error covariance diagonals relating to VLF bias estimation were set to zero i.e. no VLF bias estimation was taking place! All other initial conditions on the filter were the same as for the 'NAIVE KF' and 'SMART KF1' cases. Normally, with no VLF bias estimation taking place, any significant bias build-up in the VLF phase measurements would affect the accuracy of the filter outputs. However, according to the VLF bias shifts indicated in Table 5.3, the constant drift rate of VLF station R is the only bias shift of any real consequence. Furthermore, the groundrun noise variance for R is abnormally high, compared to the other VLF station noise variances (more than two orders of magnitude compared to that of station M), so the Kalman filter has a strong tendency to 'weight out' the influence of VLF station R in the overall position estimate. On this basis, the Kalman filter position estimate can be quite accurate without going to the extent of VLF bias estimation. As a matter of fact, allowing the Kalman filter to estimate VLF biases probably introduces an additional constraint and complexity which tends to decrease the accuracy of position estimation in this case — the known linear dependencies among VLF bias estimates also come into play here. Of course, the situation would probably be a lot different if very significant biases had developed in one or more of the critical VLF stations; then VLF bias estimation would come into its own, as demonstrated in the simulation results.

5.8 Summary of Results

The major results from the comparison study are the following:

Dead reckoning navigation using the Doppler heading system is quite sensitive to biases, even to fairly small ones, especially for the typical straight-line tracks that are flown. Any Doppler heading bias errors will result in a position error which diverges with time.

Navigation using an average of all VLF information is somewhat sensitive to VLF bias shifts and other VLF anomalies that invariably occur. Fortunately, these errors usually result in a bounded position error as a function of time, except for the drifting VLF station condition.

The Doppler VLF complementary filter is completely immune to Doppler heading biases and has a weak tendency to 'smooth out' the VLF position estimates as well as to reduce the error slightly. However, the complementary filter response is still affected by VLF biases and station drifting.

The Kalman filter has a very strong smoothing action on the position error and it can be extremely insensitive to both Doppler heading and VLF biases, depending upon the initial conditions chosen. The smart version of the Kalman filter is always found to be significantly superior to the complementary filter approach.

Output errors from a naive version of the Kalman filter can be a lot larger than those from a smart version. The naive Kalman filter navigator appears to be especially sensitive to initial condition specifications regarding the quality of the plant and the status of the various VLF stations being used.

The Kalman filter navigator has demonstrated its accuracy when applied to typical, real navigation data -- even to the extent of being able to track a real, drifting VLF station.

6.0 CONCLUSIONS

6.1 Assessment of the Kalman Filter Approach to Navigation

The Doppler/VLF Kalman filter studied in this report has shown the many advantages of this type of approach to the navigation task. Probably one of the main advantages the Kalman filter approach offers is flexibility in terms of handling redundant navigation information in some optimal fashion. Various navigation transducers can be modelled into the Kalman filter format fairly readily and, hence, can be used to their full potential. The Kalman filter is also very flexible when it comes to handling the raw data from any given navigation configuration -- in particular, the very basic transducer relationships can be modelled, if so desired. A priori knowledge concerning the quality and relative accuracy of the various navigation transducers can be put to good use by the Kalman filter witness, especially, the results obtained when attempting to track VLF biases and bias drifts. The Doppler/VLF Kalman filter has certainly demonstrated the benefits to be gained from modelling and estimating different bias error quantities, and it has also shown just how simple the modelling/estimation process can become. A bonus to be gained from estimating Doppler heading biases using the Kalman filter is the fact that improved estimates of the aircraft velocity components can then be computed. The concept of estimating the various error quantities of the overall navigation system in real time implies that, should one part of the system fail at some point in time, navigation accuracy will not be severely jeopardized.

Of course, as with everything else, one must pay the price for the improved accuracy derived from the Kalman filter approach to navigation. The cost of employing a Doppler/VLF Kalman filter would be measured in terms of the increased mathematical complexity and associated increase in computational burden compared to, say, the Doppler/VLF complementary filter scheme. However, the on-state Doppler/VLF Kalman filter described in this report is not nearly as complex as many Kalman filters that have been successfully run in real time. Nevertheless, a great deal of programming effort must go into the efficient design of a real time Kalman filter that would be run on a mainframe computer or even a dedicated microprocessor. A further drawback that results from employing a Kalman filter approach is the necessity to specify accurately the statistical and other initial condition properties necessary for correct execution of the filter algorithm. In other words, one must learn a great deal about the individual transducers comprising the complete system. The more one knows about them, the greater is the potential accuracy of the Kalman filter estimates.

In summary, a Kalman filter provides for an improved estimate of the aircraft state in a navigation system, utilizing the error states based on the concept of statistically combining the redundant/independent, redundant measurements that have a known statistical uncertainty. The on-state version of a Kalman filter is ideally suited to implementation on a computer, a computer model thereof. At the Flight Research Laboratory, the aircraft navigation system is being modelled on a computer. We are the most successful navigation scheme a Kalman filter approach to navigation and its advantages.

6.2 Future Work

Based on the results to date, several areas for future work are suggested. Some of the possibilities are the following:

- (a) Handling VLF Contingencies -- This topic was discussed in Section 5.2. It would be useful to study the VLF problem, together with suggested solutions, in order to develop a way of

simulation work or experiments involving real VLF data. As can be seen from the results presented in this report, proper handling of the raw VLF data, especially during the various 'anomalous' situations that can arise, is critical to the successful operation of the Doppler VLF Kalman filter. Much has been learned about VLF phase bias estimation, the associated linear dependencies which can occur, and the possibility of bias drift estimation. Nevertheless, a great deal more work can and should be done in this area.

- ii) **Real Time Programming Problems** — A definite challenge will be the design and implementation of a real time version of the Doppler VLF Kalman filter for use onboard the Convair research aircraft. Although the Kalman filter simulation routine does a good job of processing the real data acquired from the Convair navigation transducers, this is a far cry from simulating a real time operation onboard the aircraft. The major problem will be conversion of the Kalman filter simulation routines (written in FORTRAN IV and operating, at present, in the IBM 3032 TSS environment) to the Interdata 7/32 minicomputer onboard the Convair. At the heart of the problem will be the computational speed and accuracy required to propagate the Kalman filter matrix recursion equations. One means of reducing the computational burden might be to lengthen the update interval from ten seconds to, say, twenty or thirty seconds. Simulation studies could be done to determine the effect a longer update interval might have on basic estimation accuracy. The costs of simulation runs in the TSS environment are expensive for the ten second update case as it stands now. For example, it costs about \$50, and takes 100 seconds of CPU time for one Kalman filter run using the hour's worth of real navigation data.
- iii) **Navigation System Augmentation** — Eventually, other navigation transducers available to the Convair will be included in an augmented version of the navigation filter described in this report. The next navigation aid to be included will probably be the Litton LTN-51 inertial navigation system — two different approaches could be used to integrate the LTN-51 information into an expanded model. The simpler approach would involve treating the inertial navigator as a 'black box' and using its position and velocity outputs as additional measurements — the Kalman filter plant would stay the same as before (i.e. the Doppler heading update equations). A more complex approach to the problem would have the inertial system as the basic plant model; Doppler, heading, and VLF would then be redundant measurement quantities. This approach would imply having access to the basic inertial quantities of the LTN-51 system (i.e. linear accelerations and angular rates of change). A simulation study comparing the two approaches would help to determine which is the more effective direction to take in using the Litton data.

7.0 ACKNOWLEDGEMENTS

The author would like to thank two NRC summer students, Craig Maskell and Matthew Choptuik, for their dedication and hard work on this project. Craig was responsible for programming the various simulation routines used in the study, while Matthew was responsible for running the experiments comprising the comparison study of Chapter 5 and for creating the various comparison plots. Special thanks are also due to Doug Hardwick for supervising the collection of Convair navigation data.

8.0 REFERENCES

1. Hardwick, C.D. *Proposed Research Capabilities of the NAE Convair 580*. DME/NAE Quarterly Bulletin No. 1976/11, National Research Council Canada, January 1977.
2. Hardwick, C.D. *The NAE Convair 580 Research Aircraft — An Update for Potential Users*. NAE Laboratory Technical Report LTR-ER 64, National Research Council Canada, May 1978.

3. Anderson, B.D.O.
Moore, J.B. *Optimal Filtering.*
Prentice-Hall, Englewood Cliffs, New Jersey, 1979.
4. Barham, P.M.
Humphries, D.E. *Derivation of the Kalman Filtering Equations from Elementary Statistical Principles.*
RAE Technical Report TR69095, May 1969.
5. Barham, P.M.
Manville, P. *Application of Kalman Filtering to Baro/Inertial Height Systems.*
RAE Technical Report TR69131, June 1969.
6. Miller, I.
Freund, J.E. *Probability and Statistics for Engineers.*
Prentice-Hall, Englewood Cliffs, New Jersey, 1965.
7. Friedland, B.
Bernstein, I. *Estimation of the State of a Nonlinear Process in the Presence of Nongaussian Noise and Disturbances.*
J. Franklin Inst., Vol. 281, July 1966, pp. 455-480.
8. Richman, J.
Friedland, B. *Design of Optimum Mixer-Filter for Aircraft Navigation Systems.*
Proc. 19th Annual Nat. Aero. Elect. Conference, Dayton, Ohio, May 1967.
9. Bellantoni, J.F.
Dodge, K.W. *A Square Root Formulation of the Kalman-Schmidt Filter*
AIAA Journal, Vol. 5, No. 7, July 1967, pp. 1309-1314.
10. Kaminski, P.G.
Bryson, A.E., Jr.
Schmidt, S.F. *Discrete Square Root Filtering, A Survey of Current Techniques*
IEEE Trans. Auto. Control, Vol. AC-16, No. 6, December 1971, pp. 727-736.
11. Morf, M.
Kailath, T. *Square-Root Algorithms for Least-Squares Estimation*
IEEE Trans. Auto. Control, Vol. AC-20, No. 4, August 1975, pp. 487-497.
12. Bierman, G.J. *Measurement Updating Using the U-D Factorization*
Proc. IEEE Conference on Decision and Control, Houston, Texas, 1975, pp. 337-346.
13. Thornton, C.L.
Bierman, G.J. *Gram-Schmidt Algorithms for Covariance Propagation.*
Proc. IEEE Conference on Decision and Control, Houston, Texas, 1975, pp. 489-498.
14. Bierman, G.J. *Factorization Methods for Discrete Sequential Estimation*
Academic Press, New York, New York, 1977.
15. Hardwick, C.D.
Brownley, T.R. *An Evaluation of Aircraft Navigation Using VLF Communication Stations with the Global Navigation Inc. GNS-200 VLF Navigation System in the North Star Aircraft.*
NAE, Laboratory Technical Report LTR-FR-38, National Research Council Canada, February 1973.
16. Hardwick, C.D. *VLF Navigation Development at NAE*
DME/NAE Quarterly Bulletin No. 1973(1) National Research Council Canada, April 1973.
17. Lindorff, D.P. *Theory of Sampled-Data Control Systems*
John Wiley & Sons, New York, New York, 1965.

18. Sodano, E.M. *A Rigorous Non-Iterative Procedure for Rapid Inverse Solution of Very Long Geodesics.*
Bulletin Géodésique, Issues 47/48, 1958, pp. 13-25.
19. Sodano, E.M. *General Non-Iterative Solution of the Inverse and Direct Geodetic Problems.*
Bulletin Géodésique, Issue 75, 1965, pp. 69-89.

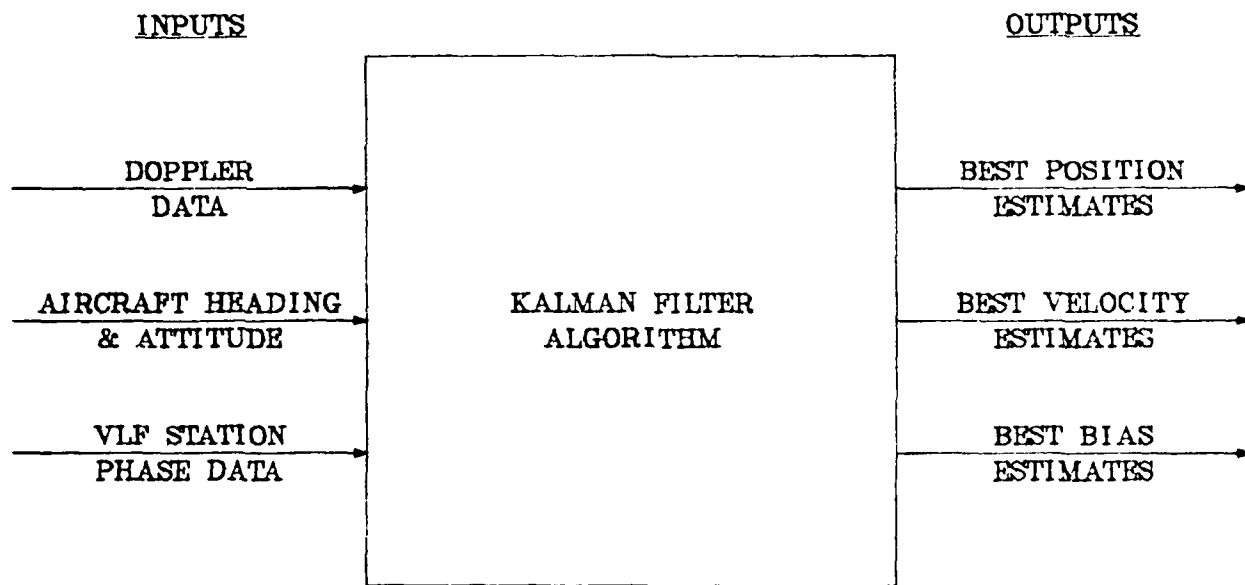


FIG. 1: PROPOSED DOPPLER/VLF NAVIGATOR

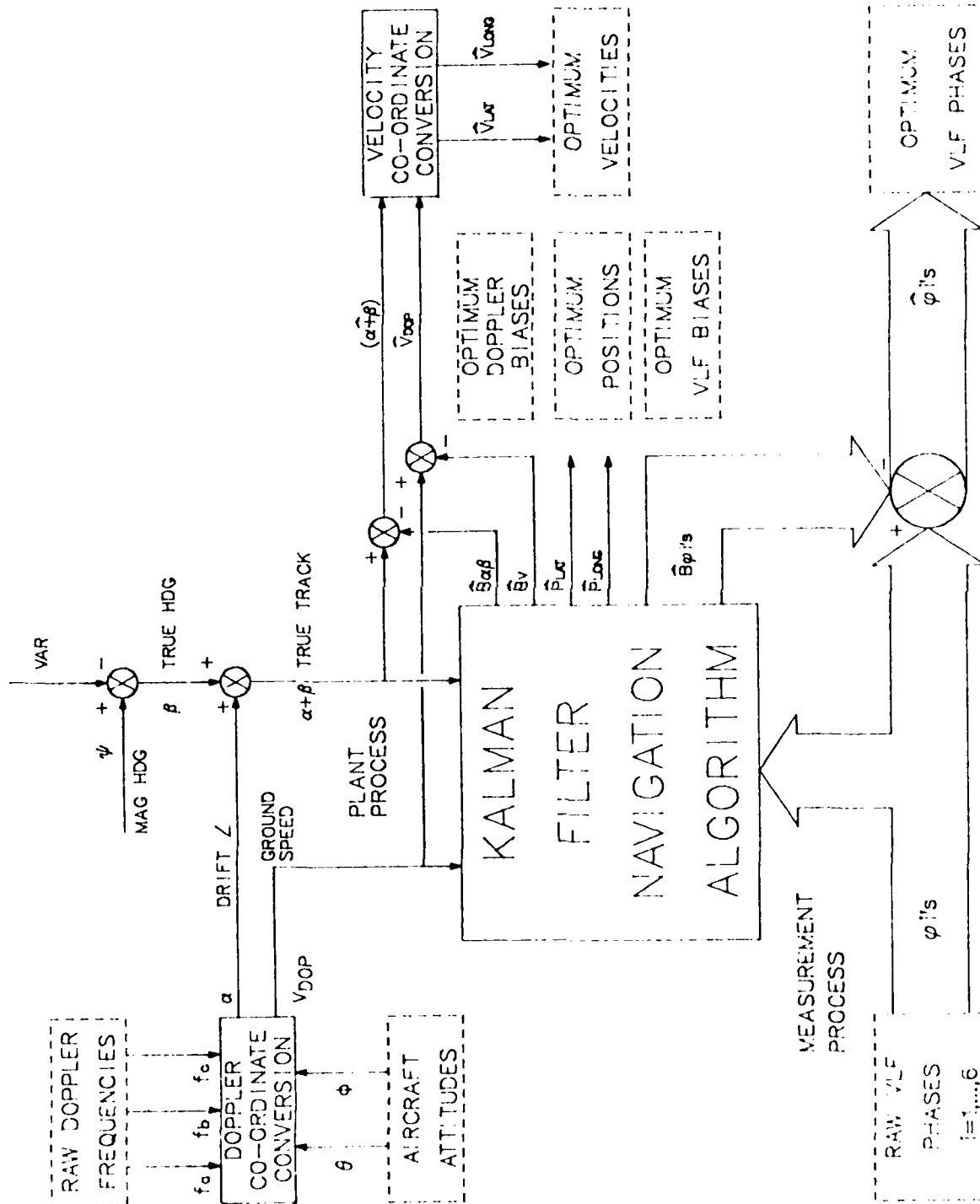


FIG. 2: DETAILED DOPPLER/VLF KALMAN FILTER NAVIGATION SCHEME

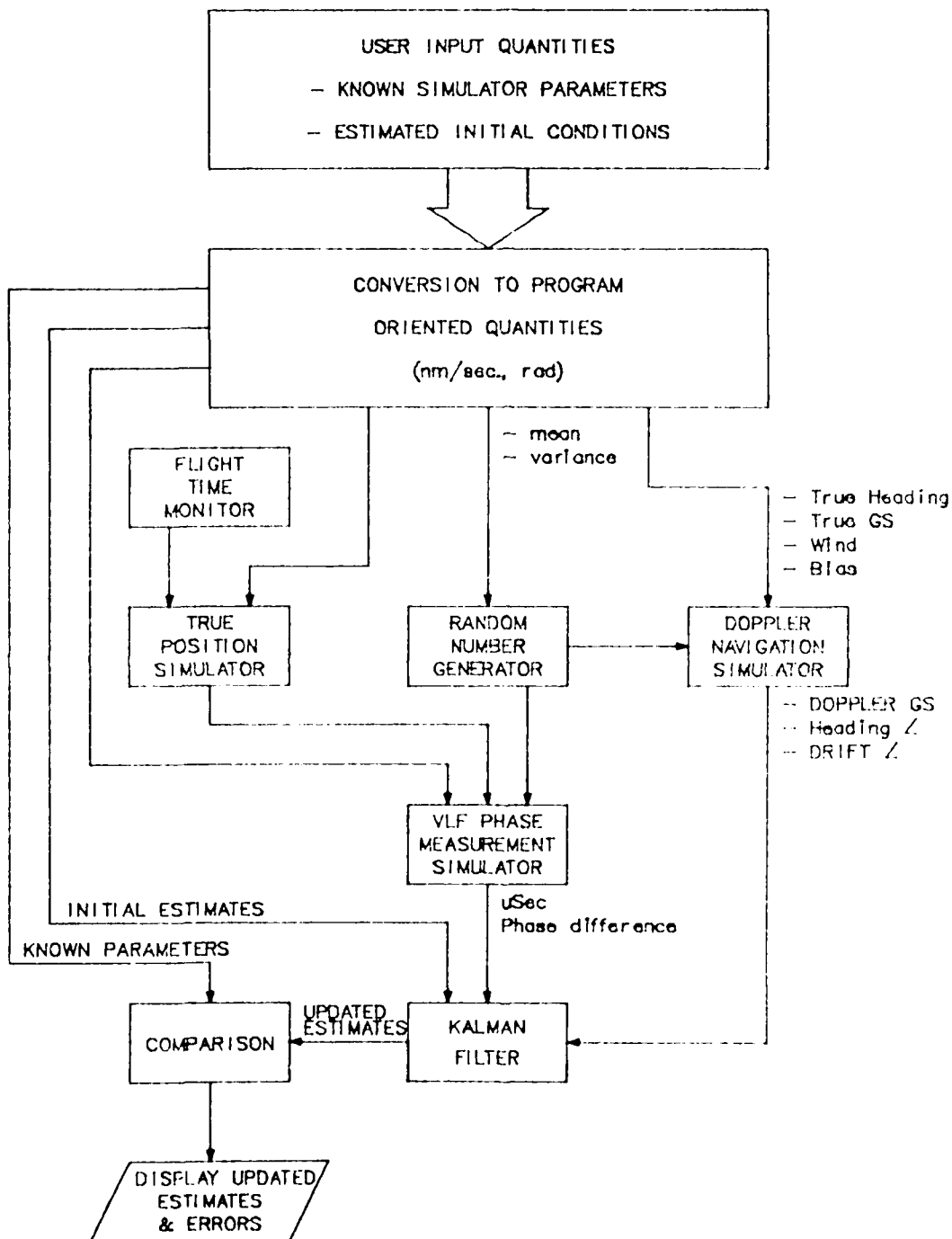


FIG. 3: BLOCK DIAGRAM OF KALMAN NAVIGATION FILTER SIMULATOR

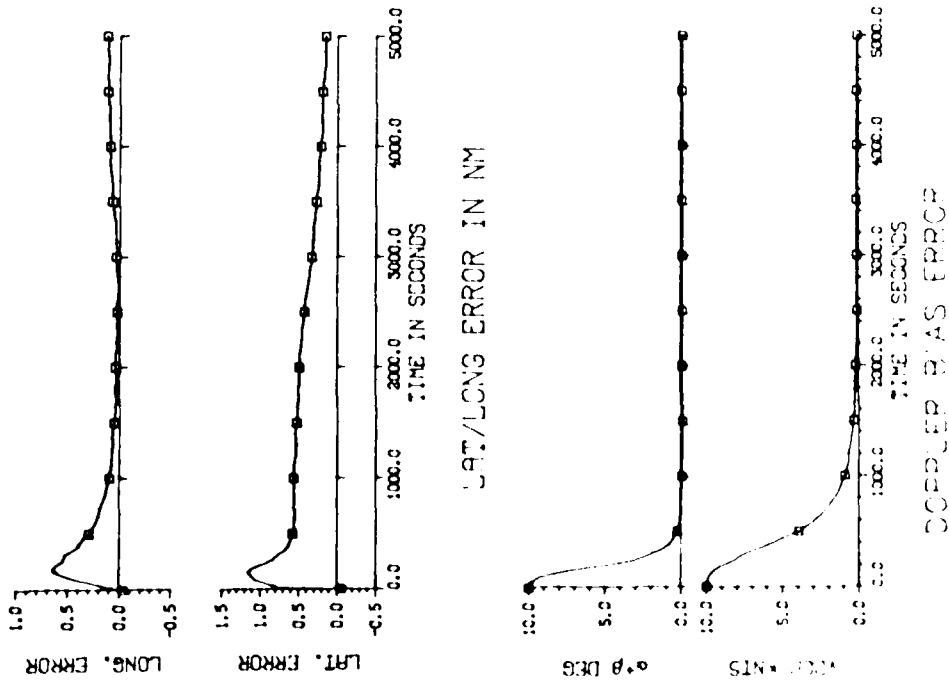
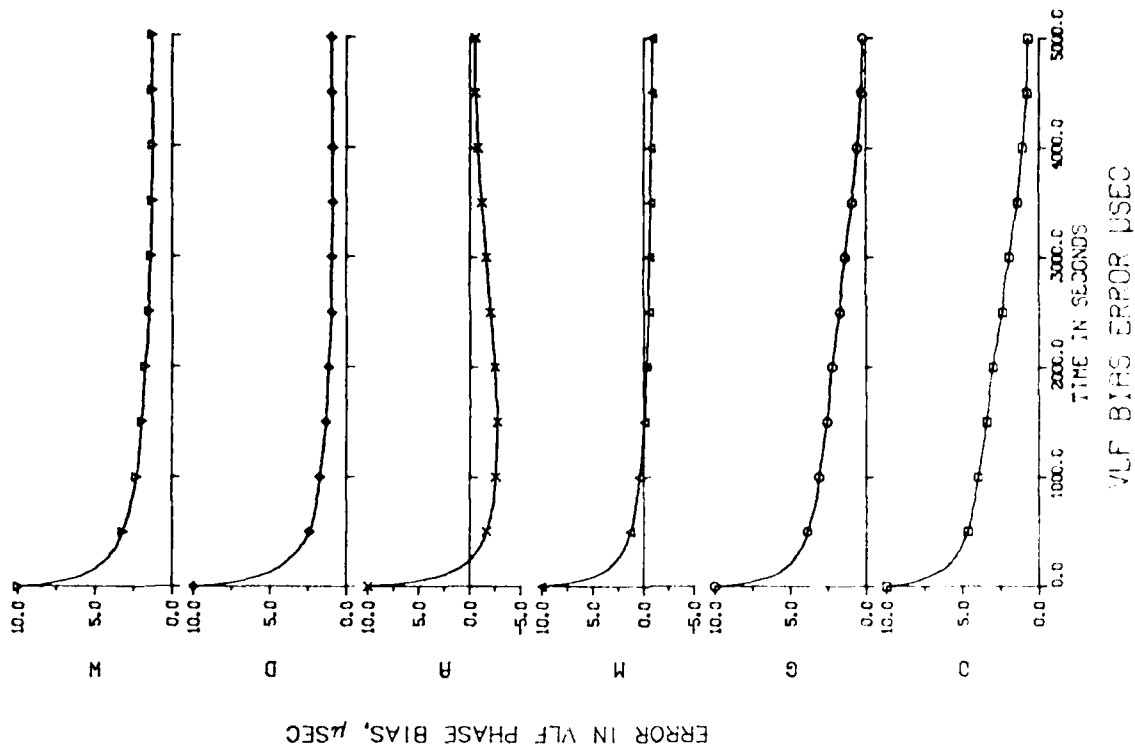
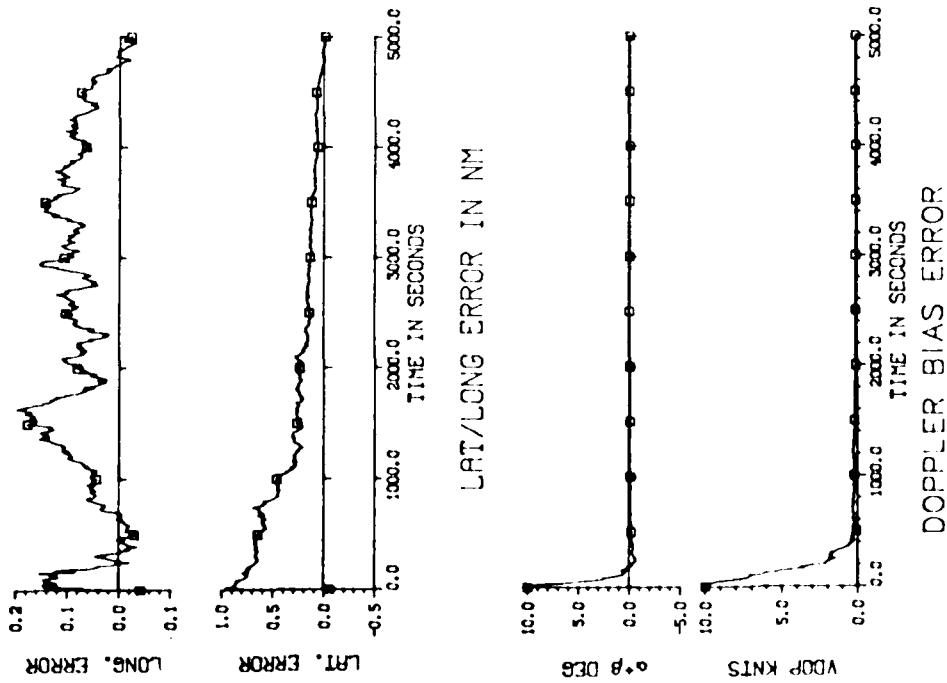
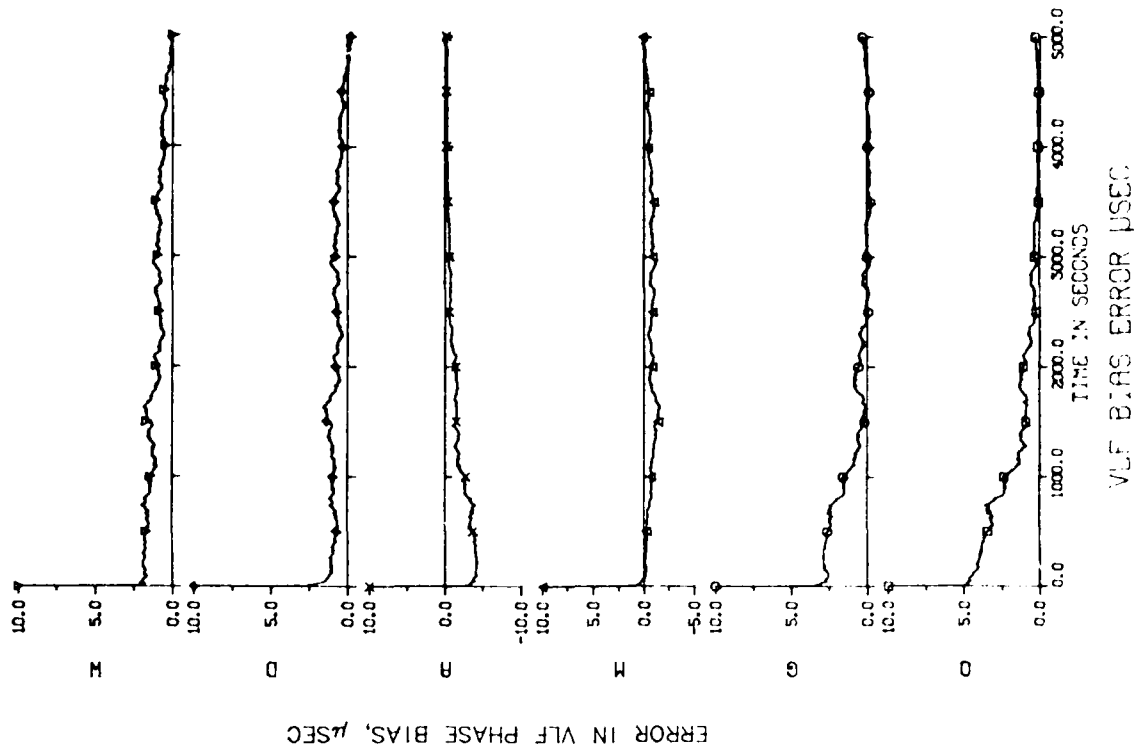
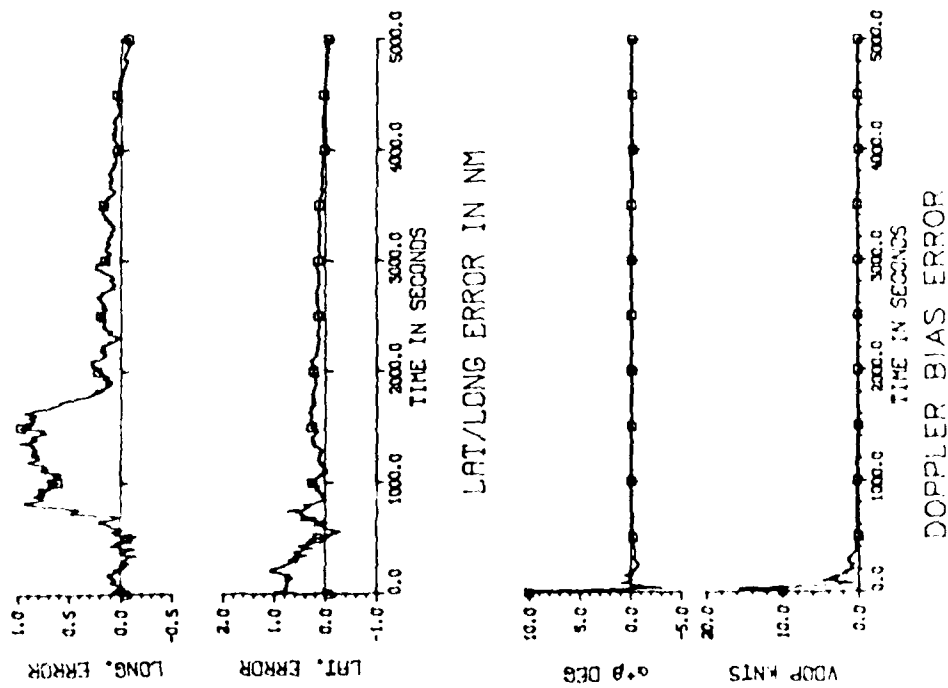
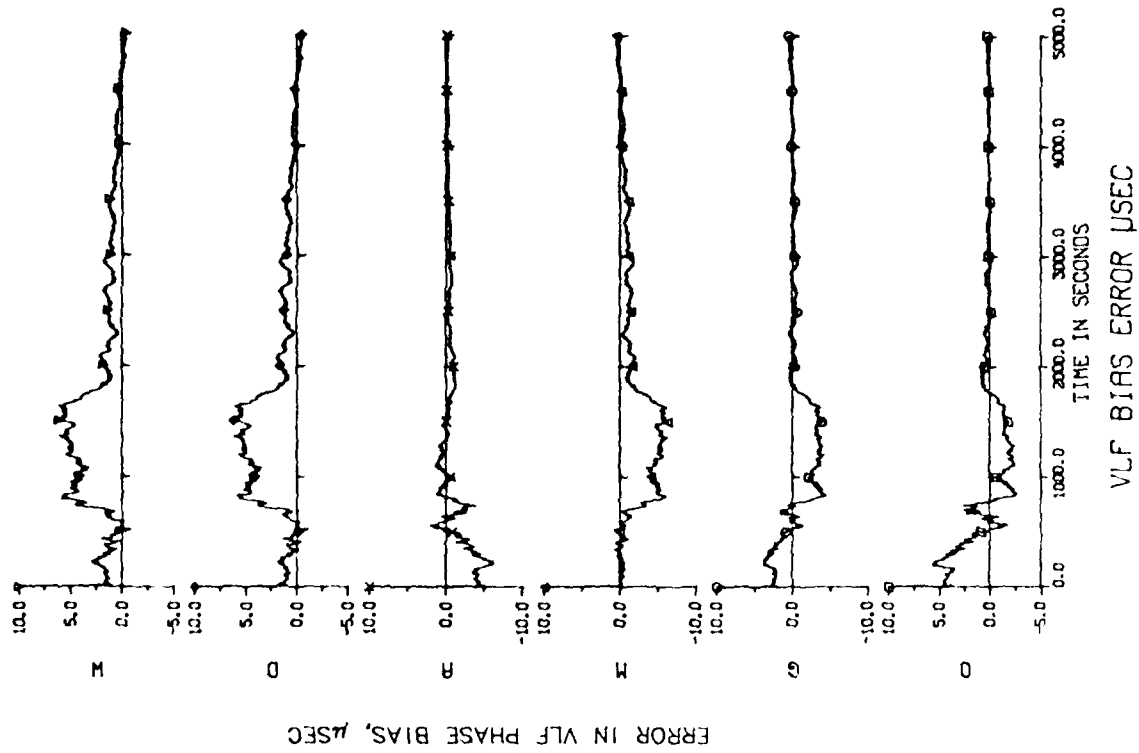


FIG. 5 KALMAN FILTER OUTPUT ERRORS FOR SMALL INITIAL ERROR VARIANCES



PLOTOUT. 2 JUL 03 1990 17:15:11

FIG. 6. KALMAN FILTER OUTPUT ERRORS FOR MEDIUM INITIAL ERROR VARIANCES



PLOTOUT. 3 JUL 03 1980 17:21:28

FIG. 7: KALMAN FILTER OUTPUT ERRORS FOR LARGE INITIAL ERROR VARIANCES

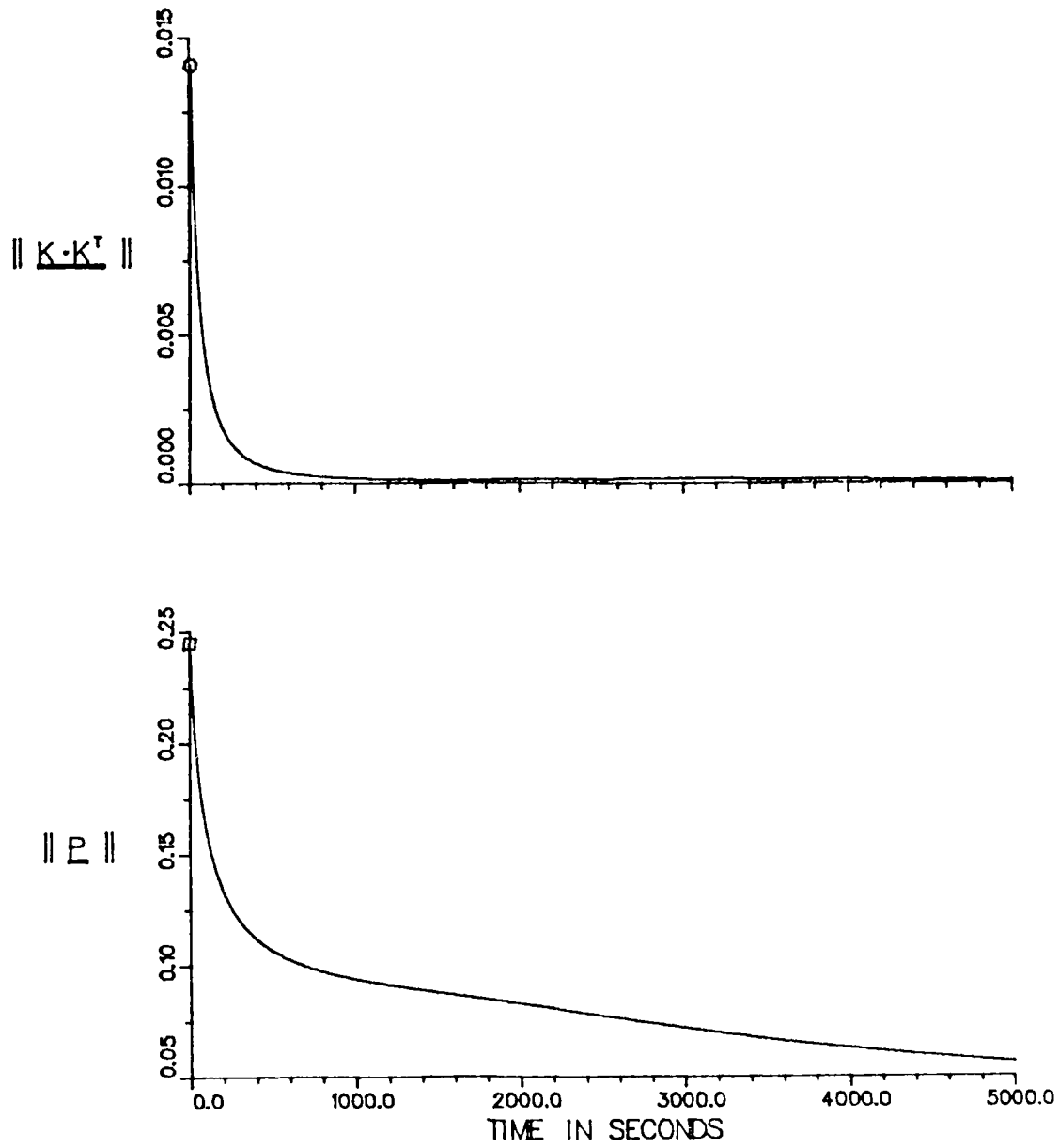


FIG. 8: STABILIZATION OF P AND K MATRICES WITH TIME FOR SMALL P_0

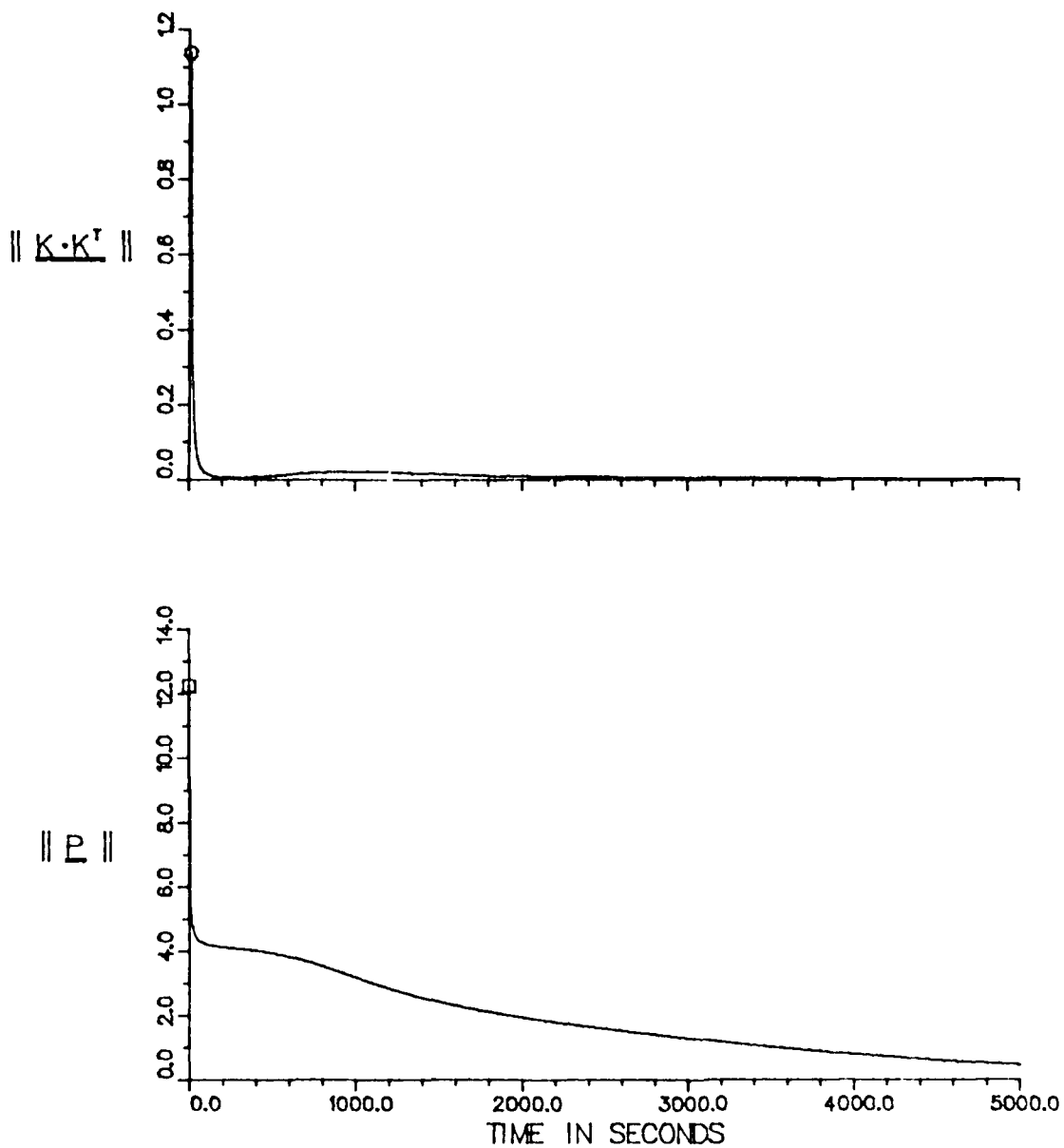


FIG. 9: STABILIZATION OF P AND K MATRICES WITH TIME FOR MEDIUM P_0 .

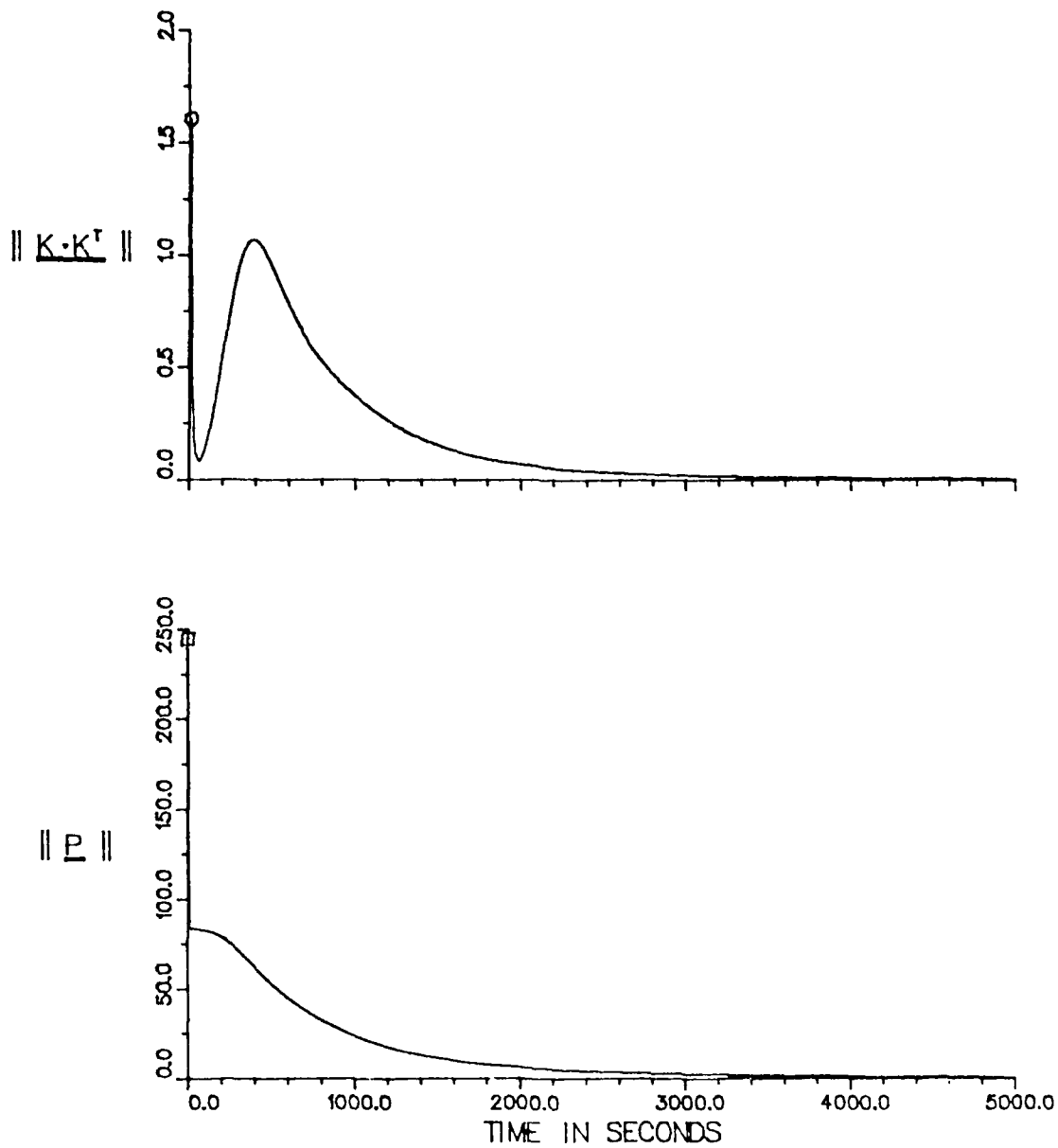
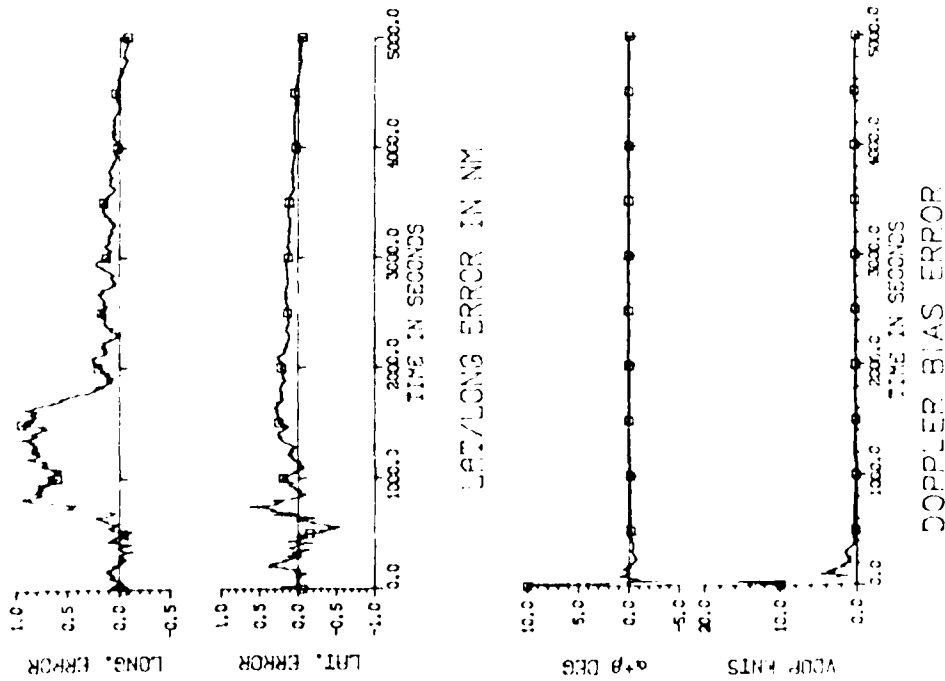
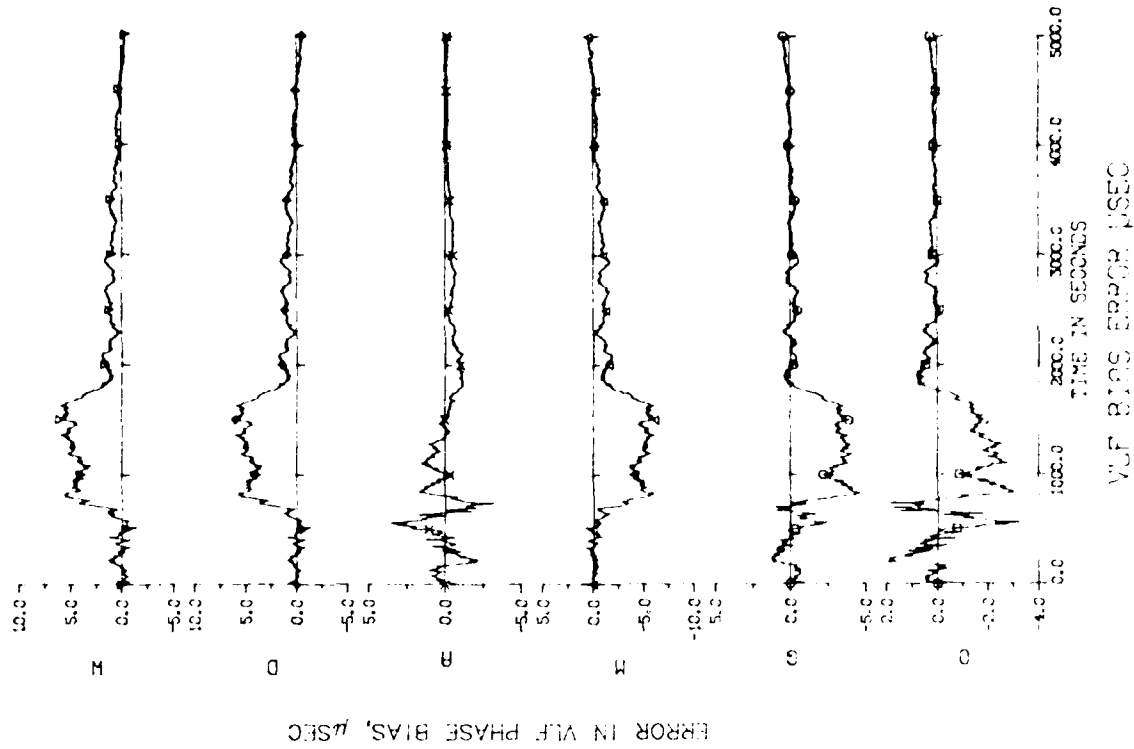
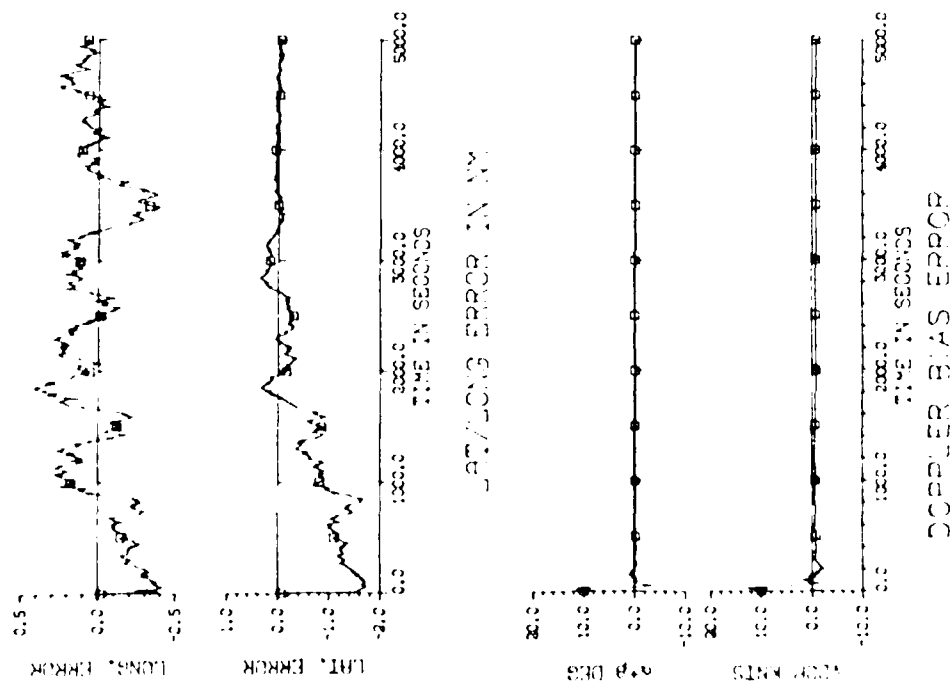
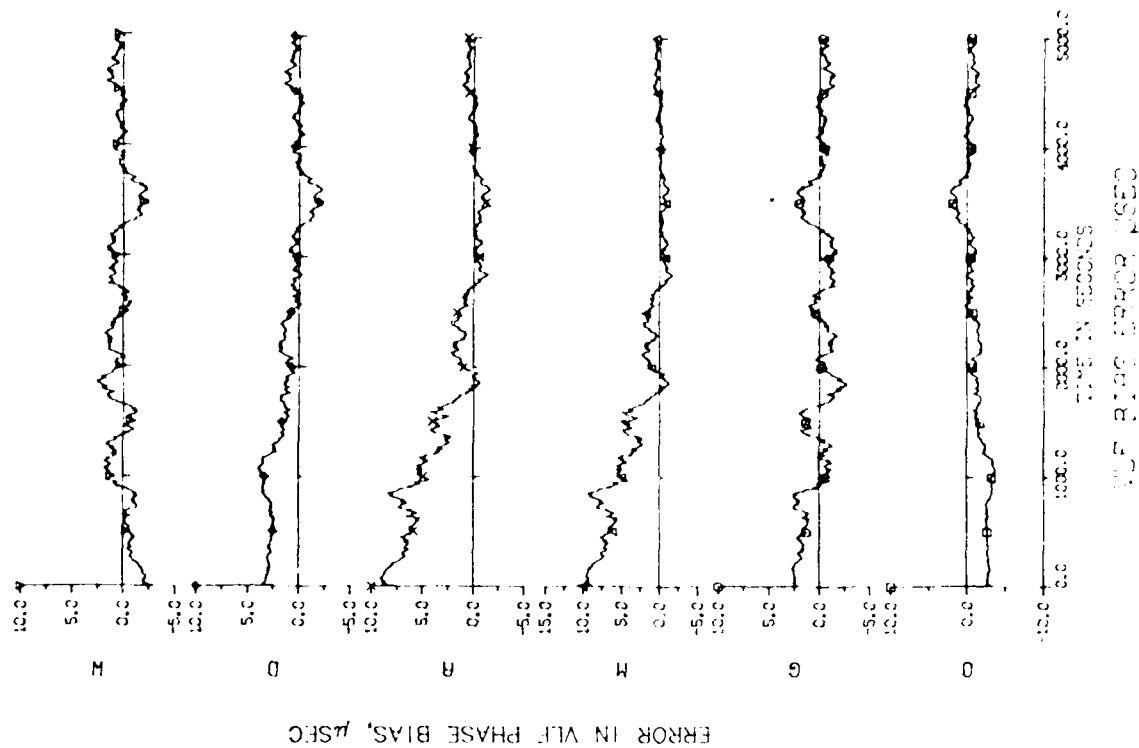


FIG. 10: STABILIZATION OF P AND K MATRICES WITH TIME FOR LARGE \underline{P}_0 .



PLCOUT. 6 JUL 67 1960 09:10:59

FIG. 11: KALMAN FILTER OUTPUT ERRORS FOR LARGE INITIAL BIAS ERROR VARIANCES -
NO VLF BIASES SIMULATED IN DATA



PL01007.4 JUL 04 1990 11:34:04

FIG. 12: KALMAN FILTER OUTPUT ERRORS FOR LARGE INITIAL BIAS ERROR VARIANCES -
DAVIS STRAIT LOCATION

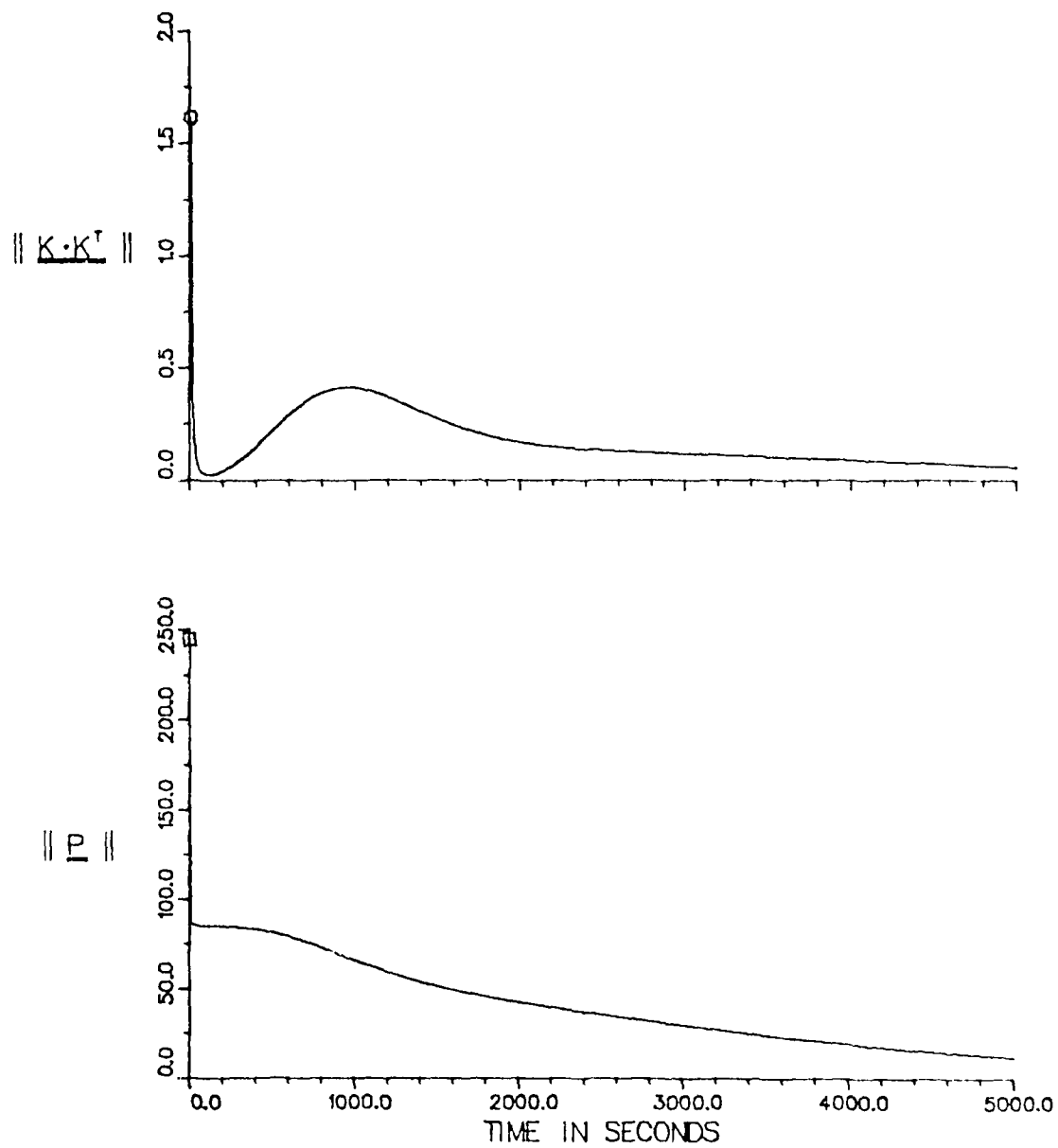


FIG. 13: STABILIZATION OF P AND K MATRICES WITH TIME FOR LARGE P_0 AND DAVIS STRAIT LOCATION



FIG. 14: VLF GEOMETRY - PROJECTION CENTRED IN OTTAWA AREA

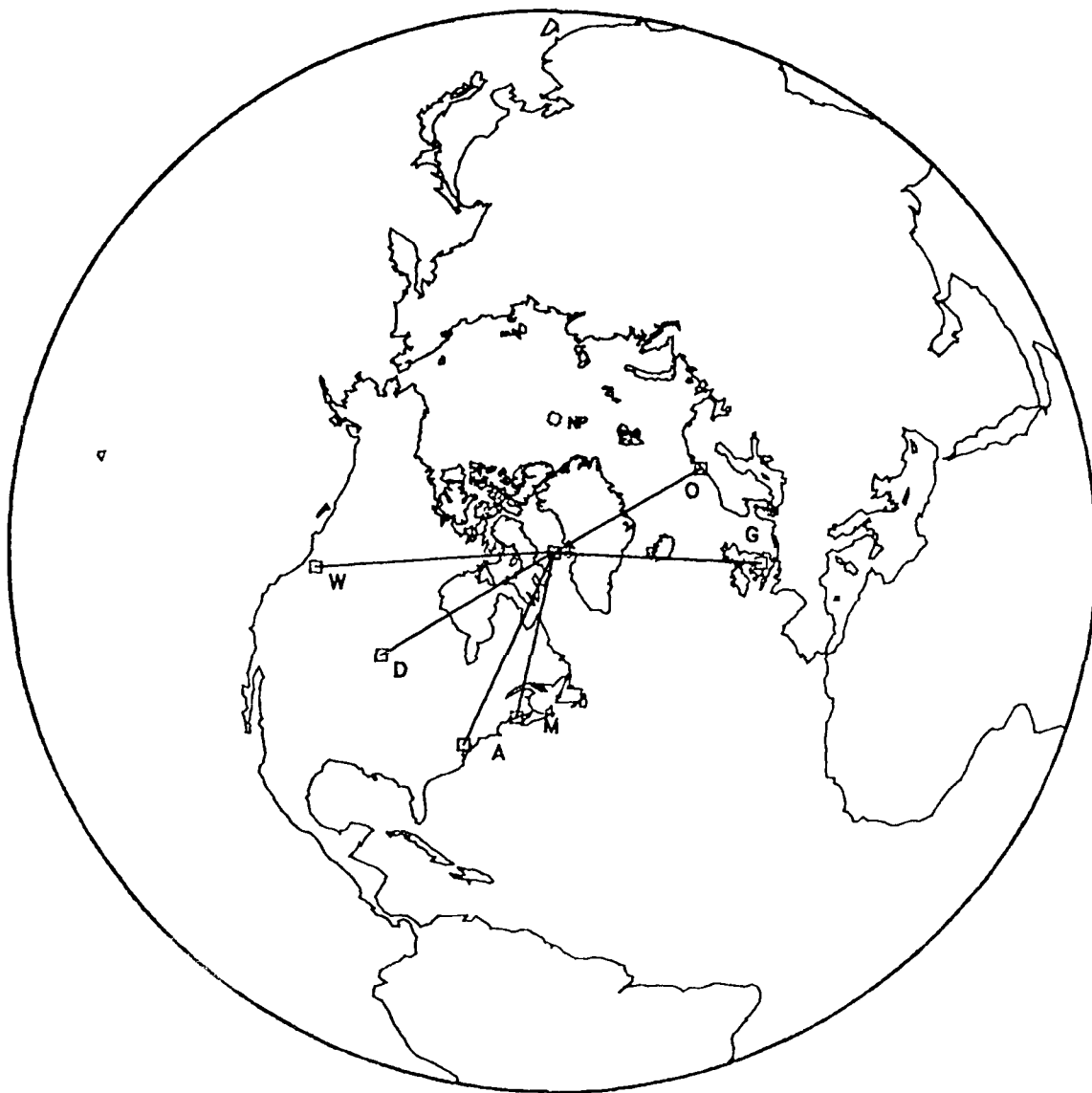


FIG. 15. VLF GEOMETRY - PROJECTION CENTRED IN DAVIS STRAIT AREA

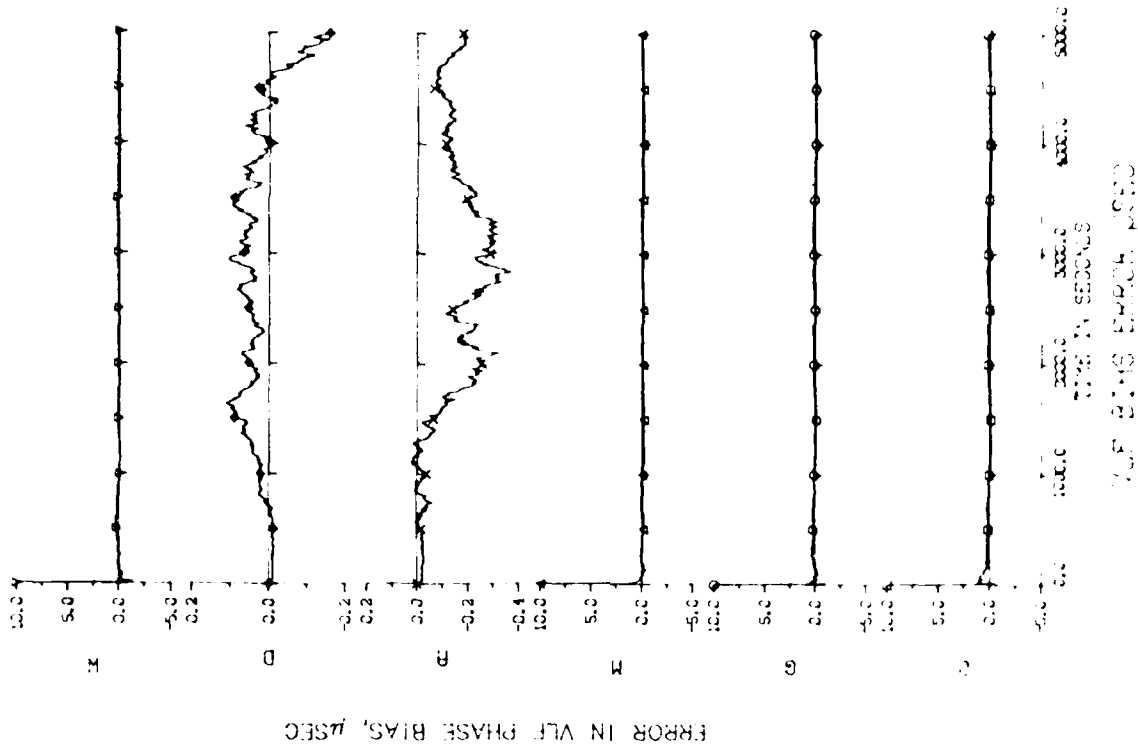
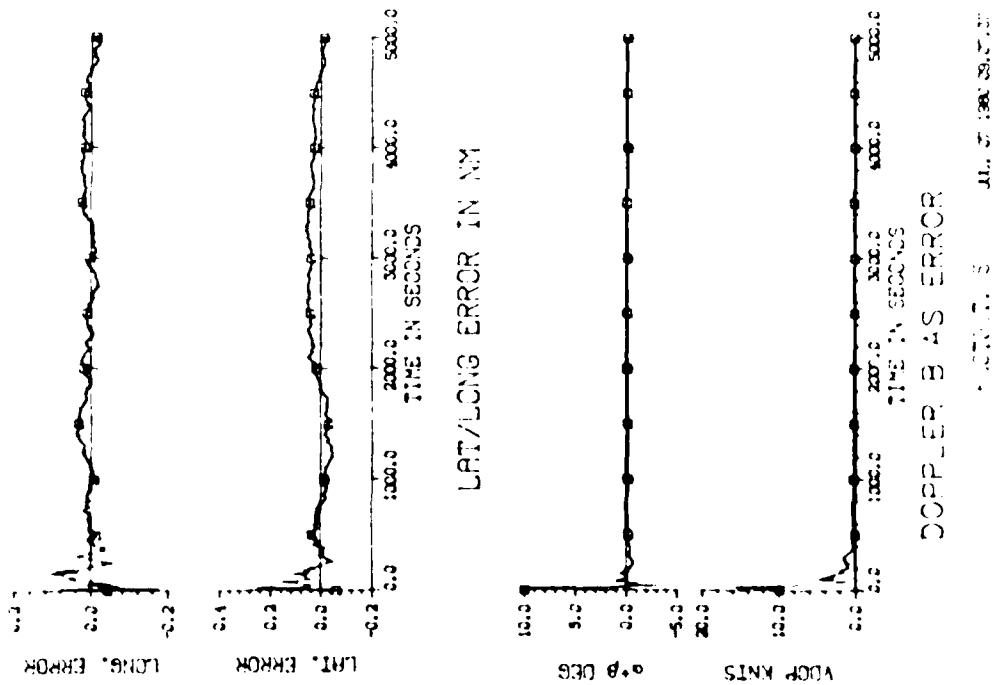


FIG. 16: KALMAN FILTER RUN WITH FOUR OUT OF SIX VLF BIASES
BEING ESTIMATED FROM POOR INITIAL CONDITIONS



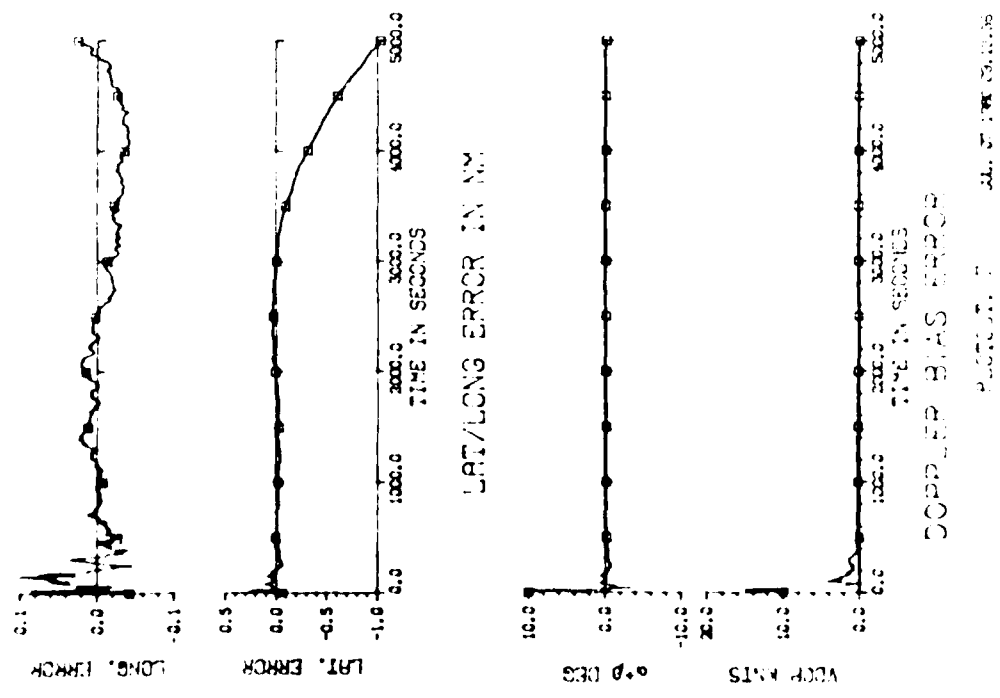
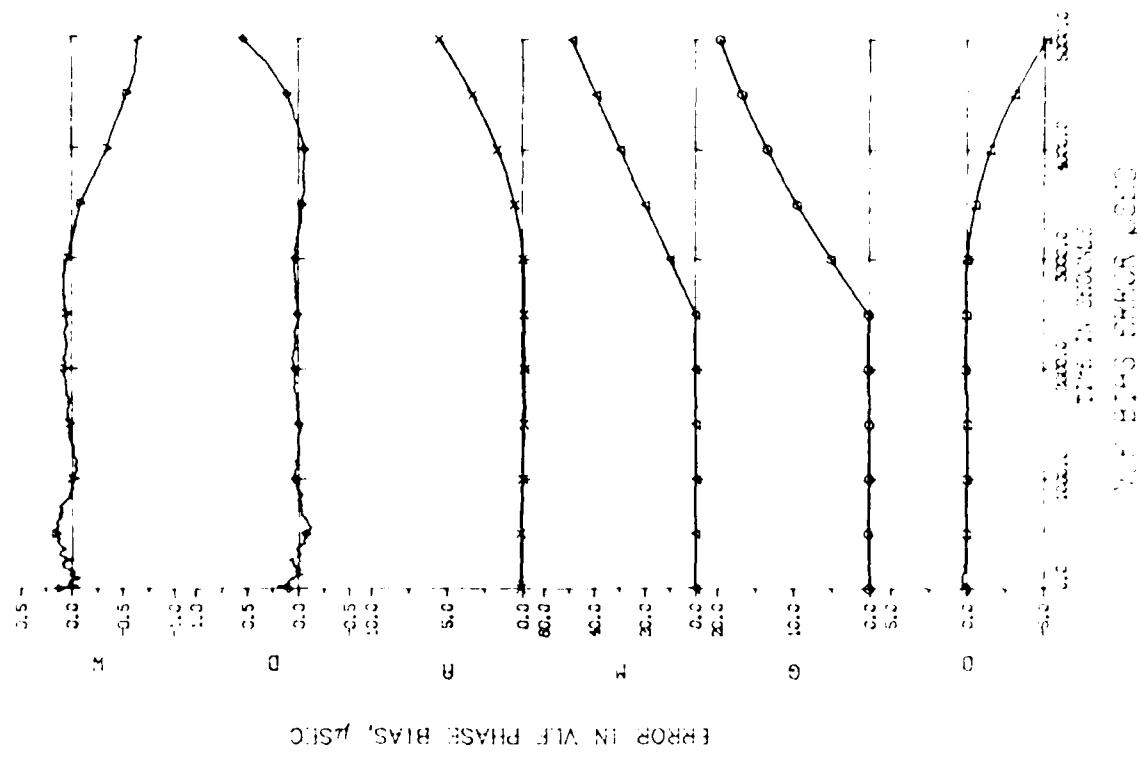


FIG. 17. KALMAN FILTER OUTPUT ERRORS SHOWING EFFECT OF LINEAR DRIFT IN TWO VLF STATIONS

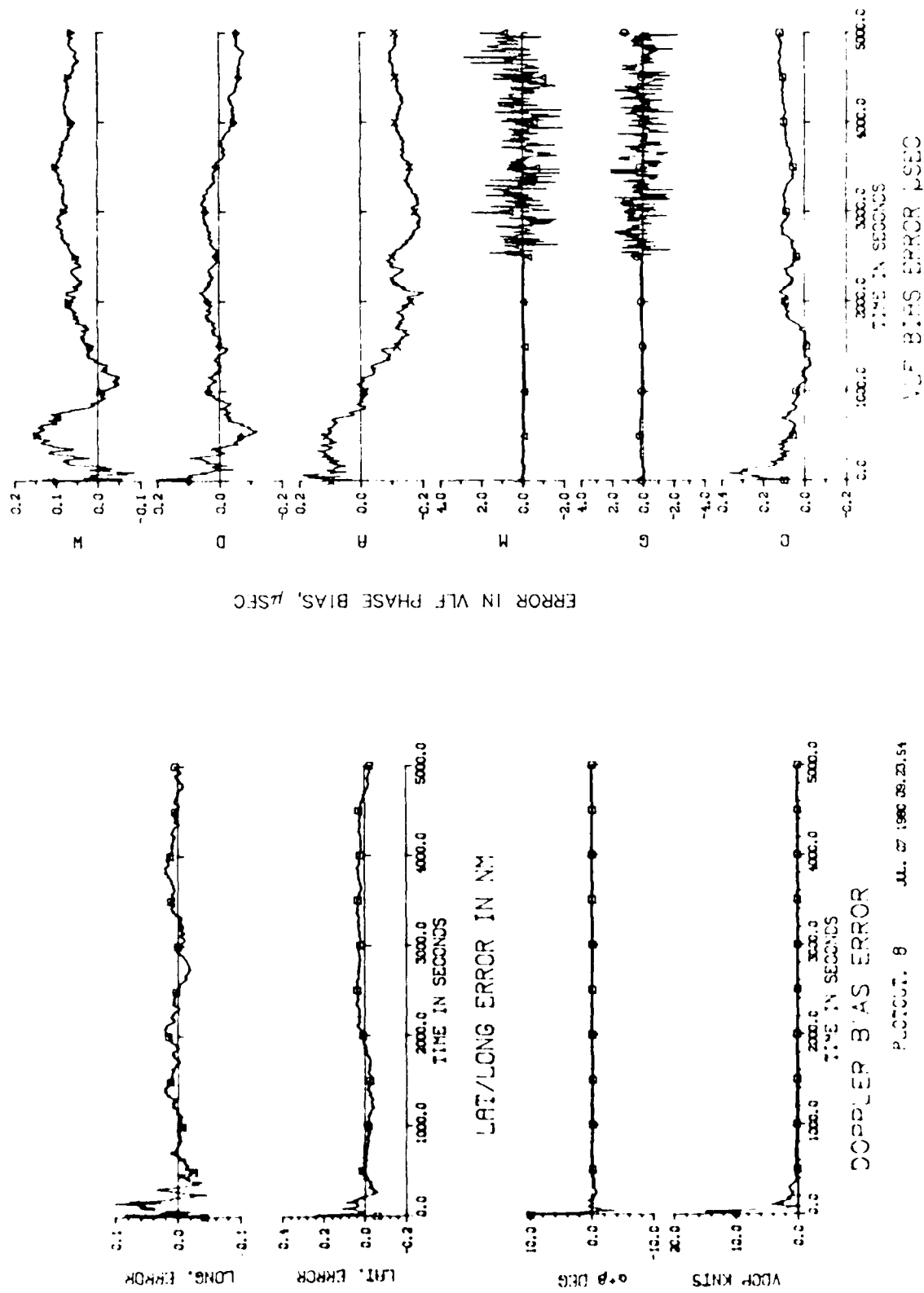


FIG. 18: KALMAN FILTER OUTPUT ERRORS - TWO DRIFTING VLF STATIONS
WITH APPROPRIATE P_0 ELEMENTS FIXED

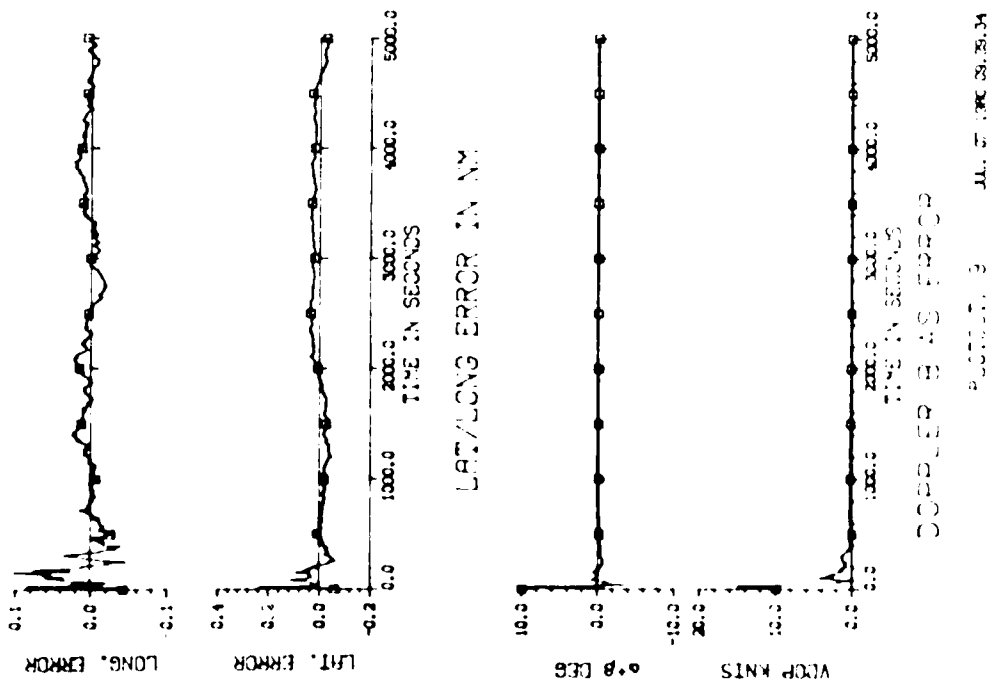
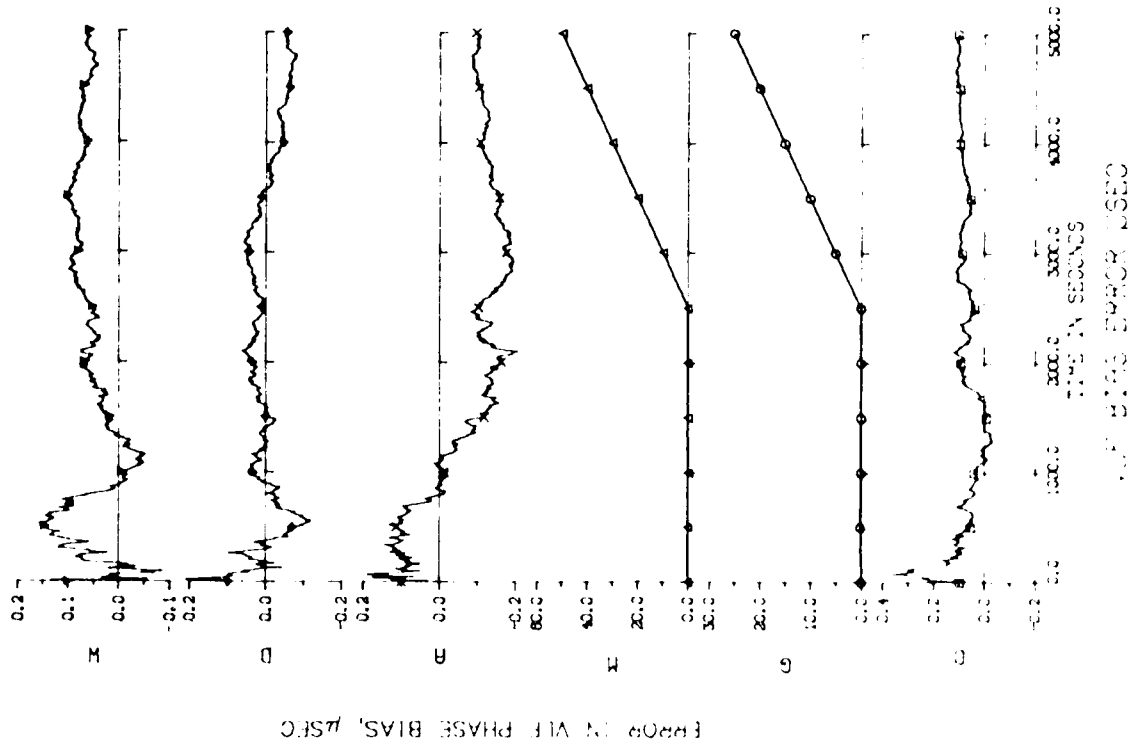


FIG. 19 KALMAN FILTER OUTPUT ERRORS -- TWO DRIFTING VLF STATIONS WEIGHTED OUT

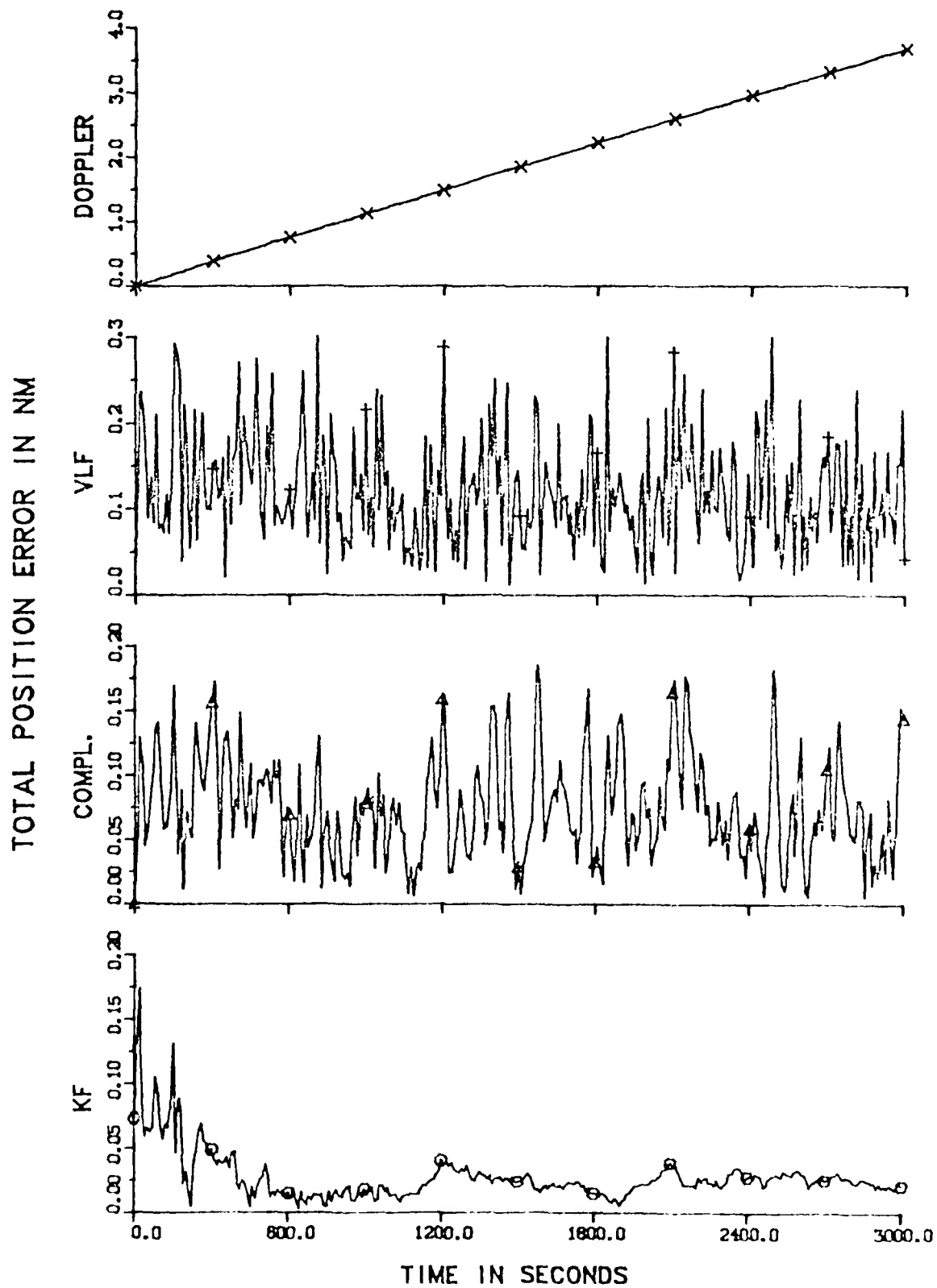


FIG. 20. COMPARISON OF TOTAL POSITION ERRORS USING BEST QUALITY DATA

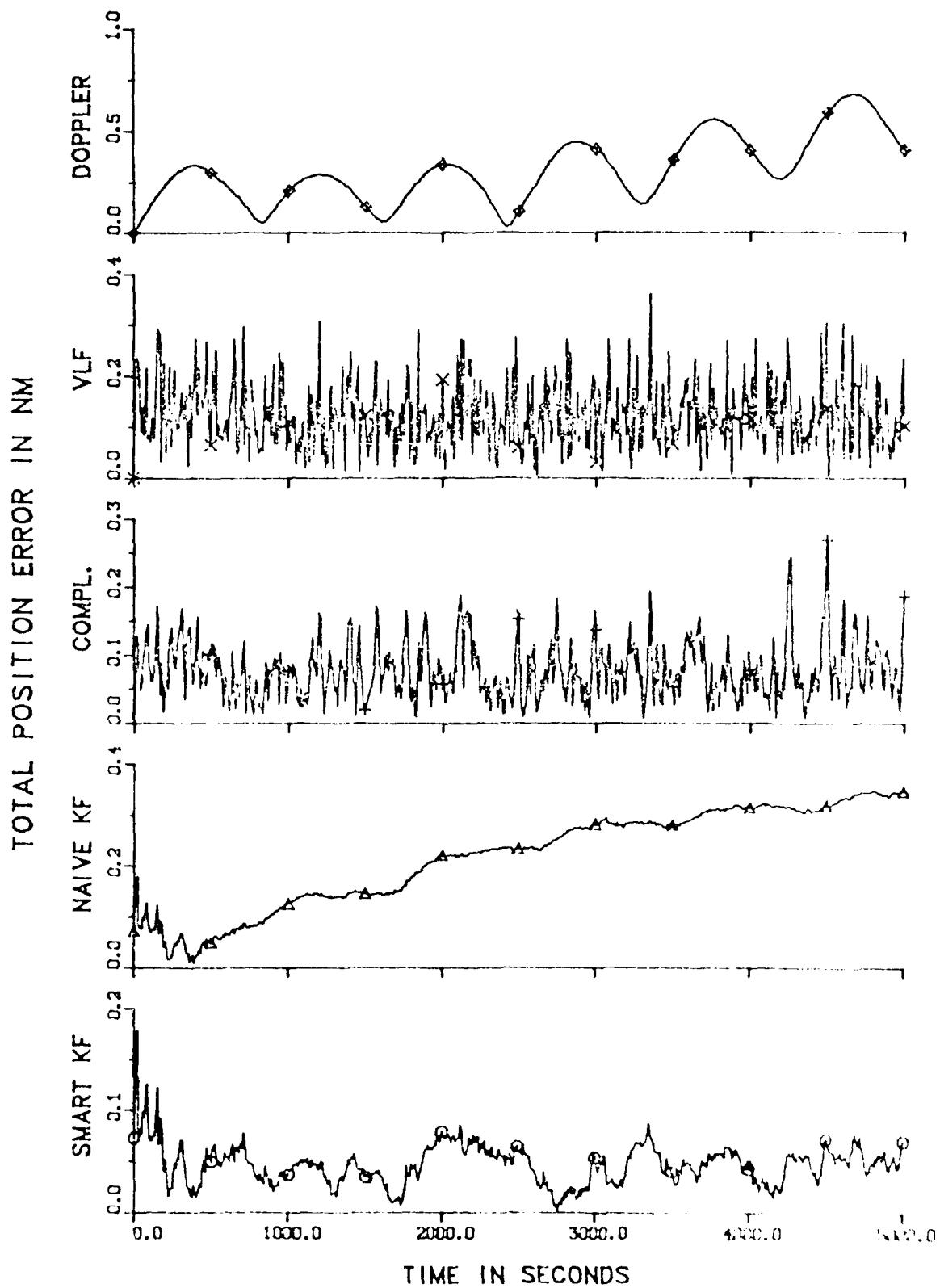


FIG. 21 COMPARISON OF TOTAL POSITION ERRORS USING BEST QUALITY DATA
AND CIRCULAR TRACK

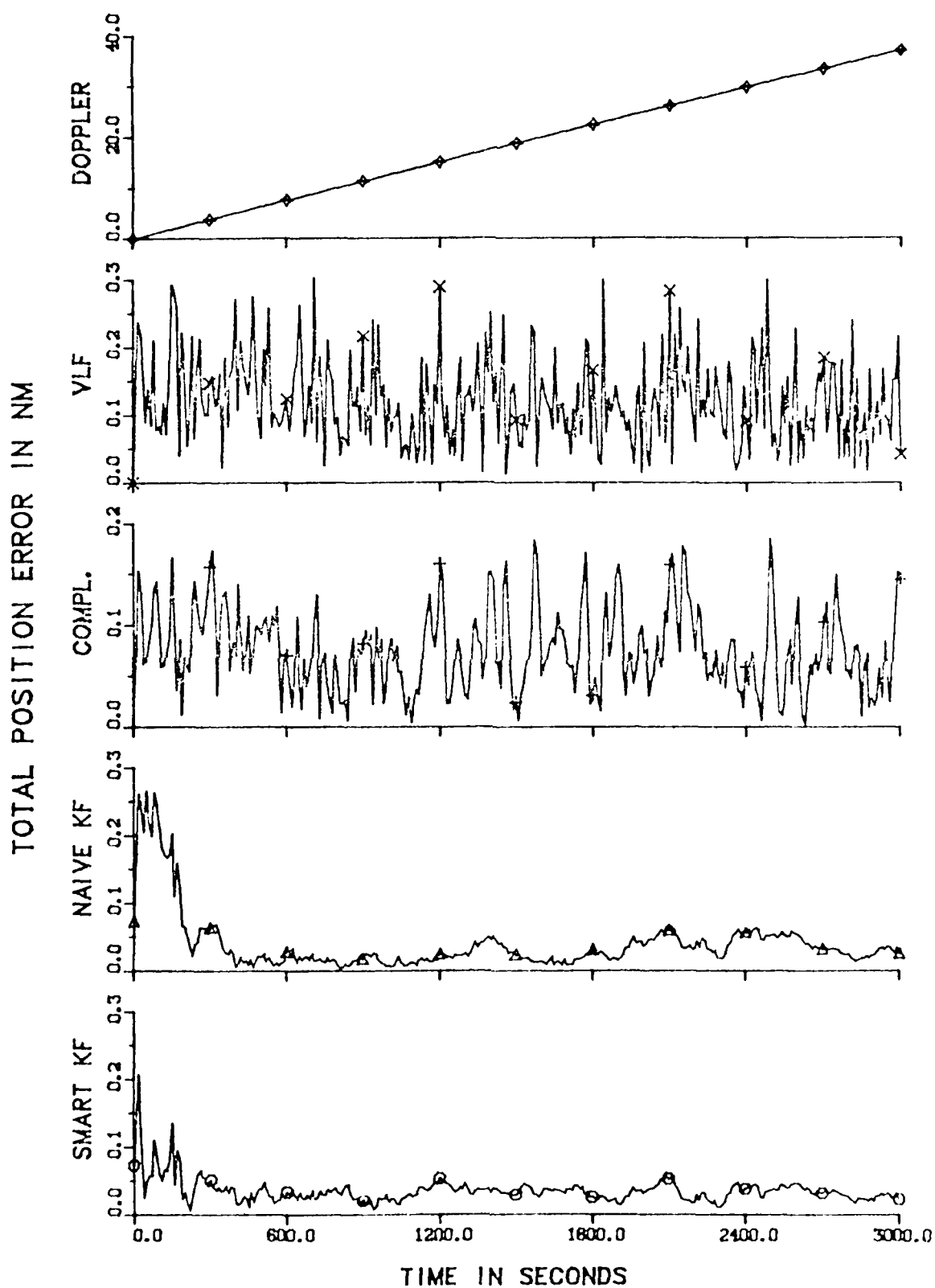


FIG. 22: COMPARISON OF TOTAL POSITION ERRORS USING DATA
WITH LARGE DOPPLER BIASES

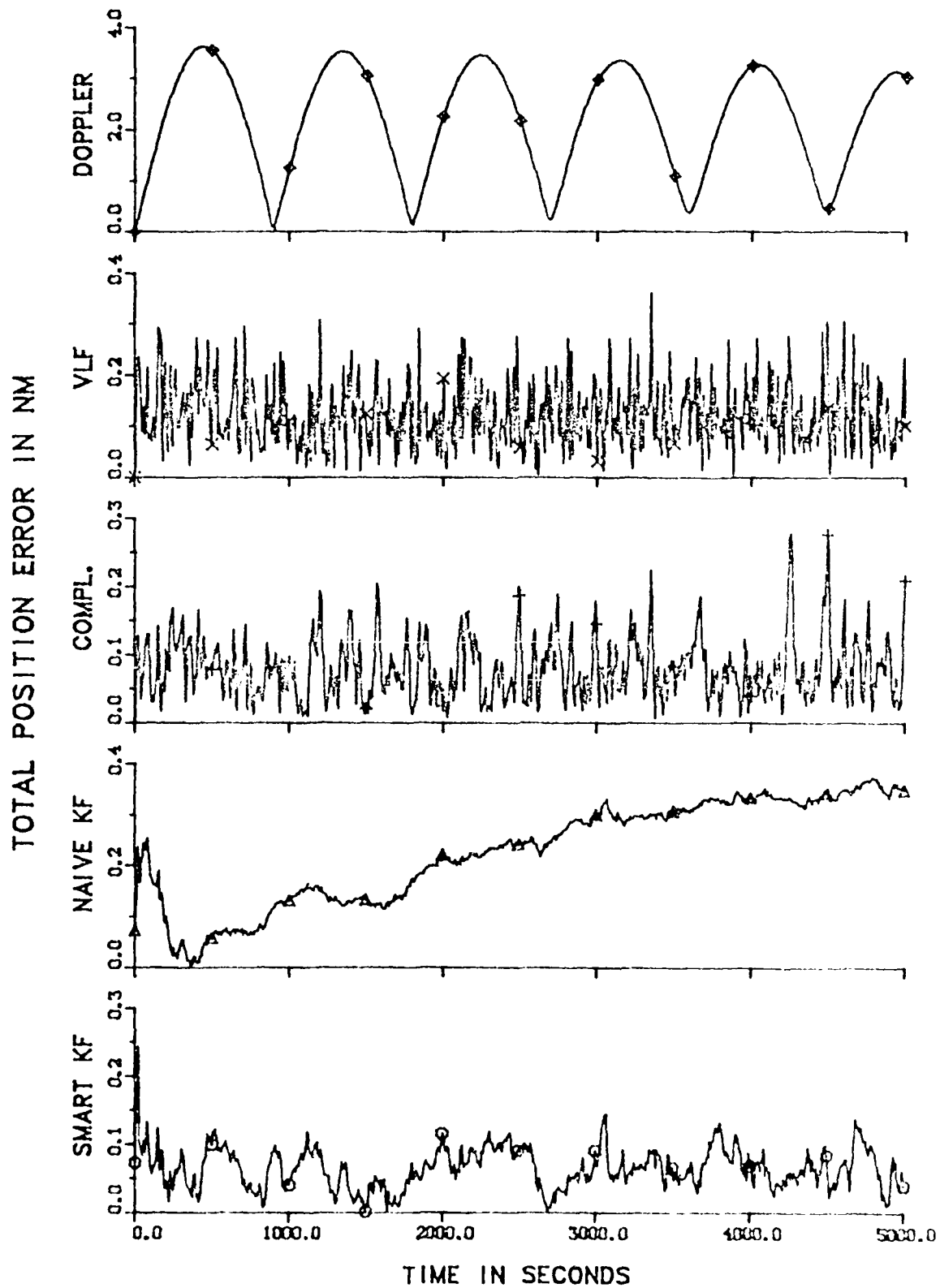
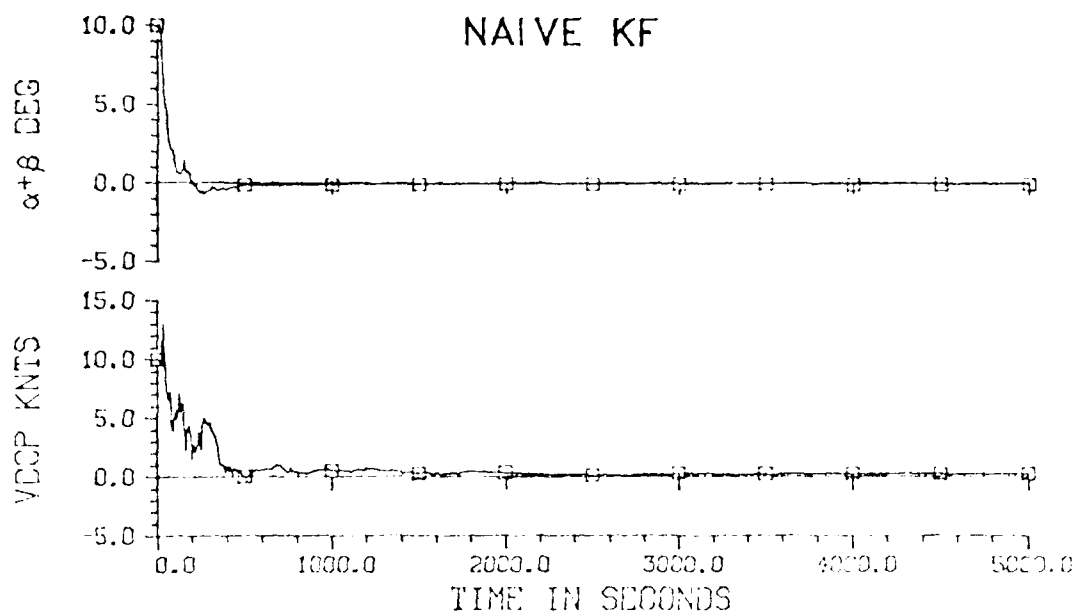


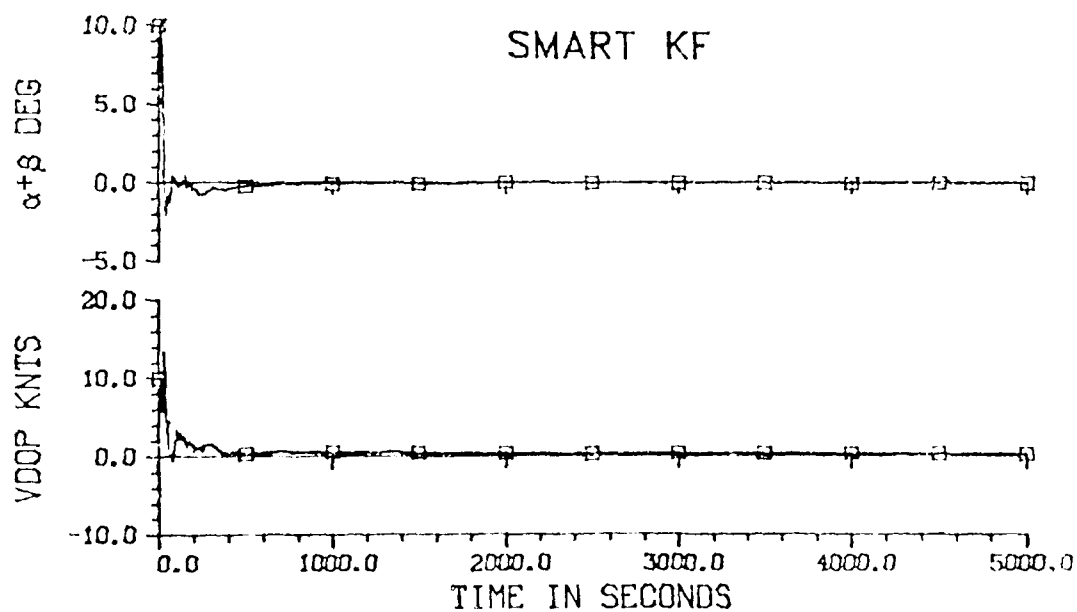
FIG. 23. COMPARISON OF TOTAL POSITION ERRORS USING DATA
WITH LARGE DOPPLER BIASES AND CIRCULAR TRACK



DOPPLER BIAS ERROR

PLOTOUT.73

JUN. 27 1960 09.27.38



DOPPLER BIAS ERROR

PLOTOUT.48

JUN. 18 1960 08.34.58

FIG. 24: DOPPLER BIAS ERROR PLOTS
LARGE DOPPLER/HEADING BIASES SIMULATED

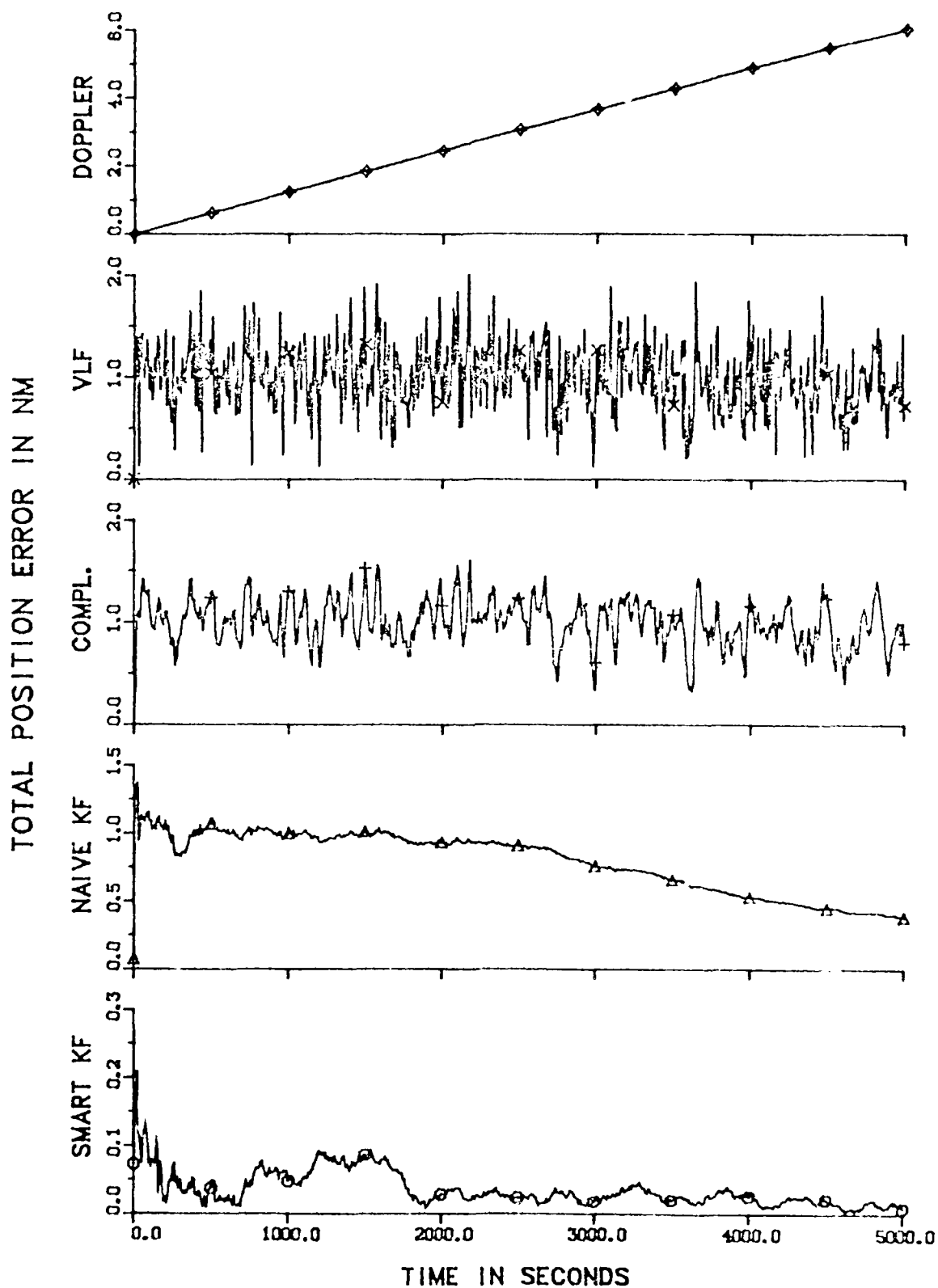


FIG. 25: COMPARISON OF TOTAL POSITION ERRORS USING DATA
WITH LARGE VLF BIASES

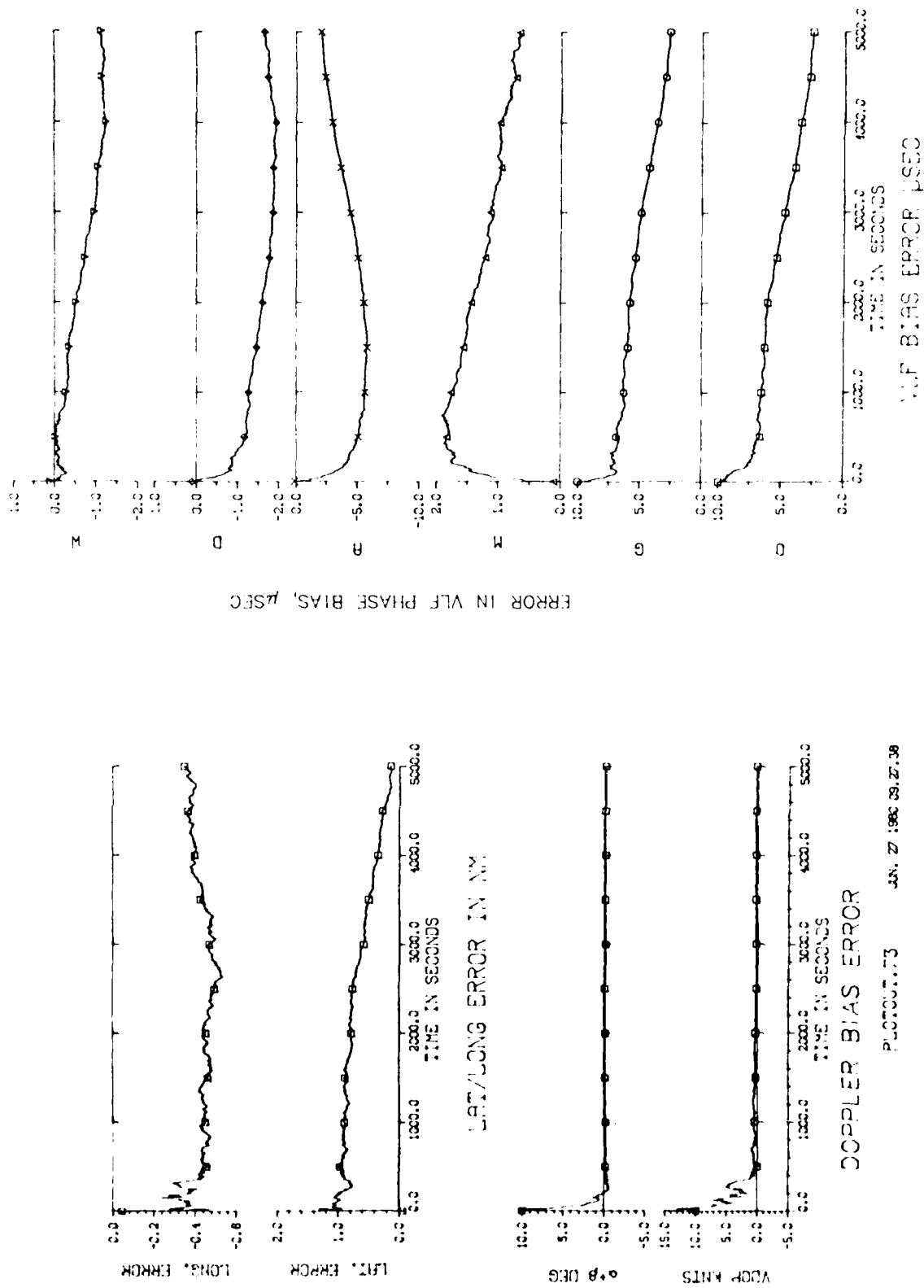


FIG. 26: NAIVE KALMAN FILTER OUTPUT ERRORS FOR LARGE DOPPLER/HEADING BIASES AND LARGE VLF BIASES

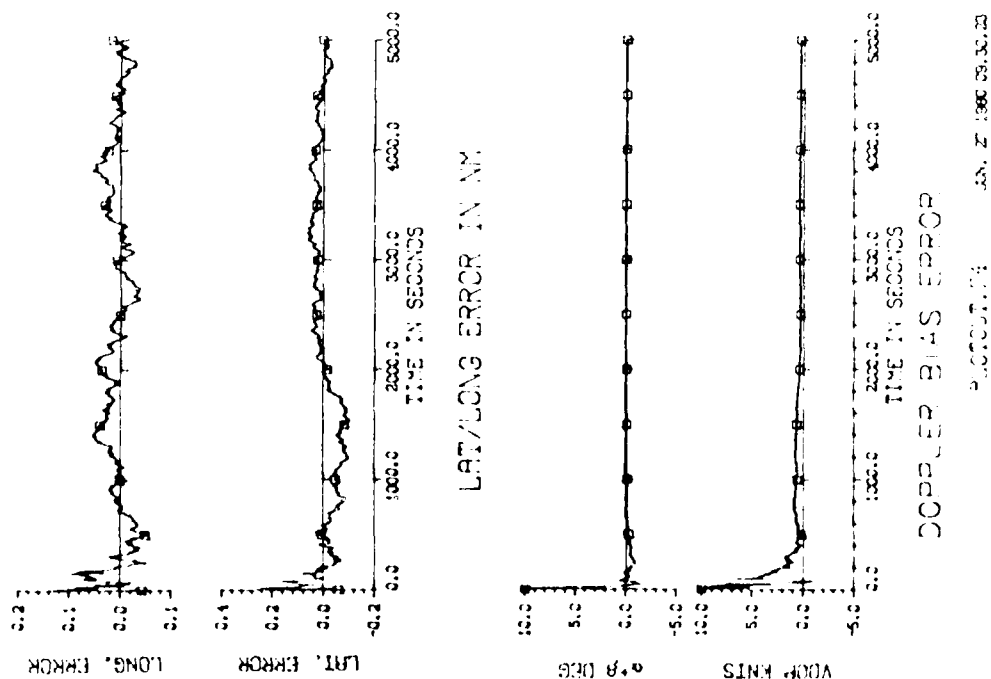
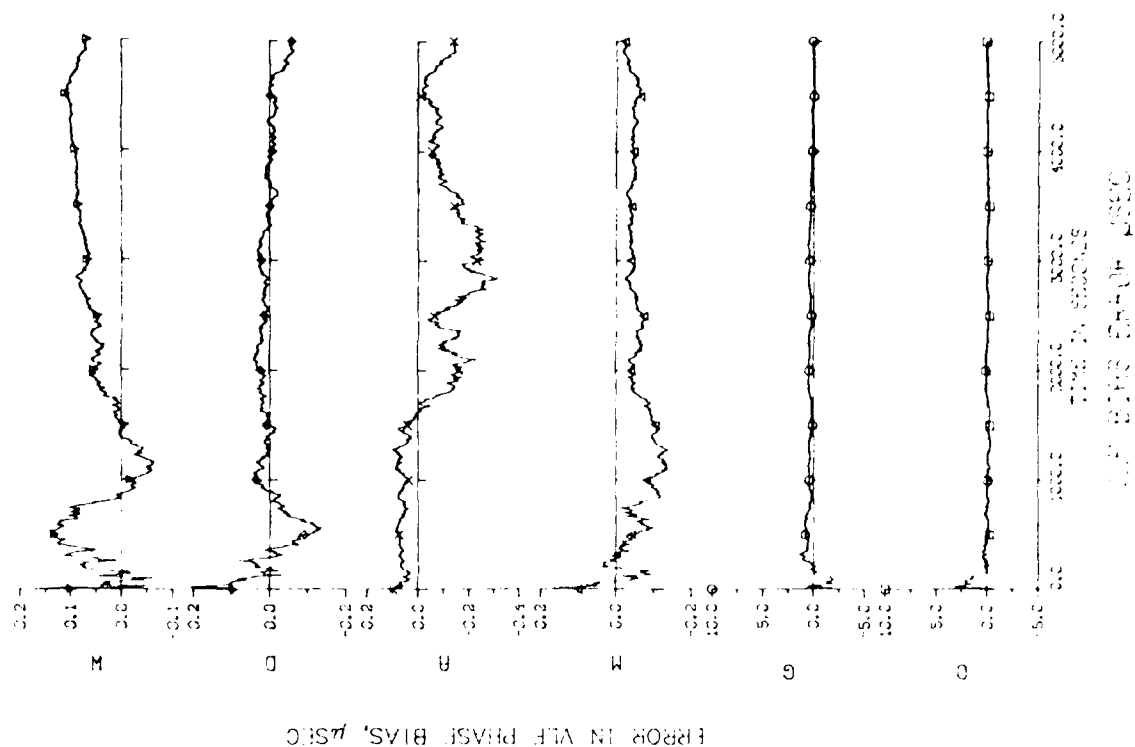


FIG. 27: SMART KALMAN FILTER OUTPUT ERRORS FOR LARGE DOPPLER/HEADING BIASES AND LARGE VLF BIASES

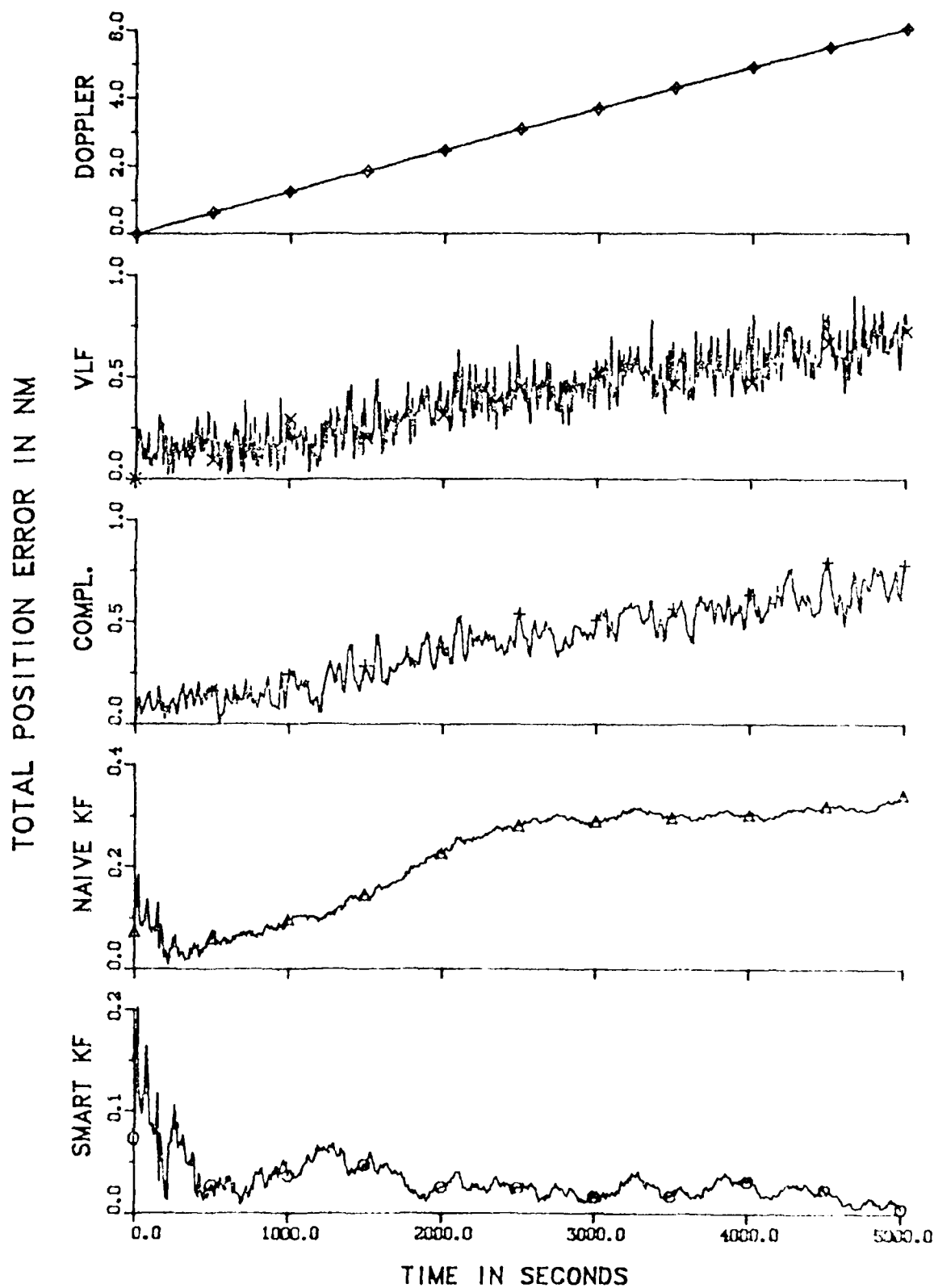
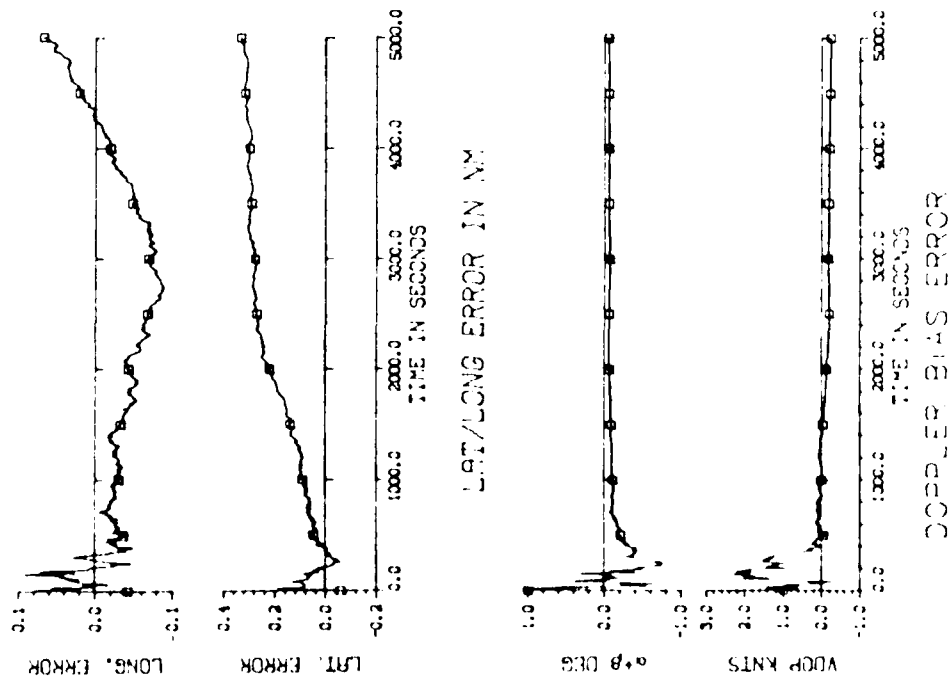
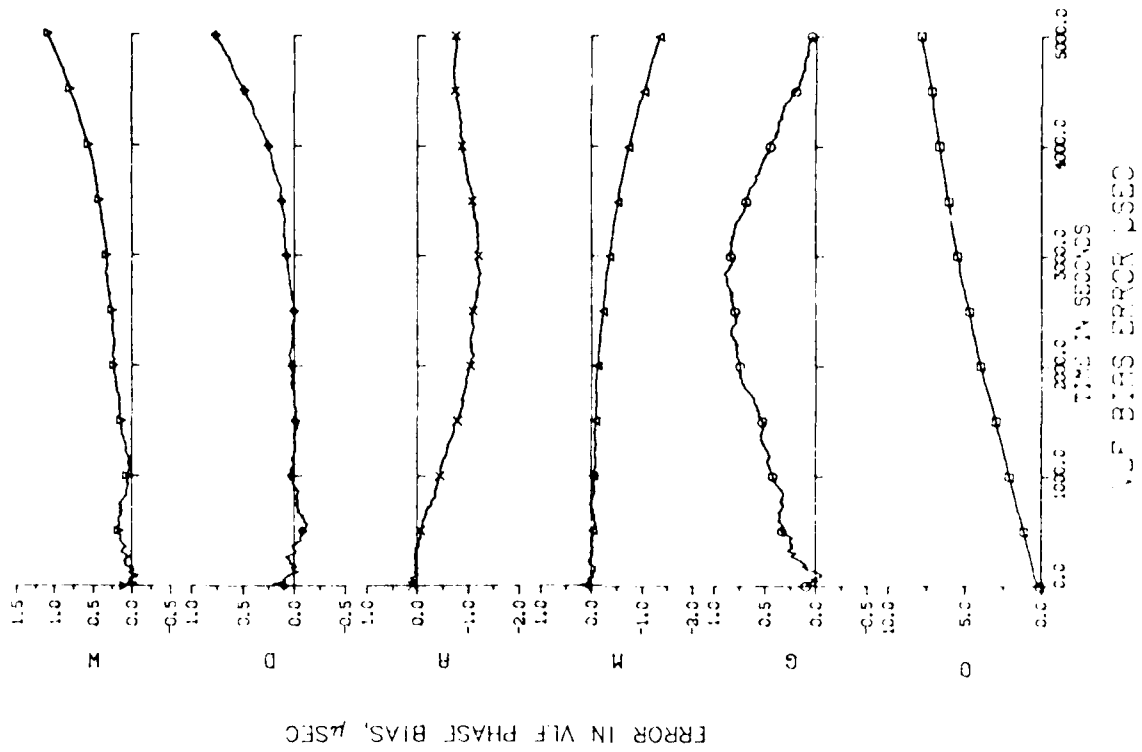
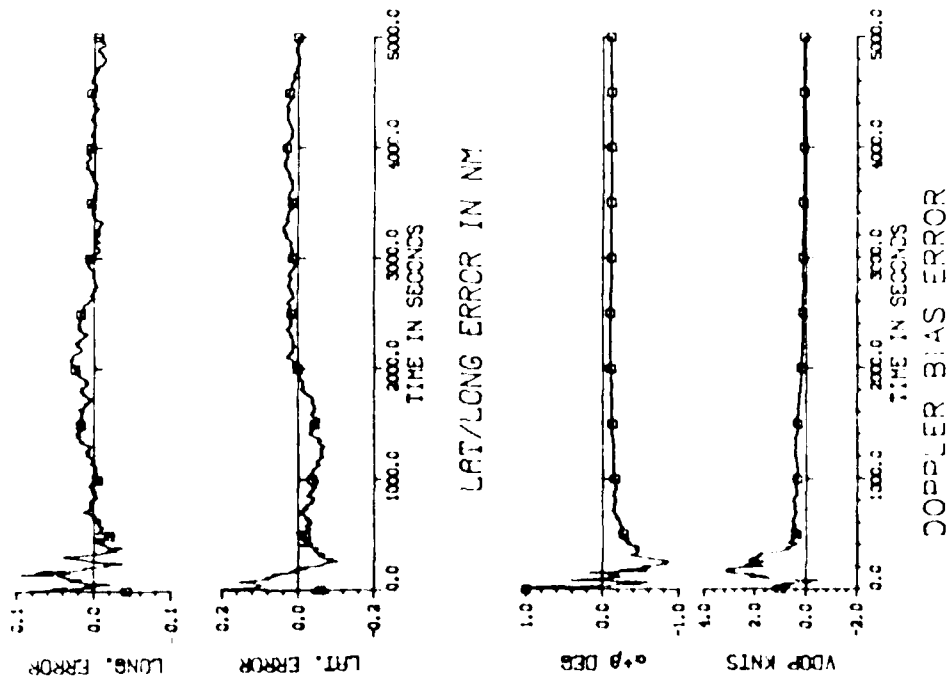
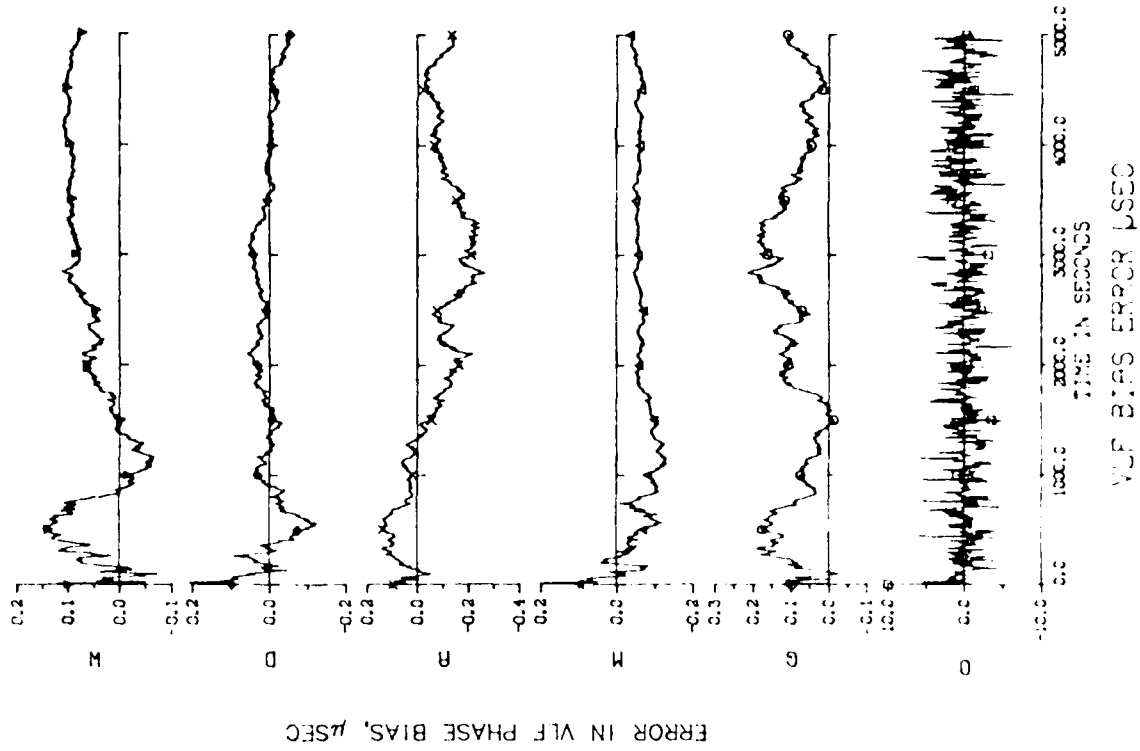


FIG. 28: COMPARISON OF TOTAL POSITION ERRORS USING DATA WITH A LARGE VLF DRIFT



PL0707.46 JUN 17 1960 14.48.04

FIG. 29: NAIVE KALMAN FILTER OUTPUT ERRORS FOR VLF DRIFT IN STATION O



PLOTOUT.56 JAN. 19 1980 11:43.24

FIG 30: SMART KALMAN FILTER OUTPUT ERRORS FOR VLF DRIFT IN STATION O



FIG. 31: VLF GEOMETRY STATIONS AVAILABLE DURING NAVIGATION FLIGHT

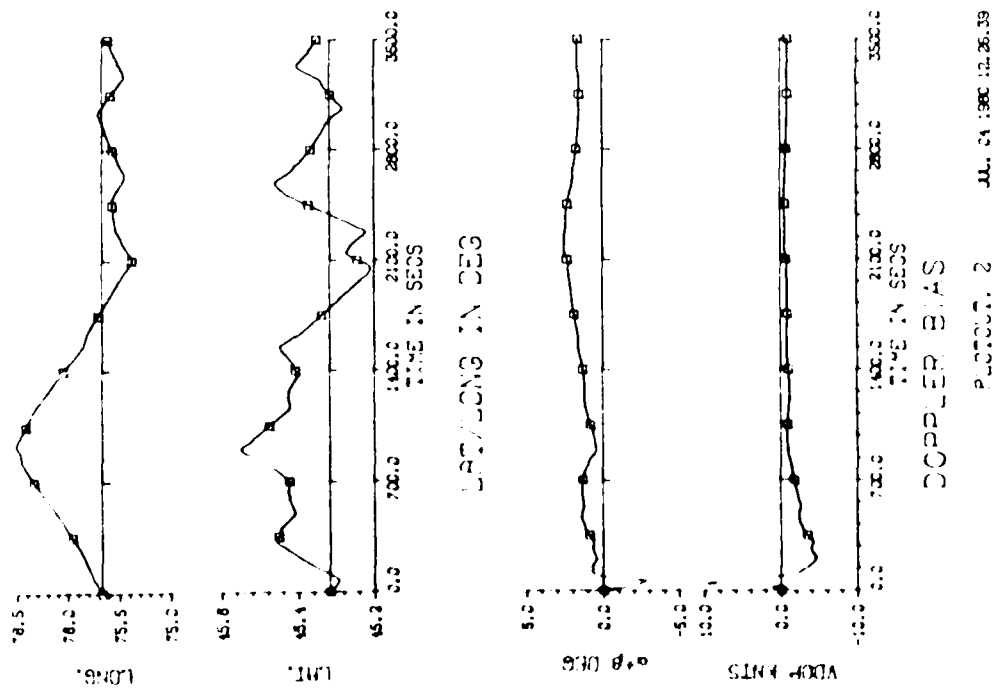
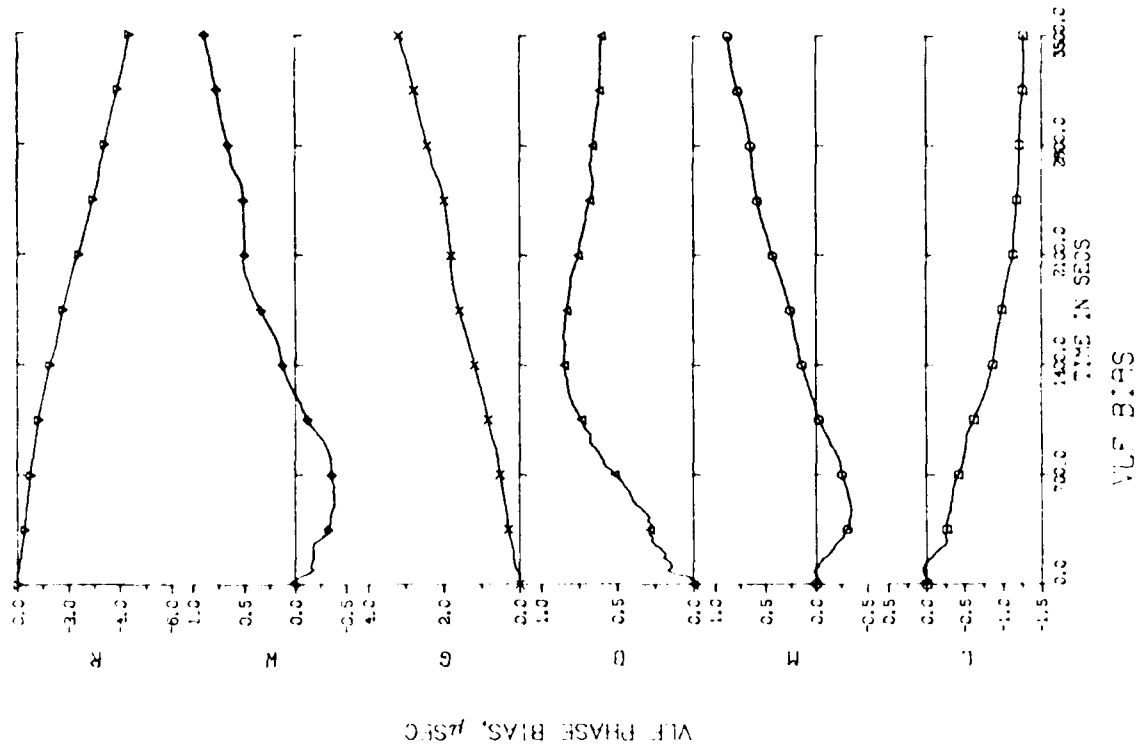


FIG. 32 NAIVE KALMAN FILTER OUTPUTS FOR REAL DATA

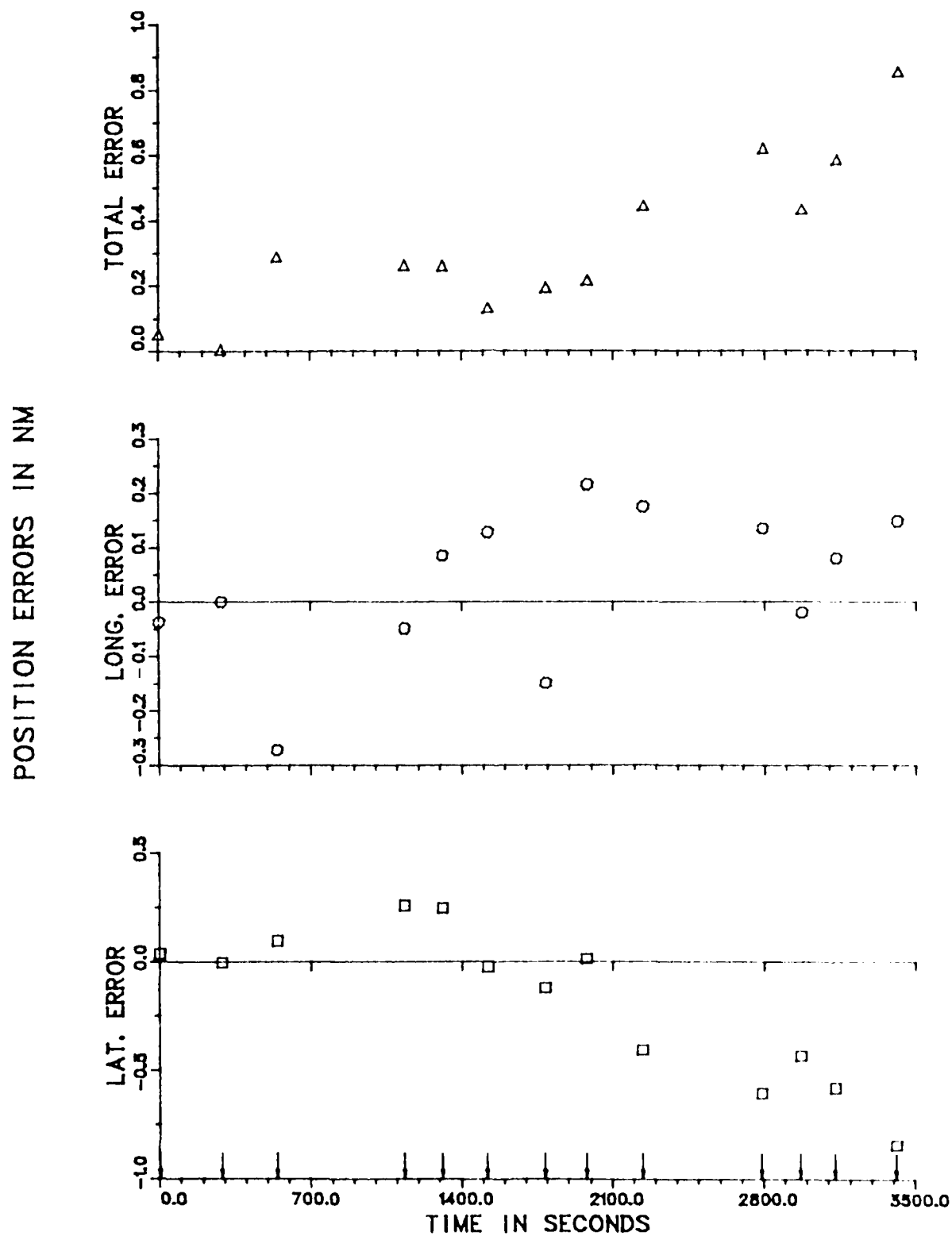


FIG. 33: POSITION ERRORS FOR NAIVE KALMAN FILTER RUN

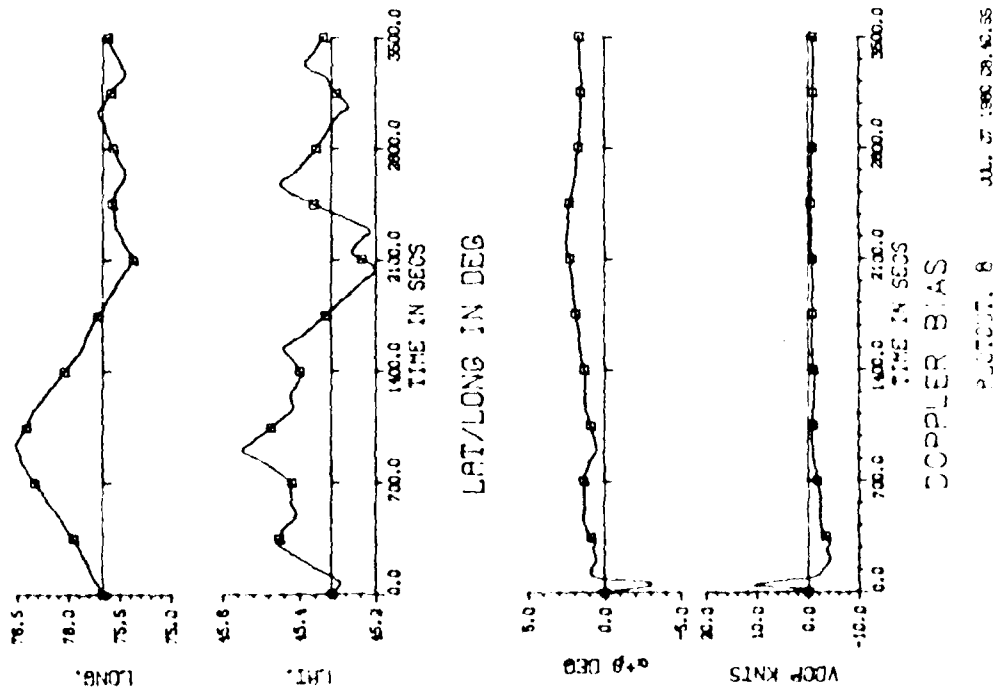
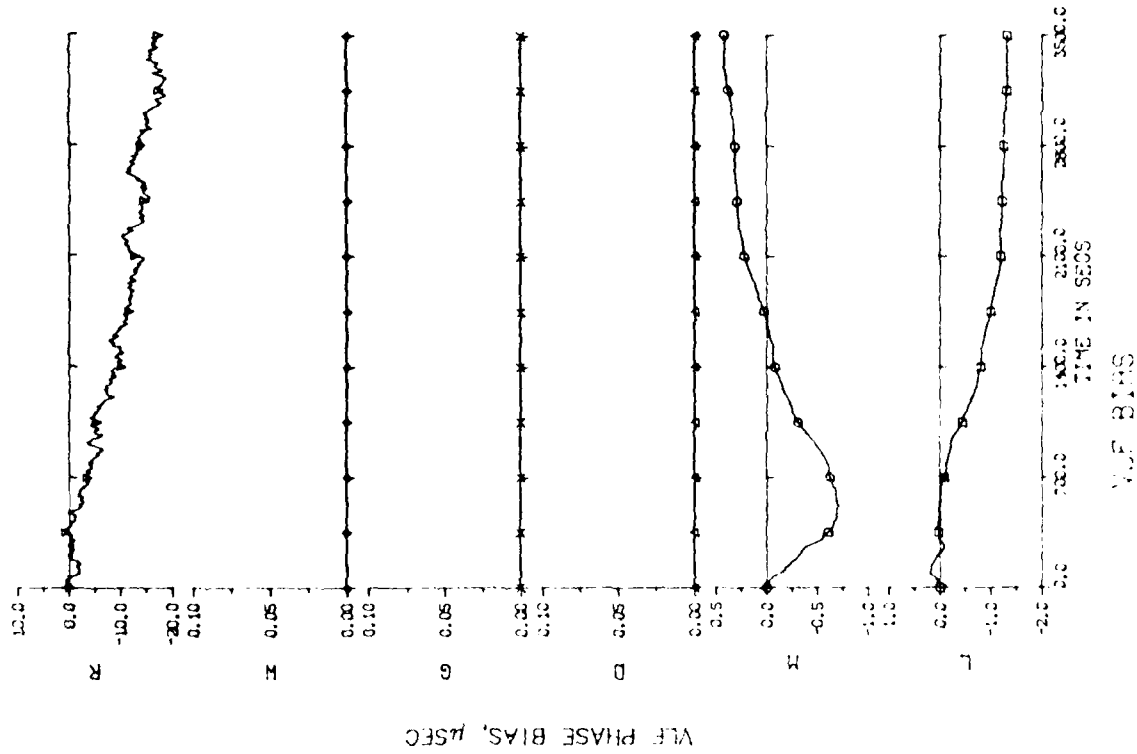


FIG. 34. SMART KALMAN FILTER OUTPUTS FOR REAL DATA

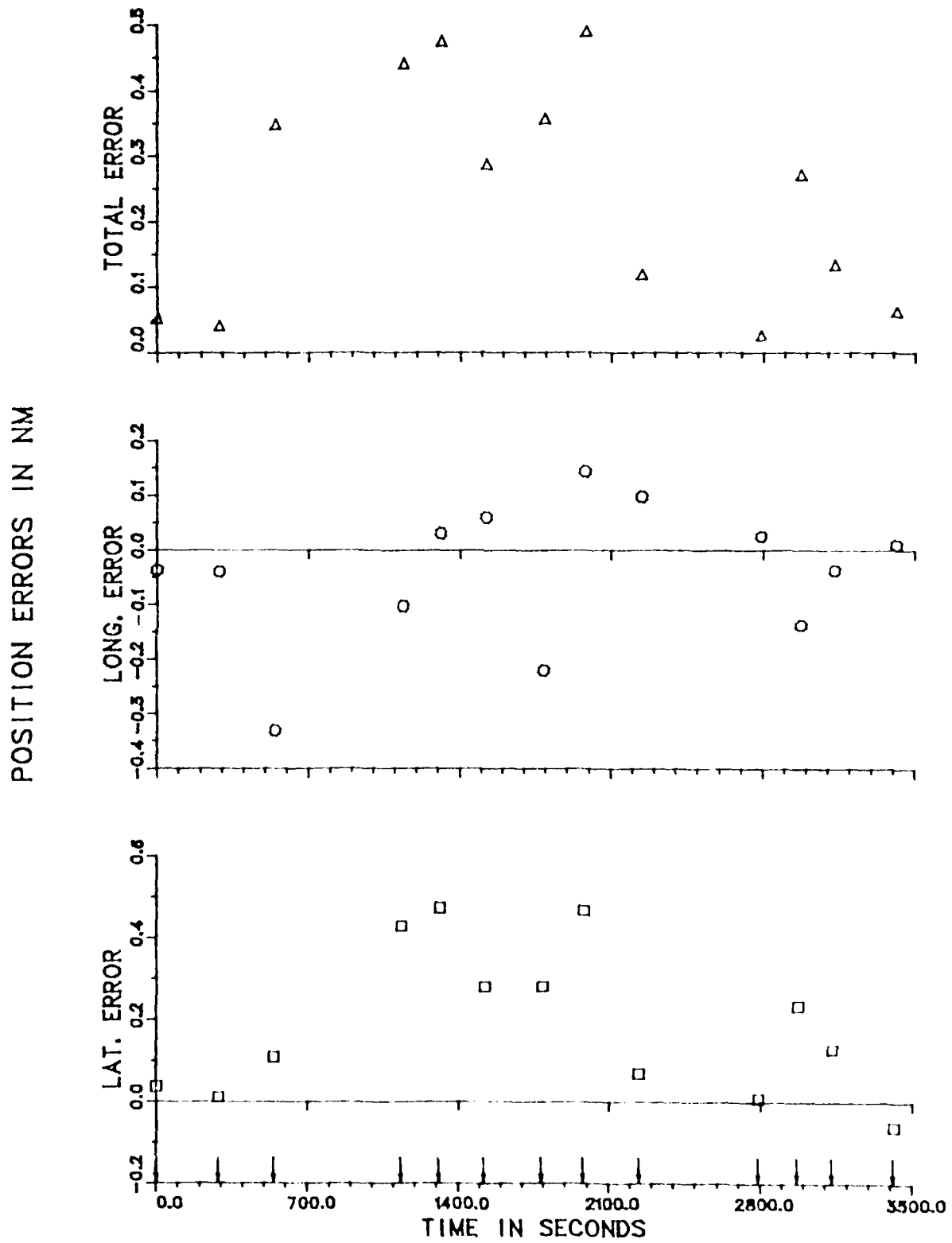


FIG. 35. POSITION ERRORS FOR SMART KALMAN FILTER RUN

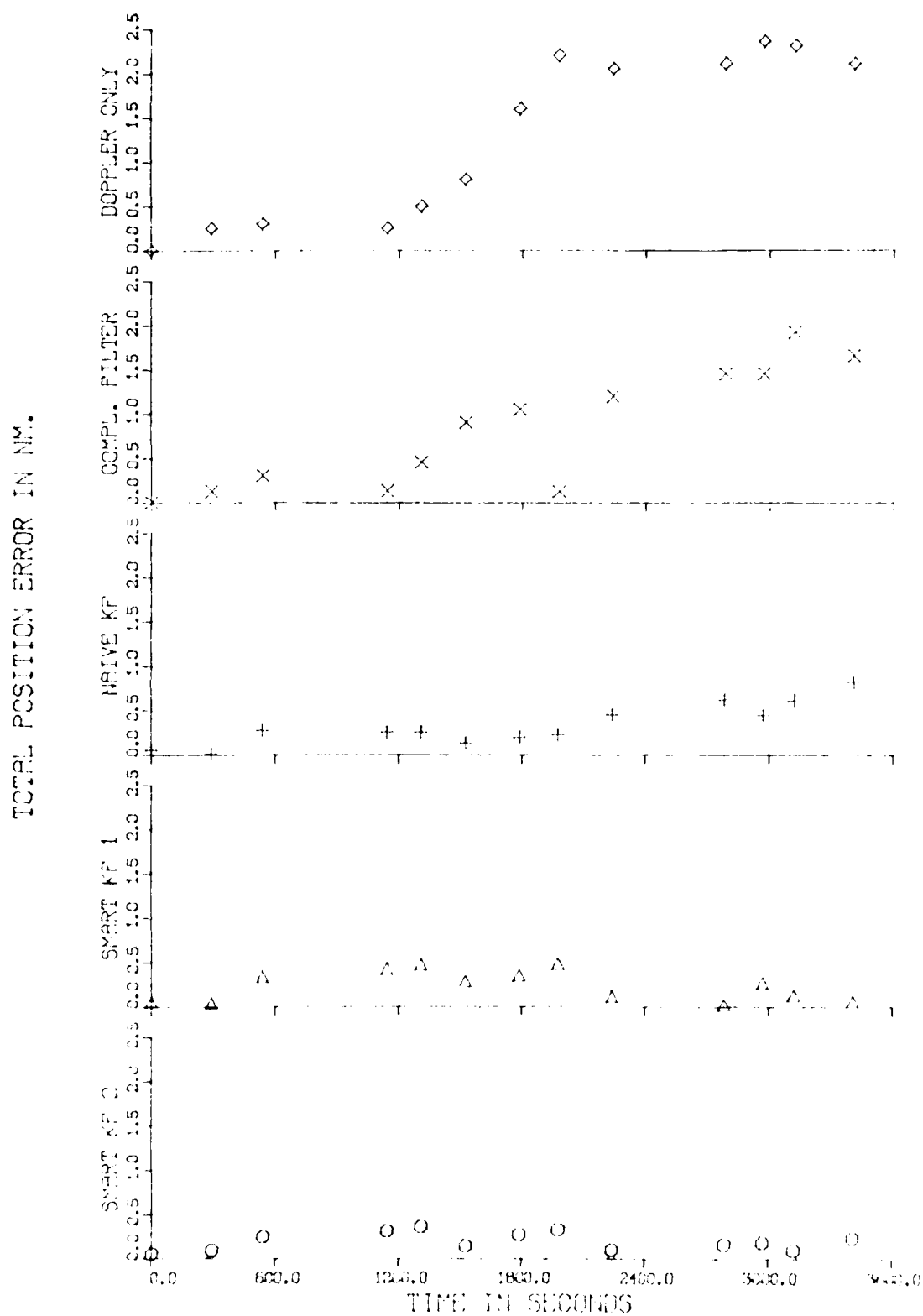


FIG 36. COMPARISON OF TOTAL POSITION ERRORS USING REAL DATA

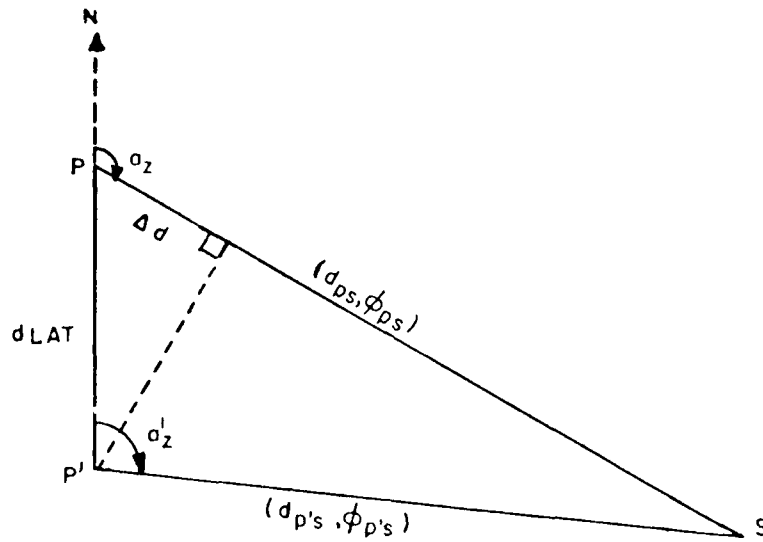


FIG. 37(a): VLF GEOMETRY FOR LATITUDE VARIATIONS

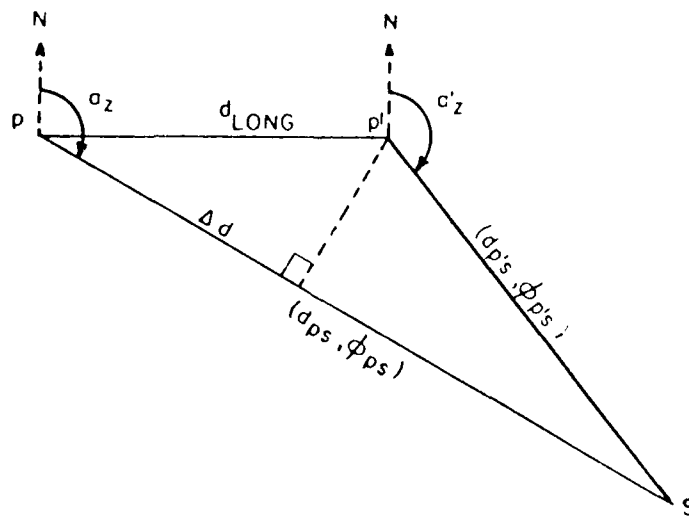


FIG. 37(b): VLF GEOMETRY FOR LONGITUDE VARIATIONS

APPENDIX A

ALGORITHM FOR HANDLING DOPPLER BEAM FREQUENCY DATA

The raw Doppler data consists of three RF beam frequencies each sampled at a twice per second rate. The beam frequencies f_a, f_b, f_c are defined as follows:

f_a : starboard forward-looking beam frequency;

f_b : port forward-looking beam frequency;

f_c : port backward-looking beam frequency.

The components of velocity in each of the three body-fixed aircraft axis directions (i.e. u: forward; v: starboard; w: vertical) can then be expressed as

$$\begin{aligned} u &= [(f_b + 50000) - (f_c + 50000)] / 8.925; \text{ (knots)} \\ v &= [(f_a + 50000) - (f_b + 50000)] / 4.4625; \text{ (knots)} \\ w &= [(f_a + f_c) - 50000] / 20.576; \text{ (knots)} \end{aligned} \quad (A1)$$

To convert the velocities u, v, and w into a straight-and-level co-ordinate system (x, y, z: x - positive forward, y - positive to starboard, z - positive local vertically upward) one must use the pitch (θ) and roll (ϕ) aircraft attitude information. Assuming θ is positive for nose-up attitude and ϕ is positive for right-wing-down attitude, the three straight-and-level components of Doppler velocity become:

$$\begin{aligned} V_x &= \cos \theta \cdot u + \sin \theta \cdot \sin \phi \cdot v + \sin \theta \cdot \cos \phi \cdot w \\ V_y &= \cos \phi \cdot v - \sin \phi \cdot w \\ V_z &= \sin \theta \cdot u - \cos \theta \cdot \sin \phi \cdot v - \cos \theta \cdot \cos \phi \cdot w \end{aligned} \quad (A2)$$

The groundspeed (V_{DOP}) and drift angle (α) quantities, more useful in the Doppler navigation model, are then expressed as

$$\begin{aligned} V_{DOP} &= (V_x^2 + V_y^2)^{1/2}; \text{ (knots)} \\ \alpha &= \arctan (V_y / V_x); \text{ (radians)} \end{aligned} \quad (A3)$$

F/G 17/7

FEB 81 B W LEACH

NAE-LR-604

NRC-19271

NL

UNCLASSIFIED

2 of 2

AD A
100636

END

DATE _____

FILMED

15

DTIC

APPENDIX B

VLF COMMUNICATIONS STATION INFORMATION

Letter Designation	Call Sign	Location	Frequency (KHz)	Radiated Power (kw)	
				Nominal	Authorized
M	NAA	CUTLER, MAINE	17.80	890	1000
W	NLK	JIM CREEK, WASH.	18.60	250	1000
L	NPM	HAWAII	23.40	140 → 630	1000
S	NWC	NORTH WEST CAPE, AUSTRALIA	22.30	1260	1000
R	GQD	ANTHORNE, G.BR.	19.00	—	—
G	GBR	RUGBY, G.BR.	16.00	250	300
J	NDT	YOSAMI, JAPAN	17.40	125	500
O	JXN	HELGELAND, NORWAY	16.40	150	350
A	NSS	ANNAPOLIS, MARYLAND	21.40	500+	1000
D*	—	LAMORE, N.D.	13.10	9 → 10	10

* D is actually an OMEGA station whose side frequency is being used in a VLF mode of operation.

APPENDIX C

DEVELOPMENT OF PLANT NOISE EQUATIONS

It is assumed that the zero mean, random noise processes u_v , u_α , and u_β occur in the measurement of V_{DOP} , α , and β respectively — the noise processes are also assumed to have constant variances σ_v^2 , σ_α^2 , and σ_β^2 respectively. The measured quantities (V_{DOP} , α , β) can then be written as follows:

$$\begin{aligned} V_{DOP} &= V_{Tr} + B_v + u_v \\ \alpha &= \alpha_{Tr} + B_\alpha + u_\alpha \\ \beta &= \beta_{Tr} + B_\beta + u_\beta \end{aligned} \tag{C1}$$

where each measurement consists of the true value + bias + random noise. It is then necessary to express $\dot{PLAT}(t)$ and $\dot{PLONG}(t)$ as functions of the noise processes to see how these noise processes are propagated through the basic Doppler differential equations. The continuous-time Doppler equations can be written as

$$\begin{aligned} \dot{PLAT}(t) &= \frac{(V_{DOP} - B_v - u_v) \cdot \cos(\alpha + \beta - B_\alpha - B_\beta - u_\alpha - u_\beta)}{60} \\ \dot{PLONG}(t) &= \frac{-(V_{DOP} - B_v - u_v) \cdot \sin(\alpha + \beta - B_\alpha - B_\beta - u_\alpha - u_\beta)}{60 \cdot \cos(PLAT \cdot \pi/180)} \end{aligned} \tag{C2}$$

For simplification, define $V_o \equiv V_{DOP} - B_v$, $B_{\alpha\beta} \equiv B_\alpha + B_\beta$, $u_{\alpha\beta} \equiv u_\alpha + u_\beta$, $\sigma_{\alpha\beta}^2 \equiv \sigma_\alpha^2 + \sigma_\beta^2$, $(\alpha + \beta)_o \equiv \alpha + \beta - B_{\alpha\beta}$. Then Equation (C2) becomes

$$\begin{aligned} \dot{PLAT}(t) &= \frac{(V_o - u_v)}{60} \cdot \cos[(\alpha + \beta)_o - u_{\alpha\beta}] \\ \dot{PLONG}(t) &= \frac{-(V_o - u_v) \cdot \sin[(\alpha + \beta)_o - u_{\alpha\beta}]}{60 \cdot \cos(PLAT \cdot \pi/180)} \end{aligned} \tag{C3}$$

If Equation (C3) is expanded, the result is

$$\begin{aligned}
 \dot{P}LAT(t) &= \frac{V_o}{60} \cdot [\cos(\alpha + \beta)_o \cdot \cos(u_{\alpha\beta}) + \sin(\alpha + \beta)_o \cdot \sin(u_{\alpha\beta})] \\
 &\quad - \frac{u_v}{60} \cdot [\cos(\alpha + \beta)_o \cdot \cos(u_{\alpha\beta}) + \sin(\alpha + \beta)_o \cdot \sin(u_{\alpha\beta})] \\
 \dot{P}LONG(t) &= \frac{-V_o \cdot [\sin(\alpha + \beta)_o \cdot \cos(u_{\alpha\beta}) - \cos(\alpha + \beta)_o \cdot \sin(u_{\alpha\beta})]}{60 \cdot \cos(PLAT \cdot \pi/180)} \\
 &\quad + \frac{u_v \cdot [\sin(\alpha + \beta)_o \cdot \cos(u_{\alpha\beta}) - \cos(\alpha + \beta)_o \cdot \sin(u_{\alpha\beta})]}{60 \cdot \cos(PLAT \cdot \pi/180)}
 \end{aligned} \tag{C4}$$

The small angle approximation applied to u_v and $u_{\alpha\beta}$ implies that

$$\begin{aligned}
 \dot{P}LAT(t) &= \frac{1}{60} \cdot [V_o \cdot \cos(\alpha + \beta)_o + u_{\alpha\beta} \cdot V_o \cdot \sin(\alpha + \beta)_o - u_v \cdot \cos(\alpha + \beta)_o \\
 &\quad - u_v \cdot u_{\alpha\beta} \cdot \sin(\alpha + \beta)_o] \\
 \dot{P}LONG(t) &= \frac{-V_o \cdot \sin(\alpha + \beta)_o + u_{\alpha\beta} \cdot V_o \cdot \cos(\alpha + \beta)_o + u_v \cdot \sin(\alpha + \beta)_o}{60 \cdot \cos(PLAT \cdot \pi/180)} \\
 &\quad - \frac{u_v \cdot u_{\alpha\beta} \cdot \cos(\alpha + \beta)_o}{60 \cdot \cos(PLAT \cdot \pi/180)}
 \end{aligned} \tag{C5}$$

In Equation (C5), the noise cross term, $u_v \cdot u_{\alpha\beta}$, can be eliminated because u_v and $u_{\alpha\beta}$ are assumed to be uncorrelated, implying that $u_v \cdot u_{\alpha\beta}$ will have only a second order effect at most. With this approximation, the equivalent noise processes in $\dot{P}LAT$ and $\dot{P}LONG$, u_{LAT} and u_{LONG} respectively, can be expressed as

$$u_{LAT} = \frac{-u_V}{60} \cdot \cos(\alpha + \beta)_0 + \frac{u_{\alpha\beta}}{60} \cdot V_0 \cdot \sin(\alpha + \beta)_0$$

$$u_{LONG} = \frac{[u_V \cdot \sin(\alpha + \beta)_0 + u_{\alpha\beta} \cdot V_0 \cdot \cos(\alpha + \beta)_0]}{60 \cdot \cos(PLAT \cdot \pi/180)}$$
(C6)

and the corresponding variances of these noise processes would be

$$\sigma_{LAT}^2 = \frac{\sigma_V^2}{(60)^2} \cdot \cos^2(\alpha + \beta)_0 + \frac{\sigma_{\alpha\beta}^2}{(60)^2} \cdot V_0^2 \cdot \sin^2(\alpha + \beta)_0$$

$$\sigma_{LONG}^2 = \frac{[\sigma_V^2 \cdot \sin^2(\alpha + \beta)_0 + \sigma_{\alpha\beta}^2 \cdot V_0^2 \cdot \cos^2(\alpha + \beta)_0]}{[60 \cdot \cos(PLAT \cdot \pi/180)]^2}$$
(C7)

The equivalent noise processes for the continuous-time Doppler system of Equation (C2) have just been defined. However, in order to calculate the \underline{G}_k needed in the Kalman filter implementation, it is necessary to look at the sampled-data version of the Doppler state equations. Including noise processes, these equations can be written as follows:

$$PLAT_{k+1} = PLAT_k + (A1_k - A3_k \cdot B_{V_k}) \cdot \sin(B_{\alpha\beta k}) + (A2_k - A4_k \cdot B_{V_k}) \cdot \cos(B_{\alpha\beta k})$$

$$+ \frac{1}{60} \cdot \int_{t_k}^{t_k + 10} u_{\alpha\beta} \cdot (V_{DOP} - B_{V_k}) \cdot \sin(\alpha + \beta - B_{\alpha\beta k}) dt$$

$$- \frac{1}{60} \cdot \int_{t_k}^{t_k + 10} u_V \cdot \cos(\alpha + \beta - B_{\alpha\beta k}) dt$$
(C8)

$$PLONG_{k+1} = PLONG_k + \frac{[(A1_k - A3_k \cdot B_{V_k}) \cdot \cos(B_{\alpha\beta k}) + (A4_k \cdot B_{V_k} - A2_k) \cdot \sin(B_{\alpha\beta k})]}{\cos(PLAT_k \cdot \pi/180)}$$

$$+ \frac{\left[\int_{t_k}^{t_k + 10} u_{\alpha\beta} \cdot (V_{DOP} - B_{V_k}) \cdot \cos(\alpha + \beta - B_{\alpha\beta k}) dt + \int_{t_k}^{t_k + 10} u_V \cdot \sin(\alpha + \beta - B_{\alpha\beta k}) dt \right]}{60 \cdot \cos(PLAT_k \cdot \pi/180)}$$

where

$$\begin{aligned}
 A1_k &\equiv \frac{1}{60} \cdot \int_{t_k}^{t_k + 10} V_{DOP} \cdot \sin(\alpha + \beta) dt \\
 A2_k &\equiv \frac{1}{60} \cdot \int_{t_k}^{t_k + 10} V_{DOP} \cdot \cos(\alpha + \beta) dt \\
 A3_k &\equiv \frac{1}{60} \cdot \int_{t_k}^{t_k + 10} \sin(\alpha + \beta) dt \\
 A4_k &\equiv \frac{1}{60} \cdot \int_{t_k}^{t_k + 10} \cos(\alpha + \beta) dt
 \end{aligned}
 \tag{C9}$$

As a simplification, assume average values for V_{DOP} , α , and β over the integration interval (i.e. for the noise terms only) by using their values at $t = t_k + 5$. Furthermore, define new random noise processes, $u_{\alpha\beta}^*$ and u_V^* , as follows:

$$\begin{aligned}
 u_{\alpha\beta k}^* &\equiv \int_{t_k}^{t_k + 10} u_{\alpha\beta} dt = \int_{t_k}^{t_k + 10} (u_\alpha + u_\beta) dt \\
 u_{V k}^* &\equiv \int_{t_k}^{t_k + 10} u_V dt
 \end{aligned}
 \tag{C10}$$

With these changes, the discrete Doppler equations become

$$\begin{aligned}
 PLAT_{k+1} &= PLAT_k + (A1_k - A3_k \cdot B_{V k}) \cdot \sin(B_{\alpha\beta k}) + (A2_k - A4_k \cdot B_{V k}) \cdot \cos(B_{\alpha\beta k}) \\
 &\quad + A5_k \cdot u_{\alpha\beta k}^* + A6_k \cdot u_{V k}^* \\
 PLONG_{k+1} &= PLONG_k - \frac{[(A1_k - A3_k \cdot B_{V k}) \cdot \cos(B_{\alpha\beta k}) + (A4_k \cdot B_{V k} - A2_k) \cdot \sin(B_{\alpha\beta k})]}{\cos(PLAT_k \cdot \pi/180)} \\
 &\quad + A7_k \cdot u_{\alpha\beta k}^* + A8_k \cdot u_{V k}^*
 \end{aligned}
 \tag{C11}$$

where

$$\begin{aligned}
 A5_k &\equiv \frac{1}{60} \cdot (V_{DOP} - B_{V_k}) \cdot \sin(\alpha + \beta - B_{\alpha\beta k}) \Big|_{t_k + 5} \\
 A6_k &\equiv \frac{-1}{60} \cdot \cos(\alpha + \beta - B_{\alpha\beta k}) \Big|_{t_k + 5} \\
 A7_k &\equiv \frac{(V_{DOP} - B_{V_k}) \cdot \cos(\alpha + \beta - B_{\alpha\beta k})}{60 \cdot \cos(PLAT_k \cdot \pi/180)} \Big|_{t_k + 5} \\
 A8_k &\equiv \frac{\sin(\alpha + \beta - B_{\alpha\beta k})}{60 \cdot \cos(PLAT_k \cdot \pi/180)} \Big|_{t_k + 5}
 \end{aligned} \tag{C12}$$

In spite of the fact that the continuous noise processes, $u_{\alpha\beta}$ and u_V , are assumed to have constant variances and zero means, the corresponding discrete-time noise processes do not necessarily have to have these characteristics, mainly because of the coloration effect that the integration process will have on the noise. Nevertheless, for the purposes of the Kalman filter implementation, $u_{\alpha\beta k}^*$ and $u_{V k}^*$ will be assumed to have the constant variances — $\sigma_{\alpha\beta}^{*2}$ and σ_V^{*2} respectively — where $\sigma_{\alpha\beta}^{*2}$ and σ_V^{*2} will be chosen to have about the same order of magnitude as $\sigma_{\alpha\beta}^2$ and σ_V^2 .

From the foregoing developments, the discrete plant noise process can be identified as

$$\underline{u}_k \equiv \begin{bmatrix} u_{V k}^* & u_{\alpha\beta k}^* \end{bmatrix}^T \tag{C13}$$

having the auto-covariance matrix,

$$\underline{Q}_k \equiv \begin{bmatrix} \sigma_V^{*2} & 0 \\ 0 & \sigma_{\alpha\beta}^{*2} \end{bmatrix} \tag{C14}$$

The associated \underline{G}_k matrix can be expressed in the following 10×2 form:

$$\underline{G}_k \equiv \begin{bmatrix} A6_k & A5_k \\ A8_k & A7_k \\ 0 & 0 \\ \cdot & \cdot \\ \cdot & \cdot \\ \cdot & \cdot \\ 0 & 0 \end{bmatrix} \quad (C15)$$

APPENDIX D

EVALUATION OF $\partial d\phi_i/\partial \text{PLAT}$; $\partial d\phi_i/\partial \text{PLONG}$

Recall that the general observation equation for expressing VLF station phase difference measurements is

$$\phi_{ik} = d\phi_i(\text{PLAT}_k, \text{PLONG}_k) + B_{\phi ik} + v_{\phi ik}; i = 1, \dots, 6 \quad (\text{D1})$$

Now $d\phi_i$ represents the relationship between a specified (PLAT, PLONG) geographical position and the theoretical phase difference of VLF station i (PLAT, PLONG in units of geographical degrees and $d\phi_i$ in units of microseconds). It is impossible to express $d\phi_i$ explicitly; however, each $d\phi_i$ is readily calculated from computer algorithms that can generate theoretical VLF station phases for any specified geographical location via the Sodano inverse routine (Refs. 18 and 19).

The partial derivatives, $\partial d\phi_i/\partial \text{PLAT}$ and $\partial d\phi_i/\partial \text{PLONG}$, can be expressed fairly explicitly using the following argument. Consider a geographical location, P, and a VLF station location, S, as shown in Figure 37(a), with d_{PS} , ϕ_{PS} , and a_z the distance, phase, and azimuth (i.e heading) respectively from P to S. Consider, also, a small change in latitude only, ΔLAT , in going from point P to a new point, P', a distance $d\text{LAT}$ away. Let $d_{P'S}$, $\phi_{P'S}$, and a'_z be the corresponding distance, phase, and azimuth from P' to S. Consider, now, the relationship between $\Delta d \equiv d_{P'S} - d_{PS}$ and $d\text{LAT}$. Based on Figure 37(a), assume that $a_z \approx a'_z$, since $d\text{LAT}$ and Δd are quite small while d_{PS} and $d_{P'S}$ are quite large distances. It then holds that

$$\Delta d \approx -\cos a_z \cdot d\text{LAT} \quad (\text{D2})$$

The relationship between d_{PS} and ϕ_{PS} is simply,

$$d_{PS}(\text{nm}) = V_S(\text{nm}/\mu \text{ sec}) \cdot \phi_{PS}(\mu \text{ sec}) \quad (\text{D3})$$

where V_S is the speed of propagation of the signal transmitted from VLF station S. The substitution, $\Delta d = V_S \cdot \Delta \phi$, into Equation (D2) yields

$$V_S \cdot \Delta \phi \approx -\cos a_z \cdot d\text{LAT} = -\cos a_z \cdot 60 \cdot \Delta \text{LAT} \quad (\text{D4})$$

or

$$\frac{\Delta \phi}{\Delta \text{LAT}} \approx \frac{-60}{V_S} \cdot \cos a_z \quad (\text{D5})$$

In the limit as $\Delta \text{LAT} \rightarrow 0$, Equation (D5) becomes

$$\partial d\phi_S/\partial \text{PLAT} = \frac{-60}{V_S} \cdot \cos a_z \quad (\text{D6})$$

In similar fashion, based on the geometry depicted in Figure 37(b), consider a small change in longitude in going from point P to point P'. Using the same kind of argument as before, an approximate expression for Δd can be determined as,

$$\Delta d \approx \sin a_z \cdot d\text{LONG} \quad (\text{D7})$$

Substituting $\Delta d = V_S \cdot \Delta\phi$ and $d\text{LONG} = 60 \cdot \Delta\text{LONG} \cdot \cos(\text{PLAT})$ into Equation (D7) yields

$$V_S \cdot \Delta\phi \approx \sin a_z \cdot 60 \cdot \Delta\text{LONG} \cdot \cos(\text{PLAT}) \quad (\text{D8})$$

or

$$\frac{\Delta\phi}{\Delta\text{LONG}} \approx \frac{60}{V_S} \cdot \sin a_z \cdot \cos(\text{PLAT}) \quad (\text{D9})$$

and, in the limit as $\Delta\text{LONG} \rightarrow 0$, Equation (D9) becomes

$$\partial d\phi_S / \partial \text{PLONG} = \frac{60}{V_S} \cdot \sin a_z \cdot \cos(\text{PLAT}) \quad (\text{D10})$$

Note that both of the partial derivatives, $\partial d\phi / \partial \text{PLAT}$ and $\partial d\phi / \partial \text{PLONG}$, are functions of PLAT and PLONG (since, in particular, a_z is a function of PLAT, PLONG). Moreover, for any specified geographical position (PLAT, PLONG) and any specified VLF station, the values of $\sin a_z$ and $\cos a_z$ come directly out of the Sodano inverse routine as it is programmed at NAE. Equations (D6) and (D10) are then used to calculate the values of the partial derivatives for the specified position and VLF station.

END

DATE
FILMED

7-18-11

DTIC